University of Stavanger

Faculty of Science and Technology

MASTER'S THESIS

Study program/ Specialization: Mechanical Engineering and Materials Science	Spring semester, 2017 Open / ~~Restricted access~~
Writer: Amanda Joela Rachel Nikolaisen	…… …… (Writer's signature)
Faculty supervisor: Prof. Dimitrios G. Pavlou External supervisor(s): Yihan Xing (ROXAR, Emerson Process Management)	
Thesis title: Evaluation of a nonlinear cumulative creep damage model for design applications	
Credits (ECTS): 30	
Key words: nonlinear cumulative creep damage model, time fraction rule, linear summation, pressure vessels, ASME, finite element analysis, material models, creep testing, Larson-Miller parameter, elevated temperature design	Pages: 91 + enclosure: 52 Stavanger, June15th 2017

Front page for master thesis
Faculty of Science and Technology

ABSTRACT

Predicting creep damage and remaining life of an engineering design is a complex task. There are many types of creep material models and they provide significantly different predictions. Furthermore, the necessary material data required for the material models are rarely available. Creep tests are typically performed in uniaxial tension under constant load and temperature. However, such similar conditions are rarely encountered in practical engineering applications where multiaxial stresses and cyclic load and temperature often are present. Creep-fatigue interaction and correlation between uniaxial and multiaxial stress states also add on to the complexity of the damage assessment in creep conditions.

Pavlou have proposed a nonlinear cumulative creep damage model (NCCDM) that considers the sequence effect from the previous load history in the damage assessment. NCCDM has been evaluated for use in design applications and compared to a widely-used linear summation method known as the time fraction rule (TFR); TFR is used in several engineering design codes. Pavlou, Grell et. al, Lin and Teng have shown that NCCDM can predict creep damage more accurately than TFR under stepwise constant uniaxial stress and temperature conditions. However, NCCDM has not been used yet in practical engineering design applications.

In this thesis, NCCDM will be applied to a X8CrNiMoNb-16-16 pressure vessel designed in accordance with ASME VIII-2 to demonstrate its use in conjunction with practical engineering problems. The pressure vessel will be subjected to elevated temperatures with applied variable two-step loading. This is used as a representative engineering example for the comparison of the two models, i.e., NCCDM vs. TFR.

Firstly, by considering proposals made by Pavlou, Grell, Lin and Teng, an evaluation of the best use of the NCCDM was made. The model behaviour was also studied by considering fictive load cases. Based on the findings, conditions for further use of the model was established. *Secondly*, rupture and creep strength data obtained from a material database were used to create fitted curves with the Larson-Miller parameter from which time-to-rupture and time-to-1% strain could be obtained for different stresses. *Thirdly*, the finite element (FE) method was used to evaluate several types of stress criteria on a generic model of a pressure vessel. Variable-step internal pressure at a constant elevated temperature was applied to the model. A linear-elastic and an elastic-plastic material model was used in the analysis. By considering high-to-low (H-L) and a low-to-high (L-H) loading sequence the remaining life to rupture and to 1% strain was calculated for the pressure vessel with both NCCDM and TFR.

It was found that the NCCDM and the TFR gave very different predictions. For the L-H type of loading sequence the NCCDM predicted more conservative remaining life than TRF. The opposite was seen for the H-L type of loading. Larger variation in stress between the two load steps resulted in an increased difference between the predictions made with the two models. Due to the difficulty of performing a time-dependent creep analysis, the NCCDM model would benefit from being combined with an elastic-analysis procedure to approximate the time-dependent stress distribution, like the procedure in ASME-NH. Because of the simple use of NCCDM, there is potential for it to gain acceptance for engineering applications. However, further analysis and research should be made to fully understand the damage processes considered in the NCCDMs remaining life assessment.

PREFACE

This thesis has been executed as a final project of my two-year Master of Technology education in Mechanical Engineering and Materials Science at the University of Stavanger. The subject was proposed by Professor Dimitrios Pavlou from the University of Stavanger in collaboration with Roxar, Emerson Process Management.

I would like to thank my supervising Professor Dimitrios Pavlou at the Department of Mechanical and Structural Engineering and Materials Science at the University of Stavanger for his help and guidance during the thesis work and for introducing me to this topic. I would also like to give a special thanks to my second supervisor Postdoctoral Senior Mechanical Analysist Yihan Xing at Roxar, Emerson Process Management for his encouragements, support and sharing of knowledge both within and outside the scope of this thesis. The guiding and optimism he has provided has been invaluable. Another thanks also go to Roxar, Emerson Process Management for providing me with an office space at their premises.

I also want to send my gratitude to PhD Student Kristen Rege who generously at one point offered his time to provide me with insight and to clear up some difficulties of a problem that was encountered during the work.

Finally, I want to thank my family and my partner for their encouragements and support during this process.

Amanda J.R Nikolasien

Stavanger, June 1017

CONTENTS

LIST OF FIGURES

LIST OF TABLES

NOMENCLATURE

Latin symbols

A, B	Constants in Lamé equations
a, b	Material specific constants for Huddleston equivalent stress
A_n	Nozzle area
A_i	Internal nozzle area
C	Larson-Miller parameter constant
D, D_c, D_f	Damage, creep damage, fatigue damage
D_i	Internal cylinder diameter
E	Elastic modulus
E_T	Tangent modulus
J_1	First invariant of the stress tensor
J_2'	Second invariant of the deviatoric stress tensor
m	Temperature dependent material constant for Norton-Bailey creep strain/strain-rate
m_2	Material factor for the multiaxial strain limit criterion (ASME VIII-2)
N_{dj}	Number of allowable load cycles to failure for stress/strain amplitude at cycle type j
n_j	Number of cycles at cycle type j
O	Point of intersection between the of the isodamage lines
P, P_i, P_o, P_n	Pressure, internal pressure, external pressure, pressure at nozzle
P_{LM}	Larson-Miller parameter
p	Fitting parameter
r, r_i, r_o	Cylinder radius, internal radius, external radius
R^2	Correlation coefficient
R_{p1}	Creep resistance corresponding to limit strain 1%
S_1	Maximum deviatoric stress
S_j	Stress corresponding to total strain range ε_{tj} (ASME-NH)
S_S	Invariant stress parameter
S_y	Yield stress
S_u	Ultimate stress
T	Temperature
T_i	Temperature at load step i
T_M	Metal melting temperature
t_{Rp1}	Allowable time to 1% strain
t_f	Failure/rupture time
Δt_2	Variation between predicted remaining life t_2 between t_{2_P} and $t_{2_{TFR}}$
t_i	Time spent at load step i
t_{fi}	Rupture time at stress and temperature i
$t_{f_{fit}}$	Rupture time from fit
$t_{f_{data}}$	Rupture time from creep data
$t_{f_{CRS}}$	Time to creep-rupture for constant, temperature load obtained from fitted curve
$t_{f_{Rp1}}$	Time-to-1% strain corresponding to constant uniaxial load obtained from fitted curve
Δt	Duration of time interval, k, at a certain stress- and temperature-level (ASME-NH)
T_d	Rupture time at stress and maximum temperature for the time interval k (ASME-NH)
t_{2_P}	Predicted remaining life obtained with nonlinear Pavlou creep damage model
$t_{2_{TFR}}$	Predicted remaining life obtained with time fraction rule
t_H	Total number of hours spent at elevated temperatures (ASME-NH)
$\bar{t}_j$	Average cycle time (ASME NH)
t	Cylinder thickness

w_i	Weights that regulate how much each response value impact the final parameter in SSE
y_i	Data points for fitted function
$\hat{y}_i$	Value in fitted function
$q_{1,2}$	Exponent in the nonlinear Pavlou creep damage accumulation model
$q(\sigma_i)$	Exponent in Rege's and Pavlou's fatigue damage model

Greek symbols

α_t	Mean coefficient of thermal expansion
α_{sl}	Material factor for the multiaxial strain limit (ASME VIII-2)
α, β	Constants for mixed criterion
$\varepsilon_t, \varepsilon_e, \varepsilon_p, \varepsilon_c$	Total strain, elastic strain, plastic strain, creep strain
ε_L	Limiting triaxial strain
ε_{cf}	Cold forming strain
ε_{Lu}	Uniaxial strain limit
ε_{peq}	Equivalent plastic strain
ε_i	Creep strain for cycle type i
ε_{fi}	Failure ductility or fracture strain for cycle type i
ε_{peq}	Equivalent plastic strain (ASME VIII-2)
ε_{cf}	Cold forming strain (ASME VIII-2)
ε_L	Triaxial limiting strain (ASME VIII-2)
ε_{Lu}	Uniaxial strain limit (ASME VIII-2)
$\dot{\varepsilon}, \dot{\varepsilon}_c$	Strain rate, creep strain rate
ν	Poisson's ratio
ρ	Material density
σ	Stress
σ_i	Stress level at load step i
$\sigma_1, \sigma_2, \sigma_3$	Principal stresses
σ_{CRS}	Creep rupture strength
σ_{CKTI}	Mixed criterion from Russian research institute CKTI
σ_e	Creep endurance limit
σ_{eq}	Mixed criteria
σ_{MPS}	Maximum principal stress
σ_{HUD}	Huddleston equivalent stress
$\sigma_h, \sigma_r, \sigma_z$	Hoop stress, radial stress, axial stress
σ_{Rp1}	Creep resistance
σ_{TR}	Tresca criterion
σ_{VM}	von Mises criterion
θ_i	Angle from creep endurance limit to arbitrary isodamage line
θ_f	Angle from creep endurance limit damage state of 100% (rupture curve)

Abbreviations

ASME	American Society of Mechanical Engineers
BPVC	Boiler and Pressure Vessel Code
CRS	Creep rupture strength
DBA	Design by Analysis
DBR	Design by Rule
EN	European Standard/European Norm
GBS	Grain boundary sliding
MPS	Maximum principal stress
NCCDM	The Pavlou nonlinear cumulative creep damage model
RMSE	Root mean squared error
SSE	Sum of squares due to errors
TRF	Time fraction rule
LRF	Life fraction rule
RT	Room temperature

1 INTRODUCTION

1.1 Background

Creep has been studied extensively ever since the creep phenomenon was recognized as a problem in design of high-temperature components [1]. One of the earliest research on creep was carried out by Andrade [2] in 1910, and by the 1920s creep strength in metals was studied systematically with short term creep tests and later in the 1950s with long term creep tests [3]. Although great advances have been made in research of understanding the creep phenomena, creep damage can be difficult to assess due to the complex nature of creep and the many factors affecting the creep damage process. Some of the main difficulties regarding creep rupture prediction is shown in Figure 1

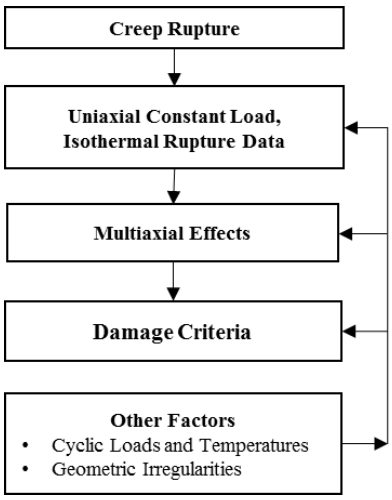

Figure 1. Details of creep-rupture problem[4]

The time-dependent damage process that constitutes creep is mainly influenced by stress and temperature. Creep and stress-rupture tests are typically performed under isothermal uniaxial constant load conditions to determine the long-term damage effect on the material due to stress and temperature. However, similar conditions are rarely found in practical engineering problems where multiaxial stress states, cyclic or variable load and temperature conditions are often present.

To predict creep deformation, it is essential to understand the material response and much work has been devoted to finding a functional relationship between stress, strain, time and temperature, nevertheless no such functional relationship has yet been generalized. The problem with predicting creep becomes even more challenging when fracture is considered, since it involves initiation and propagation of cracks. Other factors that complicates creep life prediction are the presence of geometrical irregularities and notches since these cause stress concentrations. This complicates creep rupture prediction further since notches introduce triaxiality which ultimately affect ductility and the rupture behaviour of the material. The more triaxiality, the less ductile the material behaves. Stress concentrations also lead to relaxation and stress redistributions and hence continuous accumulation of creep strain [4]. Stress relaxation is also a problem associated with variable loading when new high stresses are re-established at the beginning of each new cycle [1].

Since creep data for materials are based on uniaxial tests, it is necessary to correlate uniaxial and multiaxial stress so the same damage rules and applicable creep data can be used for predicting creep rupture. Many researchers have worked on characterizing the stress dependence of creep [5-8] and many alternative criteria have been proposed for the uniaxial-multiaxial correlation. However, which stress criterion that is best suited depends on the rupture characteristic of the material. It has been seen that materials that develops severe internal cracks which is typical for brittle material ruptures are mostly dependent on the maximum principle stress while materials with a more ductile behaviour are better described with an effective stress criterion. However, most material failures fall in a category in between and mixed stress criterions and other alternative methods have therefore been suggested [4].

Growth in computer power has made it possible to numerically solve nonlinear time dependent engineering problems and define time dependent stress and strain distributions. Although commercially available software has methods for modelling creep, it is important to understand the assumptions and material models incorporated in the software because validation of the results is necessary [1]. As mentioned no generalized procedures for correlating stress, strain, time and temperature exist and the material models that are found in literature yield predictions which can differ remarkably from one another. Thus to obtain a meaningful prediction from a creep analysis, the constitutive equations need to be carefully selected and evaluated for both the material and the load and temperature history of interest [9]. Another issue related to this is that these material models require necessary input data from experimental test which are rarely available. It will take years to collect such material data that can describe the material response well enough to justify such an analysis since the increased effort and time a creep analysis entails are not in proportion to what is reasonable in an engineering project. [1].

Because of this, instead of basing creep assessment procedures on inelastic creep analysis, most design codes try as far as they can to offer alternative assessment procedures based on elastic analysis. Another reason why elastic analysis is preferred is that it is easier than nonlinear analysis. In addition, inelastic creep analysis requires much more computational effort compared to an elastic one, especially for large components, complex load combinations and load histories [1]. ASME has made a deliberate decision not to provide too comprehensive and detained guidance for their inelastic time-dependent analysis procedure. The reason for this is because the development of material models is considered an ongoing process and that too detailed guidance would halt the development [9].

Even if a plastic creep analysis can solve the time dependent stress and strain distribution, a cumulative damage criterion is necessary to determine the remaining life of a component. Life prediction for components under variable loading conditions are based on assumptions of rules on how damage accumulates and only very simple damage rules based on linear summation are in use today [4]. The time fraction rule, also known as Robinson's rule [10] is the most common rule for assessing creep damage. To account for the creep-fatigue interaction during cyclic creep conditions the time fraction rule is combined by means of superposition with Miner's rule for fatigue, this combined cumulative creep-fatigue damage rule is sometimes referred to as the life fraction rule. However, the problem of linear summation methods is that they do not consider the damage effect due to the load and temperature sequence in the loading history. Current national standards, for instance, Boiler and Pressure Vessel Code by American Society of Mechanical Engineers (ASME) [11], UK nuclear power standard R5 [12], French RCC-MR [13], have all incorporated the life fraction rule in their rules for cyclic creep damage assessment. However, without the use of engineering corrections and safety factors that are included in the above mentioned codes, the life fraction rule is considered non-conservative [9]. More complex nonlinear rules have been proposed, but these typically require experimentally

derived material constants which can only be obtained with additional creep testing in addition to the standard uniaxial tests, something which is typically undesirable [1, 9]. This seems to be part of the reason why the linear damage rules are the only rules that have gained universal acceptance in codes and guidelines [1].

Due to the above-mentioned difficulties in predicting creep rupture accurately most damage assessments methods are based on approximations and assumptions, and methods provided in codes tend to be on the conservative side. Although the incentive of construction standards is to provide safe designs, designs should also be cost effective. Overly conservative criteria may cause designs to become expensive and are therefore not desirable. More accurate damage models might therefore be preferred.

There are many examples of equipment that encounters elevated temperatures during their operation. Some of them are hydrocrackers in petroleum refineries, boilers and pressure vessels and blades in gas turbine engines in nuclear power or chemical plants [14]. Many of the plants that are in operation today have critical components reaching or exceeding their estimated design life. Life extension of components in existing plants can reduce cost significantly comparing to building new plants [15] and more accurate assessment methods could be beneficial in a life extension project, and perhaps prohibit premature shutdown.

In a paper published in the journal Engineering Structures in 2001, Pavlou [16] derives at a nonlinear creep damage model which takes both load and temperature sequence into account in addition to being relatively easy to use. The proposed creep damage model accurately predicted the creep damage when compared with actual test results obtained from a stepwise constant uniaxial tensile creep test. Pavlou's model has later been tested by other researchers, both in its original form [17] and slightly modified [18] and did in both cases give reasonable predictions of the creep damage when variable load sequences was considered. However, the proposed nonlinear creep damage model has not so far now been used for design purposes.

1.2 Objective and scope

The main objective of this thesis is to evaluate the practical use of the nonlinear Pavlou creep damage accumulation model and compare it to the widely-used life fraction rule also known as Robinson's rule which has been incorporated in several national codes. The difference in remaining creep life between the two damage accumulation models is to be compared by studying a representative engineering example subjected to variable loads at elevated temperatures in the creep range.

The component to be studied is a generic model of a pressure vessel subjected to internal pressure at a constant elevated temperature of 700 °C (973 K). Internal pressure will be applied in a low-high sequence and high-low sequence and remaining life using the two creep models is to be evaluated for each sequence.

To reach the objectives of this thesis, the following sub-objectives are to be carried out:

- Study creep mechanisms and current creep damage assessments methods.
- Evaluate methods used in standards for design of components in high-temperature service.
- Evaluate the Pavlou creep damage model by considering suggestions from previous research.
- Study how to account for multiaxial stress states and stress concentrations in creep damage assessment. Evaluate how various stress criterions can impact damage assessment and remaining life.
- Construct a creep-rupture curve from applicable creep data for the material being used and study potential error and uncertainties from the creep data fit
- Carrey out a stress analysis in ANSYS using various material models and calculate remaining life for the pressure vessel with the linear and nonlinear creep damage models and compare the remaining life

Figure 2 shows a flowchart of the sub-objectives of the scope and work-process which is presented in this thesis.

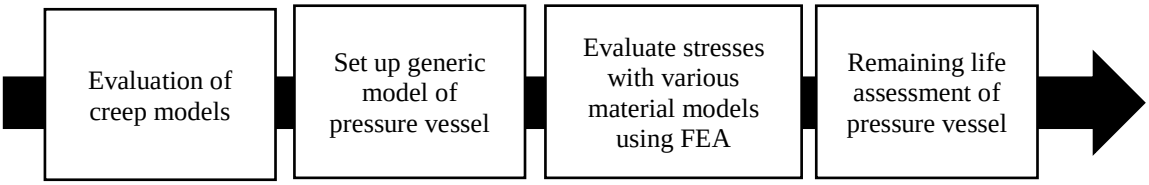

Figure 2. Scope of work flowchart

1.3 Limitations

The subject of creep is very comprehensive and in this thesis creep damage is only discussed on a macroscale level and damage from a microscale perspective is not considered nor is environmental effects that might affect material properties or load bearing capacities.

No experimental procedures can be made in conjunction with this thesis due to the lack of creep testing facilities and no new experimental data can be obtained. Any experimental data used in this work is obtained from previous research. This also limits the possibilities of validation of any obtained result.

Creep under variable loading is generally referred to as creep-fatigue. Although creep-fatigue interaction is discussed, this study will mainly be focusing on the creep damage characteristics.

Several codes are other applicable design codes for creep and pressure vessel design, this thesis will mainly discuss procedures and assessment methods given in ASME Boiler and Pressure Vessel Code.

1.4 Structure of thesis

This thesis is divided into six chapters where:

Chapter 1 of this thesis contains an introduction to the topic of study as well as the objective and scope.

Chapter 2 contains theory about creep mechanisms and creep testing. Subsequent subsections cover assessment methods for creep damage followed by a subchapter that contain a description of the nonlinear Pavlou creep damage accumulation model which will be thoroughly described. The next sections cover equivalent stress theories and the effect multiaxiality have on creep damage accumulation and material models used in finite element analysis are also described. Further the procedure in ASME-NH for elevated temperature design is explained. The last subchapter here briefly discloses pressure vessel design.

The first part of Chapter 3 contains a study of the nonlinear Pavlou creep damage accumulation model and further, creep-strain and creep-rupture curves are constructed with applicable material creep-data. Subsequent the numerical setup conditions for the finite element analysis is explained.

In Chapter 4 the remaining life results from the present study are presented.

Chapter 5 provides discussion on the creep damage assessment made with the nonlinear cumulative creep damage model based on the results and the literature study.

Chapter 6 lists the conclusions based on the current study and is followed by recommendations for future work.

2 LITERATURE REVIEW

2.1 Creep

Creep is a time dependent inelastic deformation which is induced in materials that are subjected to stress. The slow deformation can result in permanent change in shape and rates are usually less than 1.0% per minute, faster rates are generally associated with mechanical working such as forging and rolling [19]. Although creep can occur at any temperature, the point when the material experience the full effects of creep are dependent on the melting point T_M of the material. For metals this starts at the temperature $T > 0.4T_M$. At lower temperatures creep deformation occurs with continuously decreasing strain rate, while at elevated temperatures creep typically proceeds through three different stages which ultimately leads to failure [19] .

Table 1. General behaviour during creep [20]

Stage	Temperature	Characteristic
Primary	$T > 0.4T_M$ or $T \leq 0.4T_M$	$\dot{\varepsilon}$ decreases as t and ε increase
Secondary (steady state)	$T \geq 0.4T_M$	$\dot{\varepsilon}$ is constant
Tertiary	$T \geq 0.4T_M$	$\dot{\varepsilon}$ increases as t and ε increase

A typical creep curve from an uniaxial creep tensile test with constant load and temperature is illustrated in Figure 3 and it shows creep divided into three stages, namely; primary, secondary and tertiary creep. Primary creep which is also called transient or cold creep starts with an instantaneous strain ε_0 which consist of both an elastic and plastic strain, it starts with a relatively high strain rate which is then followed by monotonic decrease in creep strain rate because of strain hardening as the material deforms. For low temperatures, this behaviour can proceed indefinitely, but for elevated temperatures the deformation rate will eventually become independent from time and strain. This steady-state regime is the secondary state of creep and can also be called hot or viscous creep. Creep at the final stage before fracture is the tertiary creep, at this stage the creep rate accelerates due to microscopic cracks in the grain boundary causing damage-accumulation leading to accelerated creep strain rate behaviour. The three stages of creep and their corresponding characteristics are given in Table 1 [19, 21]

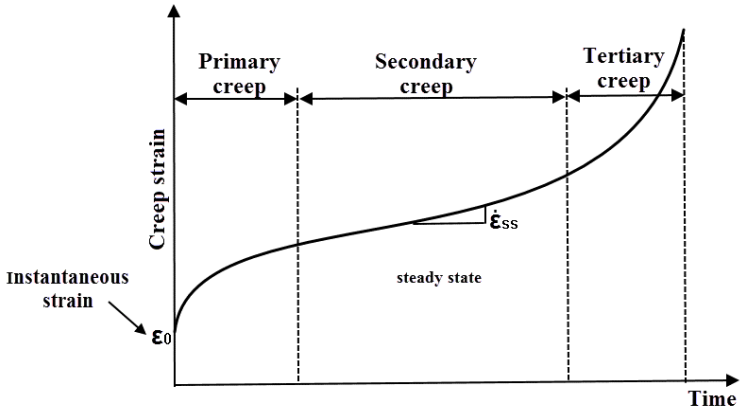

Figure 3. schematic illustration of creep curve for constant load and temperature with the three stages: primary, secondary and tertiary creep

Increasing stress or temperature ultimately increases the creep strain as schematically depicted in Figure 4, hence the time to rupture will also decrease. In addition, by increasing the stress, the time spent in each stage will shorten [19].

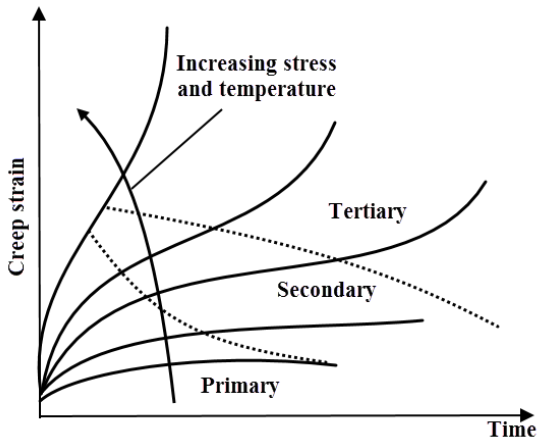

Figure 4. Schematic illustration of creep curve shapes for increasing stress and temperature [15]

The behaviour shown in Figure 4 can be explained with the following competing material reactions [15, 22]:

- Strain hardening
- Softening processes, including recovery, recrystallization, strain softening and precipitate overaging
- Damage processes like cavitation, cracking and specimen necking.

Work hardening, which is the materials ability to resist additional strain after it has been deformed, has a decreasing effect on the strain rate. Recovery is when thermal softening lead to loss of effective strain hardening. Since recovery is thermally activated it does not occur at low temperatures and explains why creep rate in the low temperature range is always decreasing. When recovery, hardening and damage is in balance the creep rate becomes nearly constant which is the steady-state creep. Increasing temperatures makes it easier for recovery processes to overcome strain hardening, which is the reason why the primary-secondary state transitions occur at lower strains as temperature is increasing. The tertiary creep stage with accelerated strain rate is due to microstructural and mechanical instabilities in the material such as cavities, separation of grain boundaries and cracks. This leads to local reductions in cross-sectional area, hence the resistance to load decreases. The coupling with softening is the cause of the rapid increase in strain rate, which ultimately leads to failure [15, 19, 22].

On a micro scale level, the first stage of creep damage is characterized by initiation and formation of isolated voids along grain boundaries. At the second stage, the voids connect with each other leading to the development of micro cracks. Finally, at the third stage the micro cracks have grown and can be detected either visually or by the aid of non-destructive testing. At this final stage, failure is impending [23].

Classification of material behaviour can be divided into three disciplines; elasticity, plasticity and creep mechanics. Other proposals differentiate them into four, where creep behaviour is divided into viscoelasticity and viscoplasticity [21]

2.1.1 Elevated-temperature fracture and creep mechanisms

Creep damage mechanisms can be represented with deformation mechanism maps as shown in Figure 5. These illustrate time- and temperature-dependent regimes and can show what damage mechanisms that dominates the creep process [1]. This helps in identifying what creep laws or creep law combination to use for modelling the creep behaviour.

The main creep mechanisms are those that are controlled by dislocation movement and those that are controlled by diffusion. The governing mechanism is dependent on stress and temperature however, many mechanisms can occur simultaneously. Higher stress and lower temperature generally promote dislocation movements while the diffusion controlled mass transport occur at low stresses and high-temperatures. Diffusion which is the atomic movement in metals is due to thermal vibration of atoms and is more difficult below the temperature of $0.3\,T_m$ but becomes more significant at higher temperatures above $0.4T_m$ when the atomic vibration increase. In dislocation creep dislocations can move through the crystal lattice both by dislocation glide along slip planes and by climbing onto parallel slip planes by the aid of diffusion [1, 24].

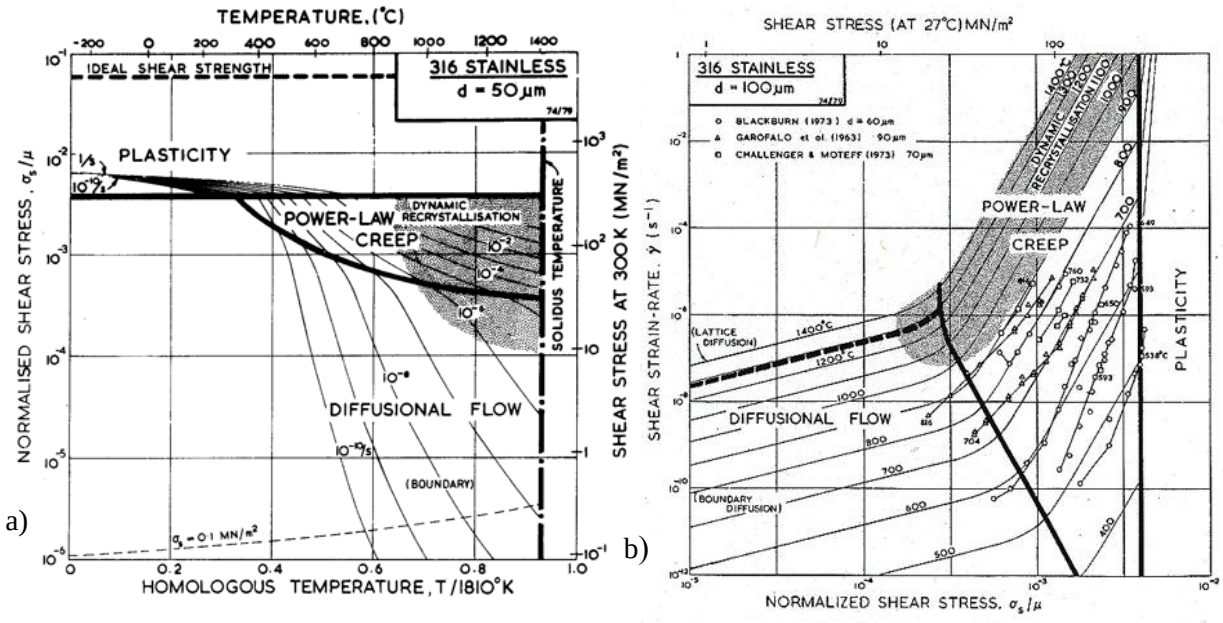

Figure 5. Typical deformation-mechanism maps for 316 SS a) Stress/temperature map of grain size 200 µm b) Strain-rate/stress map for grain size 100 µm [25]

Rupture, transgranular fracture and intergranular fracture are the three primary failure modes at elevated temperatures. Ductile rupture occurs both at temperature below $0.3T_m$ and for the ultra-high temperature regime above $0.6T_m$ at high stresses. High-temperature rupture is typically associated with dynamic recovery and recrystallization and is therefore not considered to be a creep dominated failure mode [1, 24].

In creep, transgranular fracture occur when stress and strain are reasonably high. It is initiated by void nucleation around inclusions, followed by void growth and void coalescence until fracture occurs. Transgranular fracture is similar to low temperature ductile fractures but for temperature in the creep range the process is assisted by diffusion. When temperature increase, the damage mechanism change from transgranular fracture to intergranular fracture. Which is typically the dominating failure mode

at lower stresses, higher temperatures and longer rupture times. For intergranular fracture void nucleation, growth and coalescence are restricted to the grain boundaries and the fracture appears brittle in nature since there is little macroscopic plastic flow. The two types of voids caused by intergranular fracture are known as wedge type cavities and isolated rounded cavities. The round cavities form along the boundaries normal to the axis of tension and wedge shape cavities initiates at corners or triple-points due to shear deformation along the inclined boundaries, also known as grain boundary sliding (GBS) as illustrated in Figure 6. The formation of round cavities along grain edges are promoted by lower stresses, while higher stress and lower temperature typically cause wedge crack formations [24].

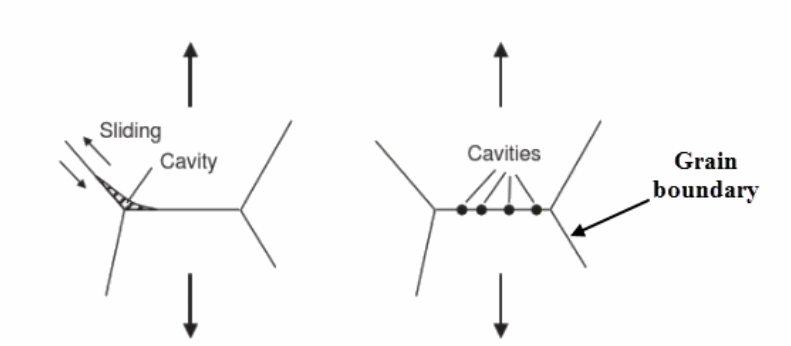

Figure 6. Intergranular fracture creep cavitation mechanisms a) wedge type cavitation at triple point and b) rounded cavities along the edge boundary [24]

If the fracture is brittle or ductile in nature depends on both the alloy, temperature and strain rate. Ductile fractures are mostly transgranular and brittle fractures are often intergranular. For fractures exhibiting both intergranular and transgranular fracture paths it is typically found that the transgranular rupture was initiated by the stress increase caused by the intergranular cracking [24].

2.1.2 Creep under cyclic actions

In primary or transient creep, redistribution of stresses occurs which eventually lead to the steady-state creep condition. Both the rate and extent of the redistribution depends on both the initial stress level, metal temperature and creep response of the material [1]. The term creep transients is the change of isotropic strength in a material because of an increase in dislocation density or by change in directional hardening [26]. Transient conditions are often important under variable loading when new high stresses are re-established at the beginning of each cycle [1].

2.1.2.1 Ratcheting

Another phenomenon that must be considered under cyclic actions is the plastic strain accumulation that may occur, called ratcheting. Below the creep range this progressive incremental plastic deformation occurs when the cyclic stresses reach the yielding point. The total inelastic strain may either be stable as illustrated in Figure 7 where the inelastic strains are constant for each cycle or the plastic strain may vary for each cycle [11]. The progressive plastic deformation finally lead to failure of the structure, a failure mode also known as incremental collapse [27]. Ratcheting in tension can cause larger tensile strains leading to necking and failure before fatigue cracks have had the possibility to form and grow [20]. In the creep range, ratcheting can occur even without plastic yielding since creep

can change the residual stresses and affect the time-independent response. It may also be enhanced due to nonlinear interaction between primary and secondary stresses [11].

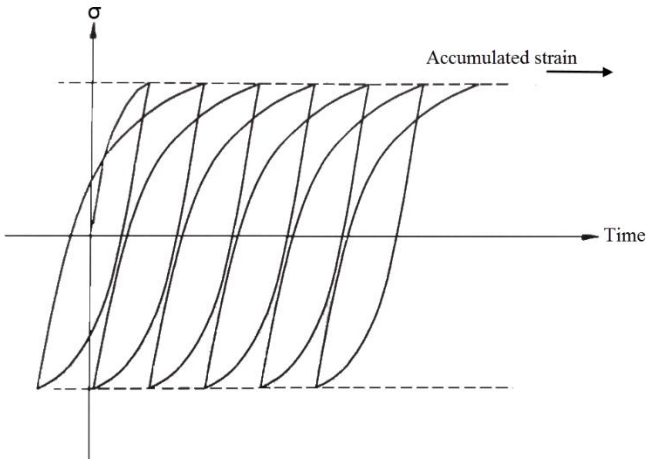

Figure 7. Stable strain ratcheting under load-controlled cycling [1]

2.1.3 Stress relaxation under cyclic loading

Time dependent stress relaxation is a kind of creep damage that occurs under hold periods at constant fixed strain. The relaxation rate is dependent on the creep strength of the material. To maintain the total strain constant, the elastic strain must decrease with a corresponding decrease in stress. A typical example where creep relaxation is an issue is for high-temperature bolting, were the stress progressively relaxes after the initial torque, therefore bolt retightening must be made on for example flanges to avoid leakage. Both relaxation and redistributions of stresses have large significance on the creep damage. Especially under cyclic operations. However, often appropriate relaxation data does not exist and relaxation analysis are made with constant load isothermal data [20, 22].

When cyclic loads are combined with hold periods, stress relaxation has been seen to influence the low-cycle fatigue endurance. Such an example of creep-fatigue interaction with stress relaxation during hold timed is illustrated in Figure 8. Test made with steel 304SS showed that hold periods at peak tensile strain are the most damaging, while compressive hold periods did not have substantial effect, in fact it was seen that it had a healing impact for hold periods at both tensile and compressive strain. The reduced fatigue life at tensile strain hold periods got more substantial when the hold periods increased. However, the reduction rate showed to progressively decrease for longer hold periods which indicated that that the limit of relaxation damage was reached within rather short hold times. The characteristics of the time-dependent cyclic relaxation damage varies between materials. Similar cyclic hold time relaxation tests made with material Udimet 700 showed the complete opposite results. For the compressive strain hold periods, it had a more detrimental effect on fatigue resistance, while tensile hold periods had only a small effect. During periods of loading and unloading the accumulated creep damage during hold periods has seen to be larger than the accumulated fatigue damage [20, 28].

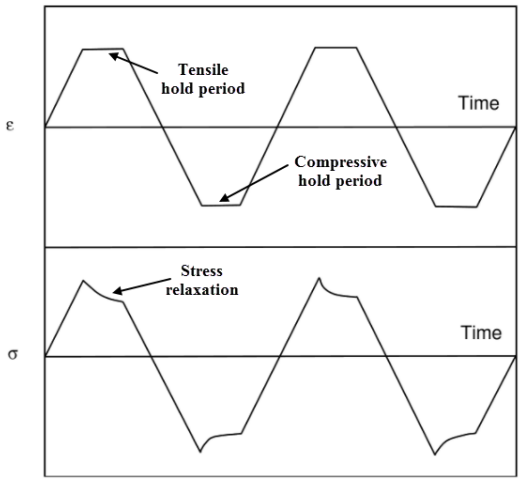

Figure 8. Example of creep-fatigue interaction with stress relaxation during hold periods under cyclic loading [24]

2.2 Temperature effect on material properties

Elevated temperatures cause changes in mechanical properties. These temperature dependent properties can be divided into time-independent and time-dependent properties. The following properties fall into the category of time independent material properties [23]:

- Modulus of elasticity
- Yield and ultimate strength
- Coefficient of thermal expansion
- Poisson ratio
- Elongation at rupture
- True stress-strain curve (the relationship between stress and strain)
- Fatigue life relationship between cyclic strain and cycles to rupture

The creep resistance and creep rupture strength of a material are often expressed in terms of temperature and time and belongs in the category of the time-dependent material properties. Other properties which fall into this category are properties which defines the relationship between applied stress and strain rate [23]. An example of this is the Norton-Bailey [29, 30] steady-state creep power law given by the following equation:

$$\dot{\varepsilon}_c = C_1 \sigma^n \qquad \textit{Eq. 2.1}$$

where $\dot{\varepsilon}_c$ is the creep strain rate, σ is the applied stress and C_1 and n are material specific temperature-dependent constants. Rate dependent plasticity theories and models for creep strain rate and creep response will be further discussed in Chapter 2.7.1.3.

2.2.1 Creep resistant steels

Creep resistant steels has been under constant developments since the beginning of the 1900s. The need to improve the high-temperature properties of steel was based on the power station industries needs to increase the efficiency of steam power plants by increasing temperature and steam pressure [3]. Today, several different alloys are used for various high-temperature applications. Typical heat

resistant alloys include carbon steels, chromium-molybdenum (Cr-Mo) steels, chromium-molybdenum-vanadium (Cr-Mo-V) steels, stainless steels, nickel and cobalt alloys and superalloys. A comparison of stress-rupture properties between different alloys is given in Figure 9 [24].

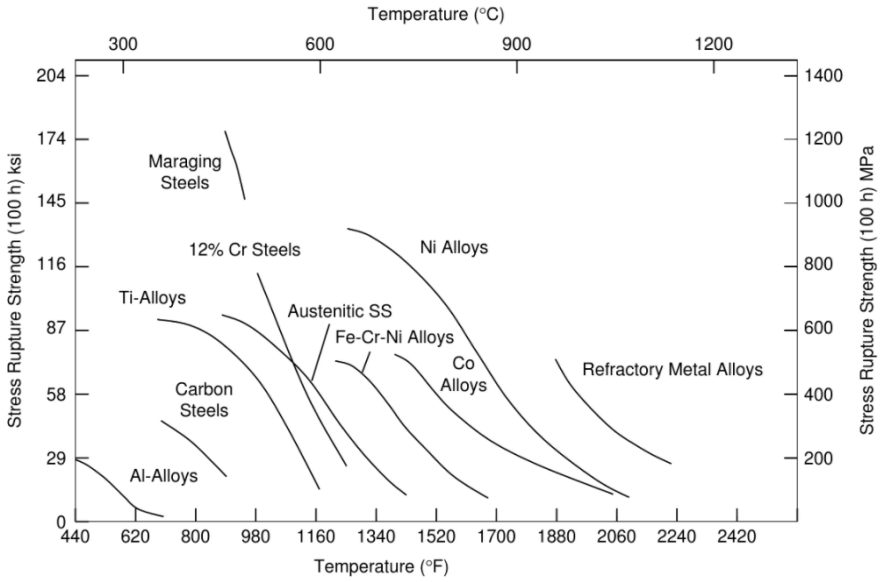

Figure 9. Stress-rupture comparison for several alloy classes [24]

Creep resistant materials typically have a high melting point since the creep rate in materials are dependent on diffusion coefficients which are proportional to the ratio T/T_m. An open metallic structure has more diffusiveness and therefore at the same T/T_m, face-centred cubic (fcc) metals generally have better creep resistance than body-centred cubic (bcc) metals which has a more open structure and hence have more diffusiveness. Depending on the dominant creep mechanism, different microstructural properties are beneficial. In diffusion creep grain size play a significant role, a larger grain size improves the creep resistance for diffusive controlled creep since mass transportation in finer grains are more rapid. Creep resistance can also be improved even further by having inert particles such as carbides on the grain boundaries which increases creep resistance since it helps to pin down the boundaries [24].

Table 2. Maximum service temperature for various alloys [24]

Alloy	**Maximum service temperature, T [°C]**
Carbon steel	400-480
Chromium molybdenum	540
Chromium molybdenum vanadium	540
Martensitic stainless steel	540-650
Ferritic stainless steel	370
Austenitic stainless steel	870
Nickel-base superalloys	1290

There is a large variation in maximum allowable service temperature for the various creep resistant alloys given in Table 2. The operating temperature for carbon steel varies depending on the in-service stress. However, beyond 480 °C, embattlement due to graphite formation becomes an issue. In Cr-Mo steels, the chromium content increase the resistance against oxidation and molybdenum

forms carbides to avoid graphitization and increase the elevated temperature strength. The addition of vanadium in Cr-Mo-V steels results in an increase of the thermal softening point for the steel. Among the stainless types of steels in Table 2, the austenitic steel has superior creep resistance and can be used for elevated temperatures up to 870°C, though a problem associated with the austenitic steel grades are their high thermal expansion coefficient which must be compensated for when designing high-temperature components. The martensitic stainless steels can be used in rather high-temperature applications up to 650 °C, but for avoiding in-service softening the martensitic steels must be tempered. Ferritic stainless steels can only be used at limited operating temperatures because of precipitation of embrittling phases that occurs at higher temperatures. The high chromium content of ferritic stainless steel does however provide it with good scaling resistance [24].

Nickel based alloys are typically used in corrosive environment at high-temperature service. The alloy elements chromium and molybdenum combined with nickel makes the steel both oxidizing and corrosive resistant. Of all nickel based alloys the Ni-Cr-Mo alloys have the best heat and corrosion resistance and they are frequently used for chemical processing and in other industries that may utilize their combination of high temperature properties [24].

The term superalloys typically designates steel with the defining feature of high mechanical strength, good fatigue resistance, high-temperature creep resistance and surface stability. They also have the ability to operate at elevated temperatures for long periods of time [24, 31]. Although there is no strict definition, the name superalloy is typically used for alloys that includes nickel, cobalt and iron with a high percentage of nickel in addition to a variety of other alloying elements. The composition of superalloys are among the most complex metallic alloys that has been developed for commercial use. The application encouraging the development of superalloys is for the use of air foils in the hot section of gas turbine engines. They have also been used successfully in other applications, for instance rocket components, nuclear reactors, heat exchangers, petrochemical equipment etc. [31]. Superalloys are often used for temperatures above 540 °C and some of them can even be used for load-bearing applications at temperatures beyond 85% of their melting temperature. Among all superalloys the nickel-base superalloys have the best creep resistance and they are used for turbine blades in engines with service temperatures up to 1290 °C, which corresponds to T/T_m=0.9 [24].The cost of superalloys are generally 30 to 200 times that of plain stainless steel and this is due to the high level of investment and the complexity of both composition and the processing [31].

2.3 Testing of creep properties

2.3.1 Creep testing

Creep strength of a material is commonly measured as rupture strength or creep resistance. Rupture strength is defined as the necessary stress level to cause failure in a certain period and creep resistance is defined as the stress level needed to produce a nominal strain within a certain time period [1].

Elevated temperature tests for creep resistance and creep rupture are similar, however rupture strength is typically measured with stress-rupture tests, which measures the time to failure for a given stress, while creep resistance is determined with so called creep tests which measure time dependent strain. A major difference between stress-rupture and creep tests is the total strain during the test. For creep tests the total strain does generally not exceed 0.5%, while the strain can reach up to 50 % in a stress-rupture test. In addition, for stress-rupture test, the specimens are typically loaded at higher stresses than in creep tests. The duration for a stress-rupture test is also generally shorter compared to the creep test. Stress-rupture tests are concluded when failure occurs, which is often approximately after 1000 hours, while the duration of creep tests can vary from a few months to several years [24].

Test specimens used to measure creep resistance and creep rupture strength are similar to specimens used in a regular tensile test [22]. Tests can be conducted either by constant stress or constant load, however the constant-stress tests are not as easy to conduct as the constant-load tests and the latter are therefore considered adequate for engineering applications because of the convenience of the constant load testing [15].

Stress-rupture and creep tests are typically carried out under constant temperature in tubular furnaces on specimens subjected to either tension or compression. The most common types of tests are those conducted under uniaxial tension under constant load conditions. Throughout these tests, the load is maintained constant and as the specimen elongates and the cross-sectional area decreases, the axial stress increase. The stress value reported from these tests is usually the initial stress value[21, 22]. A schematic illustration for a creep test setup under constant load is shown in Figure 10.

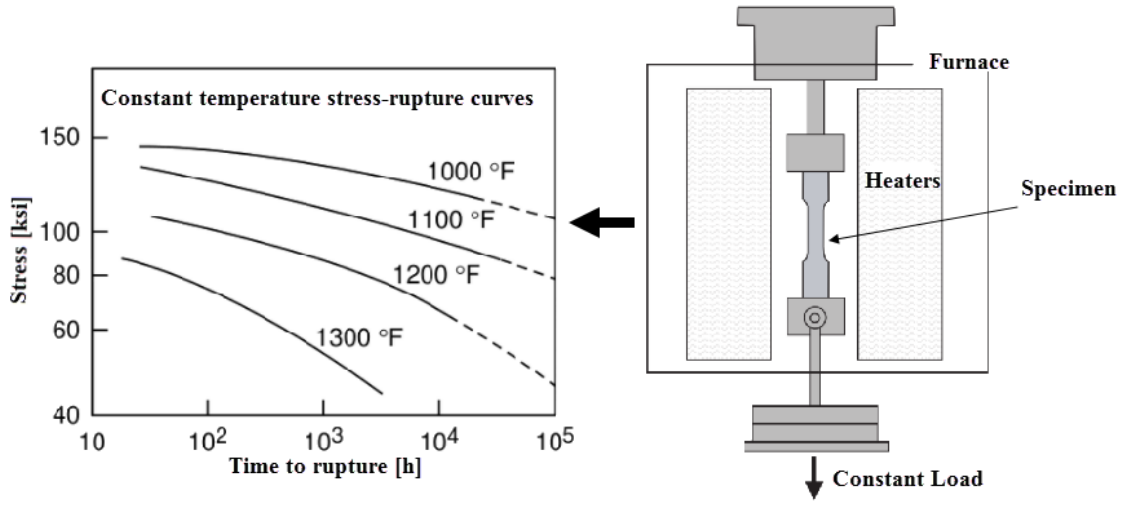

Figure 10. Typical constant load and temperature creep tensile test fixture and an example of stress-rupture data obtained from constant load and temperature stress-rupture tests [24]

Although uniaxial tensile tests are the most common in creep rupture tests, the method is not suitable for brittle materials due to its flaw-sensitivity such as crack propagation. For brittle materials, creep tests under compression is more appropriate since it better measures the inherent plastic properties of materials with brittle behaviour [22]

As previously mentioned, creep test under constant stress are more difficult to carry out than a constant load test. This is because the reduction of load must be proportionate to the degree of straining. However, in some cases, it is necessary to make constant stress creep tests, for example, when to determine the differences between temperature dependence and stress dependence of a material. To maintain the constant-stress the load is adjusted as the length of the specimen changes. Difficulties arises during necking to keep the stress constant at the neck, since stress is reduced in other points of the measured length. When this occurs, the measured strain over the measured specimen length is no longer representative, because the neck can act as a stress concentrator. Therefore, the constant-stress test is much more meaningful when elongation of the specimen occurs uniformly, instead of locally by necking. However, constant stress-creep tests are improving with the aid of computer controlled tests machines [22]. Constant-stress tests do in general not display the behaviour associated with tertiary creep. This is however not a significant problem since steady-state creep is the most important design parameter in elevated temperature design, nevertheless, the duration of

tertiary creep constitutes as a safety factor, which may allow flaw-detection in a component before failure is evident [24].

Another significant factor to consider when testing materials in the high- temperature regime is the material ductility. The importance of an acceptable creep ductility level in addition to creep strength for high-temperature steels was first recognized in the 1930s when steam turbine bolts suffered premature damage due to lack of ductility. This experience eventually led to new practices, where creep elongation and ductility was also to be considered in creep tests. The significance of studying material behaviour through long-term testing of materials was also recognized [3].

Ductility under creep conditions is particularly important to consider when selecting material for designs where stress concentrations due to localized defects and notches are present since multiaxial stress states can lead to reduced ductility. Materials with higher creep strength does in general have lower ductility [15]. This is because superalloys and engineering alloys can lose their ductility when subjected to high-temperatures because the impurities diffusing to the grain boundaries becomes more perceptible. Elongation is measured in both creep test and stress-rupture tests. For the latter, there are two significant measures of creep elongation. These are true elongation, which is measured right after the secondary creep stage, and total elongation, which is defined as the elongation at fracture. Although true elongation is considered to better represent ductility in metals at elevated temperatures it is common practice to plot both elongations versus the rupture life when presenting elongation data. The total elongation data often has more scatter than true elongation. This is because the total elongation is affected by local creep mechanisms, such as necking that occurs during tertiary creep [24].

As a conservative approach, to avoid damage due to lack of ductility, a frequently used creep design criteria is based on 1% creep [24].

2.3.2 Multiaxial creep testing

Many of the components operating in in the high-temperature range are subjected to biaxial and triaxial stresses. Nevertheless, most creep tests of materials are typically performed by uniaxial creep tensile test. The various multiaxial creep testing techniques are primarily used for modelling and validation purposes since they better represent various stress states. But since experimental testing on multiaxial creep rupture and creep damage development are not as easily executed as uniaxial testing methods, uniaxial creep testing will most likely remain to be the main creep testing method [22, 32].

One of the more common multiaxial creep testing methods is performed by applying internal pressure and axial end loading on tube specimens. This method only offer a small variation in multiaxial stress states and therefore has limited use. However, the loading on the test specimens can quite well represent the loading on piping components. Since the radial stress can be neglected for thin-walled pipes, both biaxial and triaxial stress states can be tested depending on the wall-thickness to radius configuration of the specimen. In addition, specimens can also be tested with circumferential notches [22, 32]. Creep testing with tension and torsion are also made on tubular specimens. The cheap test specimens and commercially available test machines makes the method somewhat convenient, but the stress state created by the combined tension and torsion causes second principal stress, σ_2 which is negative, and therefore cannot represent stress states in pressurized industrial components [22]

One of the most convenient multiaxial creep testing methods is uniaxial testing of notched specimens which uses measurement analysis to provide information of the deformation process. It has the great

advantage that they can be performed in regular creep testing machines, in addition specimens are inexpensive compared to other test specimens used for multiaxial creep testing [22].

There are multiaxial creep tests with cruciform specimens that offers testing for wide variety of multiaxial stress states. Such apparatus has been developed for both biaxial [33-35] and triaxial [36] cruciform specimens for which orthogonal loads of various ratios are applied to the cruciform specimen to produce a wide variety of biaxial and triaxial stress states. Although it may seem like an ideal tool researchers, test specimens are very expensive and require a highly advanced test setup [22].

Important to mention and also stated by Betten [21] is that experimental creep results can differ greatly from reality and results obtained from tests are not always representative even if similar stress states can be recreated.

2.3.3 Notch sensitivity and notched creep testing

Creep tests of notched specimen are typically used as a qualitative measure to determine the suitability of an alloy for designs that may contain stress concentrations. Rupture life testing of notched specimens can indicate a materials capacity to deform locally without cracking under multiaxial stresses. Therefore, notched specimen testing are often conducted on superalloys since these have a tendency to exhibit brittle behaviour when exposed to elevated temperatures due to precipitation of particles to grain boundaries. This leads to reduced ductility and an increase in notch sensitivity. The presence of a notch can either increase, decrease or have no effect on the rupture life. An alloy is said to be notch strengthened when the presence of a notch increases rupture life. This means that the specimen can resist higher nominal stresses compared to an unnotched specimen. On the contrary, notch weakening is when the presence of a notch reduces rupture life. Materials that exhibits this behaviour is also called notch sensitive alloys. Typically, circumferential 60° V-notch round specimens are used in notched creep testing. Nevertheless, size and shape configuration of notched test specimens should be based on requirements necessary for obtaining a representative selection of the material being studied [22].

The configuration of the notch has a major influence on the rupture life and studies that involves notch configuration usually describes the results in relation to the elastic stress-concentration factor, K_t, an ideal value which is based on linear-elastic behaviour. The design stress σ_d at the notch can then be described by the yield stress, σ_y divided by the stress concentration factor. In addition to the notch configuration there are several other factors that may affect the rupture strength or rupture time of notched specimens. Size of the specimen, notch preparation and other metallurgical effects, such as composition, grain size, heat treatment and processing histories does also influence the behaviour of notched alloys. There is therefore no straightforward way of describing the effect notches have at elevated temperatures [20].

The significance of the notch weakening or strengthening effect is often by researchers measured with a so-called notch strength ratio which is typically defined as below unity for notch sensitive alloys. This ratio can however be unreliable and can differ depending on class of an alloy and rupture-time. It is therefore not possible to use this ratio for direct comparison between materials [20].

2.3.4 Extrapolation of creep data

Even for established materials, there exist few long-term creep-rupture data up to 100 000 h. Therefore, extrapolation from short term tests data is typically necessary to determine the rupture

and creep properties over extended time periods. In addition, the continuous development of new materials for high-temperature application also make it important to know what their long-term performance will be within a reasonably short-time period. Out of necessity several extrapolation techniques have been developed and each of them with advantages and disadvantages which designers have learned to work with. One of the first extrapolation methods assumed that a plot stress versus rupture time with log-log scale was straight, an assumption that is now known to be wrong and will overestimate the rupture time [1].

The various extrapolation techniques may be divided into three main groups; parametric-, graphical- and algebraic methods and within each group there are subdivisions for empirical methods and theoretical methods trying to reflect the physical behaviour. Depending on the purpose, different methods are preferred, and it is difficult to designate one method as superior to the others, however the extrapolation techniques that uses time-temperature parameters have been very popular due to their easy use [1].

2.3.4.1 Larson-Miller parameter

Among all parametric methods used to predict allowable time to rupture for metals under constant load conditions, the Larsson-Miller parameter [37] is one of the most widely used extrapolation techniques and due to its simplicity it has got a considerable attention since it was proposed in the early 1950s [1].

The Larson-Miller parameter can be used to represent creep-stress rupture data by correlating time and temperature to one parameter in the following form:

$$P_{LM}(\sigma) = T\left(logt_f + C\right) \qquad \textit{Eq. 2.2}$$

where T is the temperature in Kelvin, t_f is the stress-rupture time in hours and C is a constant initially suggested by Larson and Miller to be of an order 20 for most metals. It has later been shown that values of C in fact varies and often has a value between 15 and 27 [14]. Figure 11 provides an illustration of how the Larson-Miller parameter joins rupture curves for various testing temperatures into one master curve by correlating the temperature on the time axis into one time-temperature parameter by using a specific value C which is dependent on the material and the temperature range [1, 14]

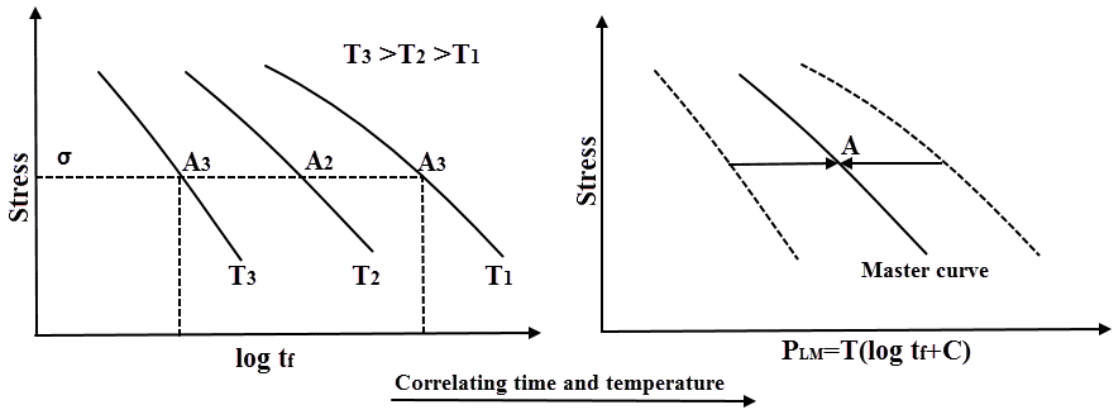

Figure 11. Illustration of rupture curves of various temperatures joined into a master curve with the Larson-Miller parameter [1]

Larson-Miller parameter plots are often used for obtaining rupture times for various stress and temperature conditions. In an assessment made by Penny and Marriott [1] of several extrapolation techniques, the semi-empirical Larson-Miller parameter was described as easy to use, simple and convenient for direct comparisons between metals, but not very accurate. However, other linear parameter extrapolation models that was assessed including Dorn and Manson-Haferd did on average not provide any better accuracy. The correlation obtained with all three methods compared well with current standards of industrial data but for extrapolation they all gave low confidence in predictions above one log cycle. Other more complex nonlinear parameter models and graphical methods were also discussed in their assessment and it was concluded that even if the extrapolation obtained with these were more accurate they were not considered practical at present. They concluded that certain methods are preferred to others depending on the purpose but until better procedure had been developed the most practical way of determining what method to choose it to use the one that best fits the data and purpose.

2.4 Linear damage models

The constant load and temperature condition used in creep testing is typically not representative for components in an elevated temperature service. For components found in power plants and petrochemical plants, repetitive cyclic loading in the creep range are considered normal operating conditions [14]. Variable load and temperature conditions must therefore be taken into consideration in damage and remaining life assessment of components.

The simplest and earliest concept of cumulative low-temperature fatigue damage was initially proposed by Palmgren [38] and later by Miner [39]. The concept which is now known as the Palmgren-Miner summation or simply Miner's rule uses linear summation to predict failure of a component by the criterion

$$D_f = \sum \frac{n_i}{N_{di}} = 1 \qquad \textit{Eq. 2.3}$$

where n_i is the number of cycles for a given load or stress level i and N_{di} is the number of load cycles until failure at that same load amplitude. Fatigue failure occurs when D_f , which represents the accumulated fatigue damage reaches unit value.

The procedure of calculating cyclic load damage at low temperatures is relatively straight forward, however at elevated temperatures where the effects of creep are significant, evaluation becomes more difficult since the cyclic life is affected by stress relaxation. In addition, factors like stress concentration and triaxiality which will be discusses subsequently, also have a significant effect on creep-fatigue life of a component[14].

2.4.1 Linear creep damage models

The same cumulative damage concept used in Miner's rule was later applied in creep damage models for evaluating damage and remaining life for components at elevated temperatures. One of the most common creep damage models is known as Robinson's rule [10] or the time fraction rule. Robinson assumed that the cumulative creep damage of a component at elevated temperature could be predicted by:

$$D_c = \sum \frac{t_i}{t_{fi}} \qquad \textit{Eq. 2.4}$$

Where t_i, is the time spent at a certain temperature level T_i and t_{fi} is the rupture time at that same temperature. The original application of Robinson's rule was to evaluate creep at various temperatures. However, since then it has also been used extensively for variable stress histories, as well as at variable temperatures [1].

An alternative to Robinson's rule is a strain-based method for creep damage assessment that builds on the concept of ductility exhaustion. The application of the method is similar to Robinson's life fraction rule, except that it uses strain fraction instead of time fraction. The accumulated creep damage is expressed as follows:

$$D_c = \sum \frac{\varepsilon_i}{\varepsilon_{fi}} \qquad \textit{Eq. 2.5}$$

Like the previously described damage models, failure occurs when the accumulated damage reaches unity. At this point, the accumulated strain has reached the materials ductility limit, which is typically obtained from the ductility measured in a constant load creep test [1].

2.4.2 Creep-fatigue interaction damage rules

When high-temperature is combined with cyclic stress, creep-fatigue interaction must be considered. As previously stated, damage assessment for cyclic loads at high-temperature is much more complicated than for low temperatures. This is because both the amplitude and the cycle duration cause damage to the material [1]. Much research has been dedicated to investigating the combination of time-dependent creep and cycle dependent-fatigue and several rules have been suggested for estimating the accumulated damage under creep-fatigue conditions. The most used method for creep-fatigue interaction is based on superposition of creep and fatigue damage [15], a concept that was initially proposed in 1962 by Tiara [40].

The life fraction rule (LFR) which is also known as the time and cycle fraction summation (TCFS) combines Miner's rule for fatigue and Robinson's time fraction rule for creep as follows [15].

$$\sum \frac{n}{N_d} + \sum \frac{t}{t_f} = D_f + D_c = D \qquad \textit{Eq. 2.6}$$

In the above formula, n_j is the number of fatigue cycles at a stress and temperature level corresponding to cycle type j and N_{dj} is the number of allowable cycles for that cycle type. Similarly, t_k is the duration of the time interval at a certain stress- and temperature level and t_{rk} is the allowable time duration until rupture for that same condition.

The basic idea with this method is that the time-dependent creep and the cycle-dependent fatigue is evaluated separately. Independently, creep and fatigue reaches failure when the time-and cycle-fraction sum add up to $D_f = 1$ and $D_c = 1$, respectively. However, when combined it was considered that the total creep-fatigue damage D would occur at unit value.

By evaluating the creep and fatigue damage as suggested above, the damage contribution from fatigue and creep can be plotted as a single point on a creep-fatigue interaction diagram, where each axis is

represented by D_f and D_c. By taking into account the failure criteria, $D = 1$ as above, the diagram can be diagonally divided with a straight line, like the dotted line depicted in Figure 12, dividing the diagram into a safe region for where failure does not occur and an unsafe region [24, 41]. However, creep-fatigue failure can occur for damage values less than one, a phenomena now known as creep-fatigue interaction [1]. By plotting experimental data on a creep-fatigue interaction diagram, Campbell [42] in 1971, was the first to demonstrate that cyclic loading at elevated temperatures could result in rupture for damage values far less than unit value.

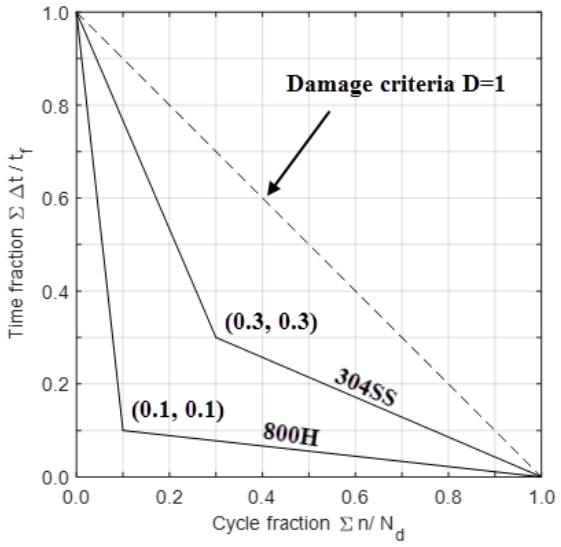

Figure 12. Creep-fatigue interaction diagram for the LFR method

By plotting experimental creep-fatigue data as proposed by Campbell, conservative approximations for safe boundary regions can be assumed for materials [41]. The safe region, which is also known as a creep-fatigue damage envelope is typically conservatively bounded by a bilinear curve with a locus point (D_c, D_f) that differ for various materials. For example, in ASME III, Subsection NH [11], the locus point is defined as (0.3, 0.3) for stainless steel 304SS and 316SS and (0.1, 0.1) for Ni-Fe-Cr Alloy 800H.

There have been many attempts to offer more complex nonlinear methods for both creep and fatigue, than the above-mentioned damage models. Nevertheless, none of these methods are regularly used today. Linear damage summation is the earliest and most simple creep-fatigue damage model and it is the only method that has found universal acceptance in design codes and guidelines regardless of its documented shortcomings [1]. The reason for this is that it is easy to use and only require standard S-N fatigue curves and creep-rupture curves [15].

Both ASME-NH [11] and French RCC-MR [13] codes uses the life fraction rule with bilinear damage envelopes based on conservative lower bounds experimental values for materials supported in the codes. British R5 [12], however differ from the other codes in that they use $D = 1$ as the damage criteria which is represented as a straight line on the damage envelope.

Important to mention is that using the linear damage summation rule given Eq. 2.6 is not equivalent to using any of the above mentioned national codes for components in elevated temperature service. Standards, such as ASME-NH, gives a very conservative life assessment due to engineering corrections and safety factors that are incorporated in the code [15].

In the companion guide to the ASME Boiler and pressure vessel code, Jetter [9] describes several comparative evaluations between the life fraction approach and other alternative methods. But even if some of these methods have given better predictions, they typically require more material testing for determination of material parameters. The most notable work has been with ductility exhaustion. Compared to only the time fraction rule, the two approaches both gave similar data scatter. However, when used with a creep-fatigue interaction diagram ductility exhaustion has shown less scatter in some situations and is also more conservative at low strain ranges and rates. However, Jetter [9] also states that there so far is no indication that the method would be sufficiently superior, compared to the current time fraction rule, to justify the tedious and complicated process of redefining and verifying rules in code.

2.5 The nonlinear Pavlou creep damage accumulation model

Linear summation models described in the previous subchapter does not account for the effect of load or temperature sequence in the load and temperature history. Although other more complex nonlinear damage methods have been suggested that more accurately predicts damage, these have not had the same success as the resilient life fraction rule, partially due to that of they require additional material testing for determination of necessary material constants.

In the journal of engineering structures from 2001 D.G. Pavlou [16] presents a nonlinear cumulative creep damage model that is analogous to a fatigue damage model proposed by Subramanyan [43] in 1976. The proposed creep damage function considers previous damage, like the time fraction rule, but in addition it also takes into consideration the sequence effect from previous load and temperature history. Pavlou proposes that creep damage can be represented by isodamage lines and builds his theory on the assumption that the curve correlating temperature, T, rupture or failure time, t_f and stress, σ on a Larson-Miller parameter plot, can be approximated as a straight line for a large variety of metals. It is also assumed that creep has an "endurance limit" σ_e, which is a stress low enough to cause no creep damage at all. This creep endurance limit is equivalent to the fatigue endurance limit which is represented as a knee-point on fatigue S-N curves.

Since each point along the rupture curve on the Larson-Miller parameter plot represent failure after the loading time t_f, Pavlou defines the rupture curve $P_{LMf} - \log\sigma$ to represents a damage state of 100% as schematically illustrated in Figure 13. The damage line representing rupture is part of a set of isodamage lines with an upper bound represent failure and a lower bound horizontal line representing the creep endurance limit $\log\sigma_e$, with the corresponding Larson-Miller parameter P_{LMe} that relates to a damage state of zero. The hypothesis is that all isodamage lines intersect at a common point O, which is the point of intersection between the line with damage state of 100% and the horizontal line representing the damage state zero as shown in Figure 14. The proposed damage function is defined as the ratio of the slope of an isodamage line to that of the original rupture curve and can be written as

$$D = \frac{\tan\theta_i}{\tan\theta_f} \qquad \textit{Eq. 2.7}$$

Where $\tan\theta_i$ is the slope of an arbitrary isodamage line and $\tan\theta_f$ is the slope of the rupture line $P_{LMf} - \log\sigma$. The damage function D has two standard damage states; zero for $\theta_i = 0$ and unity for $\theta_i = \theta_f$, when failure occurs.

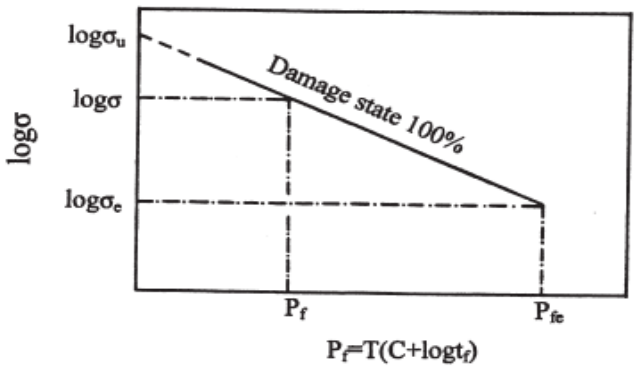

Figure 13. Schematic Illustration of the Larson-Miller parameter [16]

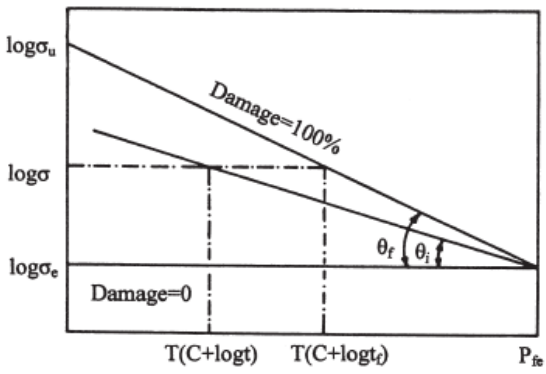

Figure 14. Definition of the damage function [16]

For a two-step loading sequence of the type shown in Figure 15 the principle of Pavlou's creep damage model can be illustrated with aid of the diagram in Figure 16. The diagram demonstrates the loading of a specimen with initial loading conditions σ_1, T_1 loaded with duration t_1 which results in a damage state D_1 indicated by A on the diagram. The specimen is further loaded under the new loading condition σ_2, T_2 indicated by C with an initial damage $D_2 = D_1$. If the specimen continues to be loaded under the same conditions until failure at $D_f = 1$, the time till failure, t_2 is represented by the line CF.

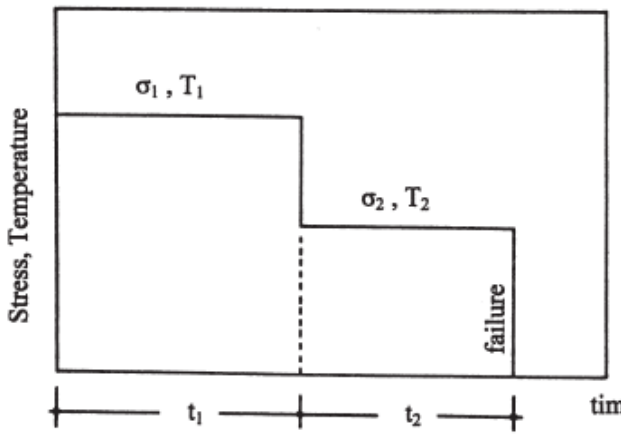

Figure 15. Two stage stress and temperature loading sequence [16]

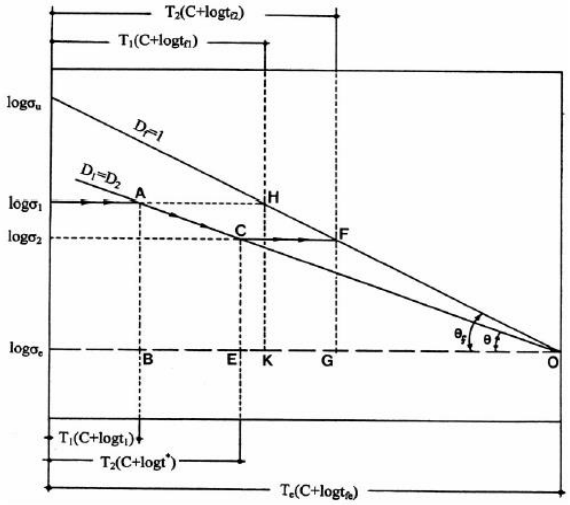

Figure 16. Creep damage accumulation under two stage loading [16]

Pavlou uses the geometric relationship of the isodamage lines and the relationship between the logarithmic stress and the Larson-Miller parameter, P_{LM} to derive the formula for a two-step loading creep damage function as follows:

$$\left(\frac{t_1}{t_{f_1}}\right)^{q_{1,2}} + \frac{t_2}{t_{f_2}} = D \qquad \text{Eq. 2.8}$$

and

$$q_{1,2} = \frac{T_1 \log(\sigma_2/\sigma_e)}{T_2 \log(\sigma_1/\sigma_e)} \qquad \text{Eq. 2.9}$$

Where σ_1, T_1 and σ_2, T_2 are the stress and temperature for the first and second step of the loading sequence, t_1 and t_2 is the duration for the first and second loading cycle and t_{f_1} and t_{f_2} is the rupture time corresponding to each stress and temperature condition. σ_e is as previously mentioned described as the creep endurance limit.

Pavlou further develops his theory and presents a generalized procedure which can be used for cumulative damage under multi stage loading.

$$\left(\dots \left(\left(\left(\frac{t_1}{t_{f_1}} \right)^{q_{1,2}} + \frac{t_2}{t_{f_2}} \right)^{q_{2,3}} + \frac{t_3}{t_{f_3}} \right)^{q_{3,4}} + \dots + \frac{t_{k-1}}{t_{f_{k-1}}} \right)^{q_{k-1,k}} + \frac{t_k}{t_{f_k}} = D \qquad \textit{Eq. 2.10}$$

where

$$q_{k-1,k} = \frac{T_{k-1} \log(\sigma_k / \sigma_e)}{T_k \log(\sigma_{k-1} / \sigma_e)} \qquad \textit{Eq. 2.11}$$

In Pavlou's study [16], it is suggested to replace the creep endurance limit, σ_e since it relates to monotonic loading and replace it with a fitting parameter p, derived from experimental values from stepped creep test. The reason for this is to consider the transient effect that occur in the material under cyclic or variable step loading.

By disregarding the physical meaning of the creep endurance limit, σ_e in Eq. 2.8 and replace it with the preferable fitting parameter p, the two-step loading damage function becomes:

$$\left(\frac{t_1}{t_{f_1}} \right)^{\frac{T_1 \log(\sigma_2 / p)}{T_2 \log(\sigma_1 / p)}} + \frac{t_2}{t_{f_2}} = D \qquad \textit{Eq. 2.12}$$

The flowchart in Figure 17 shows the outline of the creep damage evaluation procedure of the Pavlou creep damage model.

Further in the study, lifetime fractions t_1/t_{f_1} and t_2/t_{f_2} from experimental stepped creep test data were used to derive the fitting parameter by solving Eq. 2.12 with respect to the fitting parameter p. The fitting parameters obtained for the tested materials were slightly higher than the maximum applied stress, indicating that the physical meaning of fitting parameter has no relations to a creep endurance limit. Nevertheless, the theoretical results obtained with Pavlou's model correlated very well with experimental data for the materials Al-99.98 and austenitic steel X8CrNiMoNb 16-16.

As for the Submaranyan model for fatigue, the Pavlou model is unstable for stresses close to the creep endurance limit or the fitting parameter due to singularity that occurs when the logarithmic value in the exponent becomes unit value [17, 44].

More resent research by Rege and Pavlou [45] published in the International Journal of Fatigue, a one-parameter nonlinear fatigue damage accumulation model is suggested. The method is a modification of the Submaranyan's fatigue model [43] to which Pavlou's creep model is analogous to. Rege and Pavlou suggest that the isodamage lines are to be replaced with nonlinear curves. Thus, instead of using of the linear damage function $\mathrm{D} = \tan\theta_i / \tan\theta_f$ the nonlinear damage function given below is proposed.

$$D = \left(\frac{\tan\theta_i}{\tan\theta_f}\right)^{q(\sigma_i)} \qquad \text{Eq. 2.13}$$

where the exponent is a function of the stress amplitude for the current load step i. Their theory proved very successful when compared to fatigue test results. Although their proposed model is for fatigue it is likely that similar implementation of nonlinear isodamage lines can be applied to the creep model previously proposed by Pavlou.

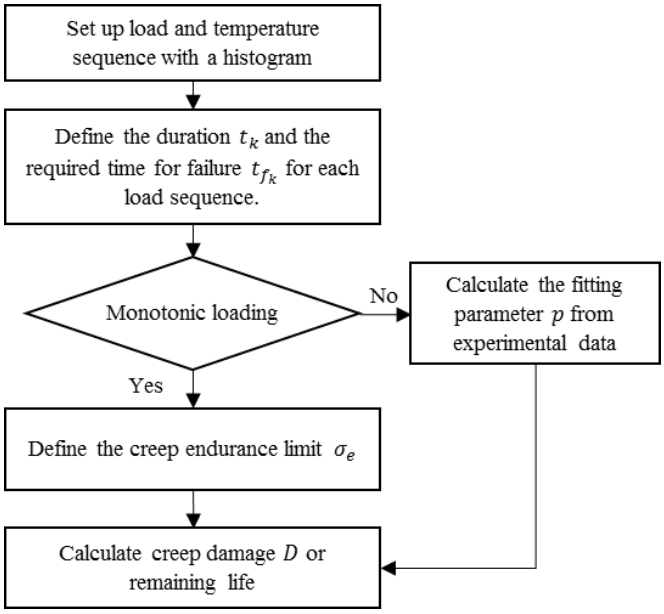

Figure 17. Flowchart of the Pavlou damage model procedure

2.5.1 Pavlou damage accumulation model applied in research

The nonlinear cumulative creep damage model proposed by Pavlou has been the subject in studies made by other researchers. It has either in its original form or slightly modified version given satisfactory predictions of variable step creep test data [17, 18].

Grell and co-workers [17] made experimental variable load creep testing for aluminium casting alloy 354 with tensile and three-point bending specimens. The experimental creep data was compared to predictions made with various creep damage models. In their evaluation, the nonlinear Pavlou damage model [16] gave the most accurate predictions for the tested material when compared with other linear summation models used in their evaluation, including the time fraction rule.

In contrary to Pavlou's analysis [16], where the fitting parameter used was higher than the applied stresses, Grell and colleagues [17] chose to use a fitting parameter that was lower than the applied stresses and closer to an actual creep endurance limit. It is recommended in their research to use the original parameter σ_e instead of the fitting parameter p, since such a parameter would limit the usefulness of the model in design applications. Grell, further states that with a fitting parameter, the material would have to be tested under similar stress and temperature conditions as expected in the component. From a design perspective, by using the creep endurance limit, a design engineer would only need to obtain the creep endurance limit for the specific material instead of having to perform tests.

Another research published in 2006 [18], used Pavlou method to analyse experimental data under variable creep conditions for the lead-free solder alloy Sn.3.5Ag-0.5Cu. However, in the study the Pavlou model did not give satisfactory predictions for the tested alloy in its original form. Instead a modified version of the Pavlou model was suggested, where the Larson-Miller parameter was replaced with a curve of normalized stresses. To include temperature, stresses were normalized with the elastic modulus for the corresponding temperature. As shown in Figure 18, the normalization makes the data points fit closer together permitting the data points to be described by a power law instead of the Larson-Miller parameter.

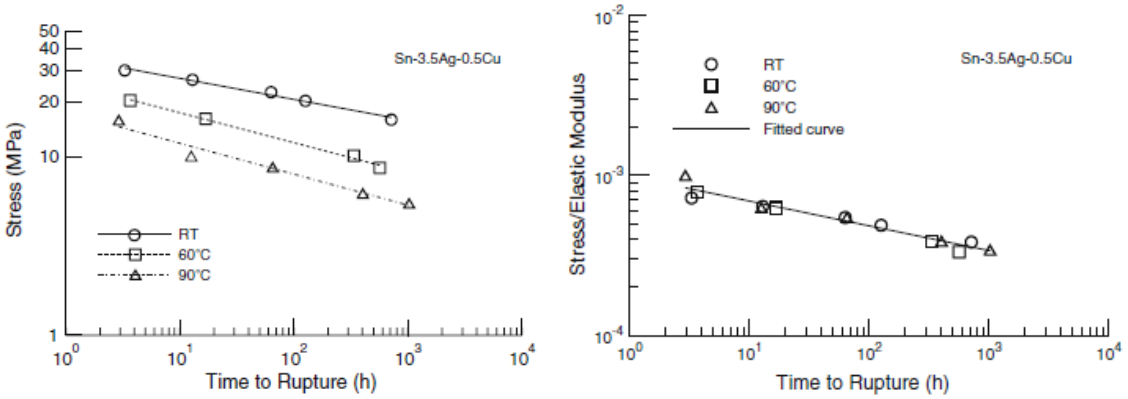

Figure 18. Correlation of stress, time and temperature as an alternative to the Larson-Miller parameter to represent damage a 100% damage state for the modified version of the nonlinear creep damage model. At the LHS stress versus rupture time for various temperatures are given as separate curves and at the RHS the normalized stress σ(T)/E(T) versus rupture time correlates stress, time and temperature into one master curve [18]

The results from their work showed that the modified Pavlou model gave reasonable predictions of the stepped creep data and well described the sequence effect from the two-step variable load and temperature creep testing. It was further observed that a high-low sequence of two-step loading at constant temperature and a high-low sequence of temperature at constant stress were much more damaging than the corresponding low-high sequence.

2.6 Influence of multiaxial stress states on creep

Any complex stress combinations with three stresses and six shear stresses can be transformed to the principal coordinate system in which no shear stresses exist. Any stress state can then be described with the principal stresses $\sigma_1 > \sigma_2 > \sigma_3$. A triaxial tress state include all three stresses, while a biaxial stress state includes only σ_1 and σ_2 and have $\sigma_3 = 0$. A uniaxial stress state is when $\sigma_1 = \sigma$ and $\sigma_2 = \sigma_3 = 0$ [22].

Most material data including creep rupture data is typically based on uniaxial testing. Therefore, the fundamental idea of equivalent stress equations is to compute a corresponding stress for complex stress states that can produce correct rupture time when applied to uniaxial creep data [22].

Creep damage development is largely dependent on the stress state of a component since stress states are known to affect the ductility of a material. The stress state also determines which stress parameter is best correlated to the creep damage rate [1]. There are many theories on how to correlate creep damage in multiaxial stress states to uniaxial stress state creep data and the most extensively used creep-rupture strength are von Mises, Tresca and the maximum principal stress criterion [46] .

2.6.1 Classical theories

Von Mises criterion, also known as the octahedral shear stress criterion or the distortional energy criterion, assumes that failure by yielding occurs when the distortional strain-energy density in the material reaches the same value as for yielding by uniaxial tension or compression [47]. Von Mises effective stress formula, when expressed in terms of principal stresses can be written as follows.

$$\sigma_{VM} = \frac{1}{\sqrt{2}}[(\sigma_1 - \sigma_2)^2 + (\sigma_2 - \sigma_3)^2 + (\sigma_3 - \sigma_1)^2]^{1/2} \quad \textit{Eq. 2.14}$$

The maximum shear stress criterion given by Eq. 2.15, also known as the Tresca criterion is based on the concept of maximum shear stress energy. Criterion for yielding is when the maximum shear stress of a point equals maximum shear stress at yield under uniaxial tension or compression [22, 47]

$$\sigma_{TR} = \sigma_1 - \sigma_3 \quad \textit{Eq. 2.15}$$

The Rankine theory base the failure criteria on the maximum principal stress (MPS). The theory states that yielding in a complex stress system occur when the maximum principal tensile stress, σ_1 reach the value of the yield stress.

$$\sigma_{MPS} = \sigma_1 \quad \textit{Eq. 2.16}$$

Important to mention is that yielding also can occur in compression if the minimum principal stress, σ_3 reaches the yield stress before yielding is reached in tension. The theory is best suited for brittle material since failure in ductile materials occur in shear, in addition, homogenous materials can resist very high hydrostatic pressures without failure, which indicates that the maximum principal stress criteria is not valid for all stress states [48].

Brittle material ruptures are generally governed by the MPS criterion while the von Mises effective stress is the controlling parameter for ductile ruptures that occurs under high stresses under short service. However, long service times in elevated temperatures can lead to a significant reduction in ductility, the rupture is then governed by either the MPS or a mixed criterion including both von Mises and MPS. Some studied has also been dedicated to finding out whether creep failure would occur at complete tensile triaxiality $\sigma_1 = \sigma_2 = \sigma_3$, a stress state for which von Mises effective stress becomes zero. It is however believed that even though no failure or deformation would occur in a short time span, long exposure time would eventually lead to a MPS controlled rupture. However, this is not easily verified due to difficulties associated with performing multiaxial testing [22].

2.6.2 Mixed criteria

Mixed criterions have often been suggested since the classical stress parameters has failed to describe material behaviour satisfactorily [22]. Much work has been devoted to characterizing the stress dependence of creep damage [5-8] and many proposals for the mixed criteria have been presented over the years. The mixed criterions are typically based on the assumption that creep damage is stress dependent and that the parameters von Mises effective stress, σ_{VM} and the maximum principal tensile stress, σ_{MPS} are the most relevant [1]. The models differ on how much each stress parameter

contributes to the equivalent uniaxial stress and on how the relative importance of the stress parameters are defined.

A general model [1] that uses α to determine influence of the stress parameters σ_{VM} and σ_{MPS} correlates creep damage under uniaxial stress with multiaxial stress conditions by the formula

$$\sigma_{eq} = \alpha\sigma_{VM} + \beta\sigma_{MPS} \qquad \textit{Eq. 2.17}$$

where

$$\beta = 1 - \alpha \qquad \textit{Eq. 2.18}$$

This method divides materials are into α materials and β materials, whereas α materials are only depending on effective stress (α=1), this is typically the case for aluminium alloys. Similarly, β materials, such as copper is only dependent on the maximum principal stress. However, most materials used for engineering purposes have a combination of both α and β behaviour. β materials are more sensitive to notches and stress concentrations and α dominant materials are often selected in engineering applications [1].

Another alternative empirical equivalent stress developed by the Russian research institute CKTI uses the Norton creep exponent n in their proposed mixed criteria for high-temperature alloys [22].

$$\sigma_{CKTI} = (\sigma_{MPS}^{n} + 0.47\sigma_{VM}^{n})^{1/n} \qquad \textit{Eq. 2.19}$$

The Principle Facet Stress, σ_F concept was proposed for materials that experience grain boundary sliding (GBS) [49]. The suggested criterion is based on the observation that the creep damage process is dominated by cavitation on the transverse axis of the MPS and is coupled with shear deformation governed by von Mises along the inclined grain boundaries as illustrated in Figure 19.

$$\sigma_F = 2.24\sigma_1 - 0.62(\sigma_2 + \sigma_3) \qquad \textit{Eq. 2.20}$$

The principle facet stress has been successful in predicting multiaxial creep rupture from uniaxial creep data, especially for austenitic and ferritic steels. Since stresses calculated with the above equation are high, it cannot be used directly in engineering calculations. However, it has been observed to coincide with von Mises stress on the outer surface on a pressurized tube by normalizing with a factor of 2.4 and Huddleston's stress by normalizing with a factor of 2 [22]. The criterion is not suitable for specimens subjected to large hydrostatic stress and it is only valid when grain boundary cavitation is the dominant failure mechanism [49].

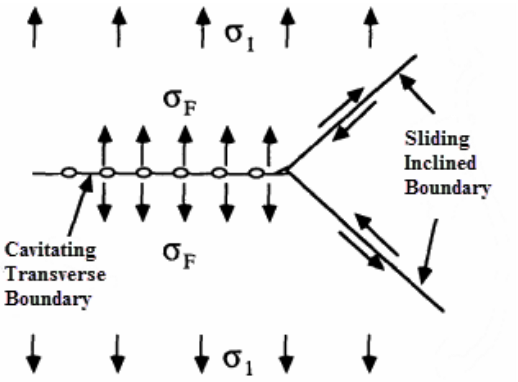

Figure 19. Grain boundary sliding with round shaped cavities forming on the transverse axis of the maximum principal stress and shear deformation along the inclined boundaries [49]

2.6.3 Huddleston's theory

Although it has been shown that classical criterion suggested by von Mises, Tresca and Rankine all give a comparatively poor fit for compression- tension stress states. Tresca and von Mises have been the most commonly used strength theories used in high-temperature structural design codes [46, 50, 51]

Huddleston [46, 50, 51] developed an isochronous rupture surface when studying creep rupture in stainless steel. The concept can be considered a modified version of the von Mises criterion and a comparison between biaxial isochronous contours of classical theories and Huddleston's theory is shown in Figure 20.

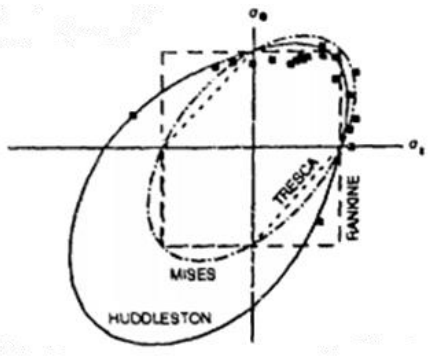

Figure 20. Biaxial isochronous stress-rupture contour for Inconel 600 at 816 °C [51]

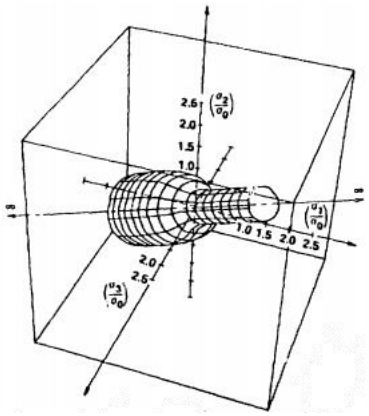

Figure 21. 3D Isochronous stress rupture surface for type 304 stainless steel at 593 °C [51]

The model proposed by Huddleston has shown to give more accurate stress-rupture life predictions than the classical theories of von Mises, Tresca and Rankine (MPS) for stainless steel alloys tested under various biaxial stresses. The model can also differentiate creep life under tensile versus compressive stress states. The bottleneck in the 3D isochronous rupture surface depicted in Figure 21 indicates that larger stresses are required under compressive stress states to cause the same amount of damage as produced in tension. The model translates a multiaxial stress state to an equivalent uniaxial stress that causes creep damage at a similar rate. The proposed equivalent stress σ_{HUD} given by Eq. 2.21 [46, 50, 51].

$$\sigma_{HUD} = \frac{3}{2} S_1 \left(\frac{2\sigma_{VM}}{3S_1}\right)^a \exp\left[b\left(\frac{J_1}{S_S} - 1\right)\right] \quad \text{Eq. 2.21}$$

Where σ_{VM} is von Mises effective stress, a and b are material specific constants, J_1, the first invariant of the stress tensor, S_1, the maximum deviatoric stress and S_S, an invariant stress parameter that includes $J_1$and the second invariant of the deviatoric stress tensor J_2'

$$J_1 = 3\sigma_H = \sigma_1 + \sigma_2 + \sigma_3 \quad \text{Eq. 2.22}$$

$$S_1 = \sigma_1 - J_1/3 \quad \text{Eq. 2.23}$$

$$S_S = \sqrt{\frac{6J_2' + J_1^2}{3}} = (\sigma_1^2 + \sigma_2^2 + \sigma_3^2)^{1/2} \quad \text{Eq. 2.24}$$

The model is not sensitive to small changes of the constants a and b, biaxial data from 304, 316 and Inconel stainless steel also showed that the values of material specific constants a and b had a limited range. Based on this, Huddleston proposed that universal values a=1 and b=0.24 may be applicable. This leads to a simplified form of Eq. 2.21 , given by

$$\sigma_{HUDS} = \sigma_{VM}\, exp\left[0.24\left(\frac{J_1}{S_S} - 1\right)\right] \quad \text{Eq. 2.25}$$

Although the material specific values produced more accurate predictions, the model with the universal constants still produced better predictions for the tested steels 304, 316 and Inconel, than the classical theories [46]. The Huddleston criteria which was initially developed for stainless steels has also been confirmed useful for ferritic high-temperature engineering alloys and was included into the ASME Code Case N47-29 in 1990, is today known as ASME III, Subsection NH [11, 22, 50]

2.7 Finite Element analysis

Finite element analysis (FEA) is a numerical method used to solve field problems for example displacement, stress and temperature distributions. Differential equations or integral expressions are used to describe the field problem and a field or structure is discretized in to smaller parts which are called finite elements. Each finite element is only allowed to have a limited spatial variation which can be modelled by simpler equations. This yields an approximate solution of the field problem since the actual variation is often more complicated [52].

2.7.1 Material models

Finite element analysis use material models for describing the material response for various loading conditions. The various material models have different stress-strain relationships and a description of a selection of material models are presented below.

2.7.1.1 Linear-elastic material model

The linear-elastic material model is the most used material model in solid mechanics. The linear-elastic model assumes a linear behaviour of the material, where stress is proportional to strain, commonly known as Hooke's law, $\sigma = E\varepsilon$. Material subjected to small strains has a reversible behaviour and when released after loading the material recover to its original form and the strain returns to zero. If

the material has been strained within the linear elastic limit, the material is considered perfectly elastic. This material model assumes that stress is proportional to strain and it is represented by the linear part AO in Figure 22. [47, 53]

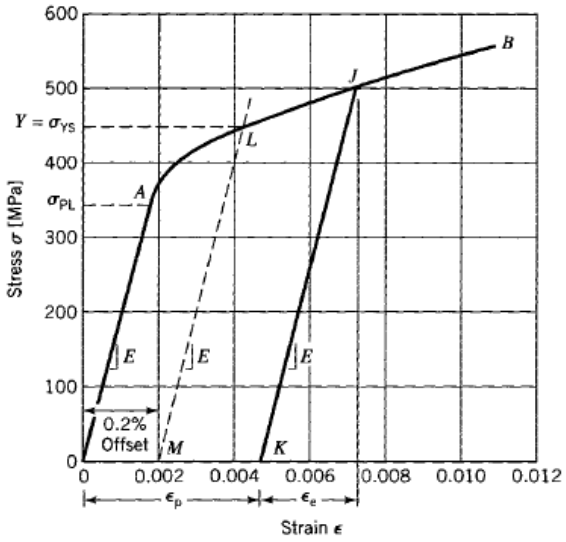

Figure 22. Engineering stress-strain diagram for tensile specimen [47]

2.7.1.2 Rate independent plastic material model

When a metallic material is loaded beyond the elastic limit and deforms at low temperatures (below the creep regime) the material response is described by rate independent plasticity models.

A material subjected to load beyond its elastic limit have a total strain equal to the sum of the elastic and a plastic strain component $\varepsilon_t = \varepsilon_e + \varepsilon_p$. Upon unloading, the elastic strain is recovered but the plastic strain remains and the material has a sustained non-recoverable plastic deformation. Figure 22 illustrates a material loaded to its plastic region to point J and unloading occurs along the line JK which corresponds to the recovered elastic strain, ε_e. The plastic strain, ε_p remains as permanent in the material [47].

In theoretical analysis, the stress-strain curve can be bilinear or multilinear as shown in Figure 23. The simplest bilinear stress-strain curve is represented by the elastic-perfectly plastic model. The material has a linear stress-strain relationship until the yield point and exhibits no hardening behaviour. As the material is loaded to its yield point, the material will continue to elongate without increasing the load [54]. This material model is an idealized model which can be used when strains are small [47]. The elastic-perfectly plastic stress-strain curve has a plastic region beyond the yield point which is represented by a horizontal line with tangent modulus, E_T equal zero.

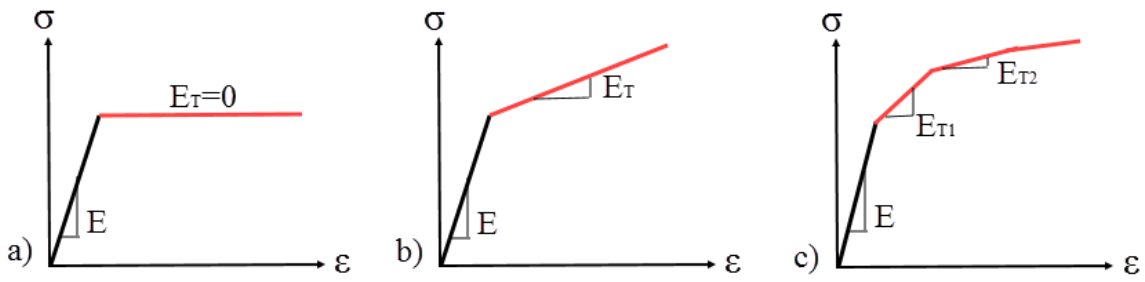

Figure 23. Stress-strain representations: a) Elastic-perfectly plastic stress strain curve b) Bilinear stress-strain curve c) multilinear stress-strain curve

Strain hardening is a material's ability to resist additional strain when loaded beyond the yield stress, as the material deform the elastic proportion of the curve and yield stress increases until the ultimate stress limit has been reached [47, 54]. To include strain hardening behaviour a bilinear or a multilinear stress-strain curve representation can be used. The tangent modulus for the plastic region is constant for bilinear curve while for the multilinear curve each segment of the plastic region is represented by a different value [53].

Hardening rules are used to describe the change in yield criterion due to plastic deformation. Figure 24 provides a graphical illustration with two isotropic and kinematic hardening rules which are commonly used for plasticity modelling. For isotropic hardening the yield surface keeps its shape and has a uniform increase in size around its symmetric axis, which results in a corresponding increase in elastic range and in yield stress. For the kinematic hardening law the yield surface moves in stress space but the shape and size remains the same so that the elastic range remains constant. Isotropic hardening best describes material behaviour under monotonic loading and elastic unloading while the kinematic rule can be used for both monotonic and cyclic loading because of its ability to model the behaviour of plastic ratcheting, which is the buildup of plastic strain during cyclic loading and the Bauschinger effect, which is when compressive yield strength is reduced in response to tensile hardening [53].

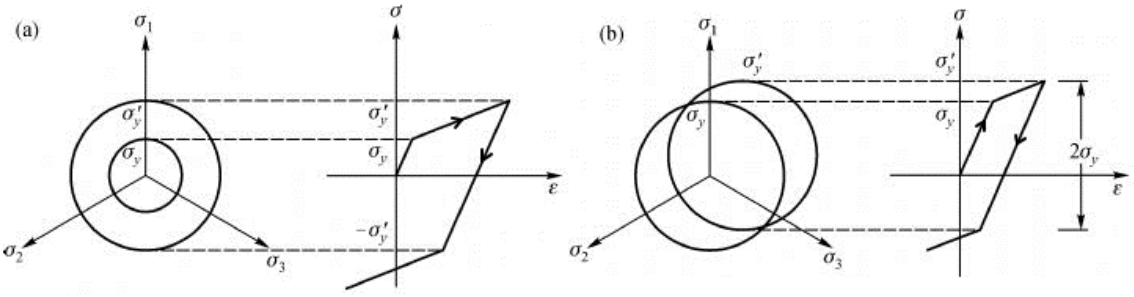

Figure 24. Illustration of hardening models with bilinear stress-strain curve (a) Isotropic strain hardening; (b) kinematic strain hardening [55]

2.7.1.3 Rate dependent plasticity

Creep is a time dependent deformation which is described with rate dependent plasticity models. The inelastic time dependent creep response of a material when loaded at elevated temperature is also sometimes referred to as viscoplasticity. Creep response is modelled by functions describing creep strain rate and as previously described in Chapter 2.1 the three stages; primary; secondary and tertiary creep are characterized by decreasing, constant and accelerating strain rate. There is not yet a single

model that can describe all three stages. However, in structural analysis, it is typically the two first stages that are considered. Various constitutive equations and theories have been proposed over the years for modelling time-dependent plastic behaviour. Many of these has been gathered in work made by Penny and Marriott [1]. The following general descriptions of rate-dependent plasticity models has been obtained from their work and is described in terms of uniaxial state of stress, however multiaxial generalizations can be made by using hypothesis and concepts that has been proposed in plastic deformation theory.

Creep under uniaxial constant load depends on functions of stress, time and temperature. Most work on creep has treated functions as separate parameters and a general approximation on creep strain can be described in the following form

$$\varepsilon_c = f_1(\sigma) f_2(t) f_3(T) \qquad \textit{Eq. 2.26}$$

Several suggestions for how to describe the various parameters have been made and some common forms for describing the stress and time functions are given in Table 3 and Table 4 respectively.

Table 3. Stress functions $f_1(\sigma)$ [1]

		$f_1(\sigma)$	
Norton	1929	$K\sigma^n$	*Eq. 2.27*
Soderberg	1936	$B\{\exp(\sigma/\sigma_0) - 1\}$	*Eq. 2.28*
Mc Vetty	1943	$A\ sinh(\sigma/\sigma_0)$	*Eq. 2.29*
Dorn	1955	$C\ exp(\sigma/\sigma_0)$	*Eq. 2.30*
Johnson, Henderson & Kahn	1963	$D_1\sigma^{m_1} + D_2\sigma^{n_2}$	*Eq. 2.31*
Garofalo	1964	$A\ \{sinh(\sigma/\sigma_0)\}^n$	*Eq. 2.32*

* $K, A, B, C, D_1, D_2\ n, n_1, n_2$ and σ_0 are temperature dependent material constants

Most work on stress dependence has been made for secondary creep. The most common form of the stress functions in Table 3 is the Norton power law. One of the reasons it has gained popularity, besides from its simplicity is because it describes stress distributions as independent from the load magnitude.

Table 4. Time functions $f_2(t)$ [1]

	$f_2(t)$	
Andrade	$\left(1 + bt^{1/3}\right)exp(kt) - 1$	
Bailey	Ft^m	*Eq. 2.33*
Mc Vetty	$G\{1 - exp(-qt)\} + Ht$	*Eq. 2.34*
Graham & Walles	$\sum a_i t^{m_i}$	*Eq. 2.35*
Garofalo	$\theta_1\{1 - exp(-\theta_2 t)\} + \dot{\varepsilon}_s t$	*Eq. 2.36*

* $F, G, H, a_i, b, k, m\ , m, q$ are temperature dependent constants

The time functions are mostly based on empirical expressions for which researchers have tried to apply physical meaning and they do not necessarily describe the actual creep behaviour. Although they do describe time dependence under constant stress rather well, it is typically due to the many coefficients used in the curve fitting procedure. The temperature dependence $f_3(T)$ in equation Eq. 2.26 is essential to all creep rate processes and is described with Arrhenius law $exp(-Q/RT)$, where Q is the activation energy, R is the Boltzmann's constant and T is the absolute temperature.

It is more complicated to predict strain rates under variable load than it is for constant loading. Since most available creep data are from uniaxial, constant stress and temperature conditions, creep equations for variable stresses are established purely from hypothetical generalizations from constant stress creep equations. These generalizations do however predict very different results under the identical load histories and none of these methods are considered entirely satisfactory.

One of the proposals for describing creep strain rate for varying stress is the time hardening theory. This considers the hypothesis that the only thing affecting strain rate, except for stress is time-dependent structural changes. Time hardening theories suggest that creep strain rate is a function of stress, time and temperature and can be stated in the form

$$\dot{\varepsilon}_c = f_1(\sigma)\frac{df_2(t)}{dt}f_3(T) \qquad \textit{Eq. 2.37}$$

The material changes described by the time hardening approach are mainly of softening character and cannot adequately describe primary creep. It can however be correct to use for material that only displays secondary creep and may in some cases be adequate for material that exhibits secondary and tertiary creep.

Another theory is the strain hardening theory. This assumes that the hardening effect is caused by deformation and describes creep strain rate as a function of stress, accumulated strain and temperature in the following form

$$\dot{\varepsilon}_c = f_1(\sigma)f_2(\varepsilon_c)f_3(T) \qquad \textit{Eq. 2.38}$$

The strain hardening assumption describes creep that is predominantly primary and has also given satisfactory results for describing creep in very short-time creep tests. Since strain hardening is generally associated with primary creep and time hardening may be related to time dependent effects, these theories can be combined to better fit experimental data. Such combinations are however generally considered as purely empirical refinements. A general expression for the combined theories can be expressed in the following form

$$\dot{\varepsilon}_c = f_1(\sigma)f_2(\varepsilon_c)f_3(t)f_4(T) \qquad \textit{Eq. 2.39}$$

In addition to the above-mentioned theories, numerous other suggestions have been proposed for describing creep rate under variable stress, some of which were also included in the work by Penny and Marriott [1]. These include phenomenon such as reverse creep which is the reverse creep strain upon unloading and recovery, which is the loss of strain hardening due to thermal softening. However, a more detailed explanation of these is beyond the scope of this thesis.

One of the most commonly used laws for describing primary and secondary creep strain is obtained by combining the Norton [29] and Bailey [30] stress and time functions as

$$\varepsilon_c = C_1\sigma^n t^m \qquad \textit{Eq. 2.40}$$

Where C_1 (with unit $MPa^{-n}\cdot h^{-m}$), n and m are temperature dependent parameters. As described by Betten [21] the above expression in Eq. 2.40 can be differentiated with respect to time to obtain the time-hardening version Norton-Bailey law is given by

$$\dot{\varepsilon}_c = C_1 n\,\sigma^n t^{m-1} \qquad \textit{Eq. 2.41}$$

And by solving Eq. 2.40 with respect to time and insert into the time-hardening expression in Eq. 2.41 the Norton-Bailey strain-hardening version in Eq. 2.42 can be obtained.

$$\dot{\varepsilon}_c = mC_1^{1/m}\sigma^{n/m}\varepsilon_c^{(m-1)/m} \qquad \textit{Eq. 2.42}$$

What is typically known as the Norton-Bailey creep power law previously given in Eq. 2.1 is obtained by taking m=1 [21]. Another form of the Norton-Bailey power law often used in literature is given by

$$\dot{\varepsilon}_c = C_1'\sigma^{n'}t^{m'} \qquad \textit{Eq. 2.43}$$

Where Creep C_1', n' and m' still are temperature dependent constants but C_1' have different units $MPa^{-n'} \cdot h^{-m'-1}$. However, this form is limited to values for C_1' that are larger than zero [56]. All of the temperature dependent constants given in the above equations need to be obtained from creep test data which is not always easily obtained.

2.8 High-temperature design code: ASME III Subsection NH

As previously mentioned in the introduction, there are several national codes that provide rules and guidelines for design of components at elevated temperatures. In the following sections, the design rules for construction at elevated temperatures according to ASME, Section III, Subsection NH are discussed.

Behind the rules in standards, engineering corrections and safety factors are often based on extensive research and detailed analysis. However, the fundamental principles behind the methods are not often apparent to the user [22]. ASME provide extensive rules for evaluating components in the creep regime and only the outline of the method provided in the code will be presented.

2.8.1.1 Background of ASME III Subsection NH

Many industries consider their design procedures and guidelines as property and information is typically classified as commercially confidential. Many industries also appear to have no systematic design procedures at all. Historically, it has been necessary for the pressure vessel industry to implement regulatory design methods due to the substantial risk associated with failure in pressurized components. Due to this there has been an open forum for its procedural methods and the experience gained during the process of working with other industries has suggested that the design practice used in the pressure vessel industry can be used for high-temperature design in general [1].

The main difference between high- and low-temperature design requirements is not so much the effect of temperature but rather the time-dependency it introduces [1]. ASME Boiler and Pressure Vessel Code, section III subsection NH [11] contains rules for construction of Class 1 components for nuclear service at elevated temperature. Its purpose is to offer comparable construction rules as subsection NB [57] does for Class 1 components (components in primary reactor system) below the temperature regime for which creep effects are significant [9].

The first predecessor to ASME-NH that covered design rules for elevated temperature Class 1 components was issued in 1963 under the name Code Case 1331. The initial versions of this was very limited in scope and it was not until 1971 that the basic requirements used in ASME-NH was included. Since then, many additions, modifications and revisions has been made. A series of code cases 1592-1596 were released in 1974 covering all aspects of elevated temperature construction [9]. Subsequently this became Code Case N-47 before it finally was called ASME-NH.

The main contributor to the development of ASME-NH has been the Oak Ridge National Laboratory. In addition, many organizations, both in the United states and worldwide has contributed through exchange agreements and voluntary contributions [9].

2.8.1.2 Creep assessment method in ASME-NH

Subsection NH can be considered and extension of Subsection NB, and deals with construction of components at elevated temperatures where the effects of creep are considered significant, which has been specified as temperatures above 370 °C for ferritic steels and 425 °C for austenitic steels and nickel based alloys [9, 11].

One major difference between Subsection NB and subsection NH is the number of allowed materials [9]. The permitted materials included in the code of Subsection NH are listed in Table 5.

Table 5. Permitted materials in ASME-NH [11]

Material	Permitted use	Condition
304SS	Structural and bolts	Annealed
316SS	Structural and bolts	Annealed
Ni-Fe-Cr Alloy 800H	Structural	Annealed
2¼Cr-1Mo	Structural	Annealed
9Cr-1Mo-V	Structural	Normalized and tempered
Ni-Cr-Fe-Mo-Cb Alloy 718	Only for bolts	Precipitation hardened

Except for Alloy 718 which is precipitation hardened and only allowed for bolts and 9Cr-1Mo-V, the allowed materials are specified in the annelid condition. The annealed condition was specified for Subsection NH material because of concern for long-term stability and predictability of mechanical properties. In 2004, structural material 9Cr-1Mo-V with the normalized and tempered condition, was the last material to be added to the list of structural materials to take advantage of its higher yield strength, which tend to reduce distortion and strain accumulation due to ratcheting and superior creep rupture strength [9].

2.8.1.3 Analysis of components at elevated temperature service

As indicated in Figure 25, the analysis of a component at elevated temperature in the creep regime, require limits for both the load-controlled stresses and strain- and deformation-controlled quantities to be satisfied. The limits have been set to avoid the following failure modes: (1) ductile rupture from short term loadings; (2) creep rupture from long-term loadings; (3) creep-fatigue failure; (4) gross distortion due to incremental collapse and ratcheting; (5) loss of function due to excessive deformation; (6) buckling due to short-term loading and (7) creep-buckling due to long-term loadings. For failure modes (5) to (7) there are only brief guidelines provided in the code [11].

First a design should meet the requirements given in an ASME code of construction such as ASME I, VIII-1 or VIII-2, and then comply with requirements in ASME III-Subsection NH. It should however be mentioned that the temperature dependent allowable stress values vary with the different sections [14].

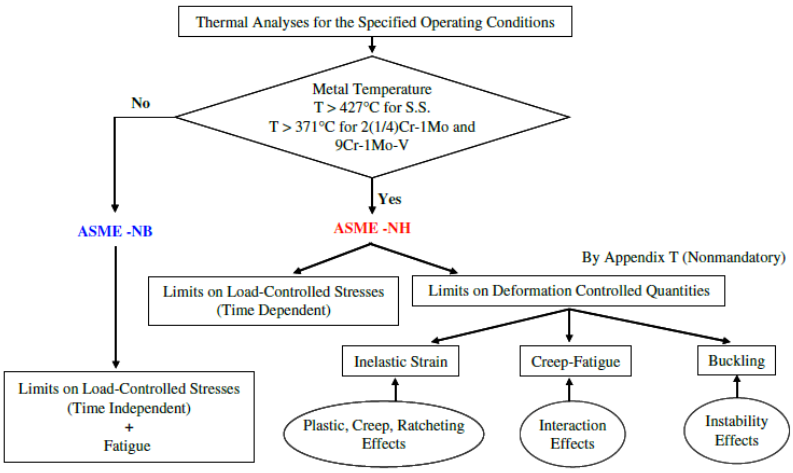

Figure 25. Procedures for structural integrity evaluations for nuclear class 1 components by the ASME Rules [58]

In subsection NH, the following maximum accumulated inelastic strain limits has been established to ensure functional requirements and structural integrity [11] :

- Strains averaged through thickness, 1% (membrane strain)
- Strains at the surface, due to an equivalent linear distribution of strain through the thickness, 2% (bending strain)
- Maximum local strains, at any point, 5%

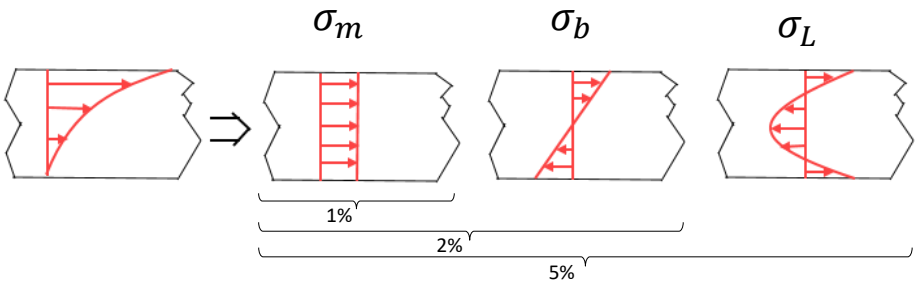

Figure 26. Illustration of strain-limited quantities [9].

The limits above are the accumulated limits over the expected operating lifetime of a component and are to be computed for a steady state period at the end of the specified life to avoid significant effect of transients [11]. These limits require an inelastic analysis to be carried out. Due to the difficulties associated with performing inelastic analysis (which will be further discussed below) subsection NH has provided alternative methods that are based on elastic analysis [9].

The strain- and deformation-controlled limit evaluation in Subsection NH [11] can be performed using one of the three following analysis methods:

1. Elastic analysis
2. Simplified inelastic analysis
3. Inelastic analysis

These are arranged in the order from simplest to most difficult and least accurate to most accurate. Also, the amount of material data required for the analysis and the cost to perform them increase for

method two and three. Of all the three criteria, the elastic limits are set to be most conservative, due to difficulties of accurately predicting inelastic strain with elastic analysis. As illustrated in the flowchart in Figure 27, when stresses from the elastic analysis cannot satisfy the elastic limits, either the component need to be redesigned or a simplified inelastic analysis can be performed. Similarly, if the simplified analysis does not meet the requirements for the simplified inelastic stress limits, the component must either be modified or an inelastic analysis be carried out [11, 14].

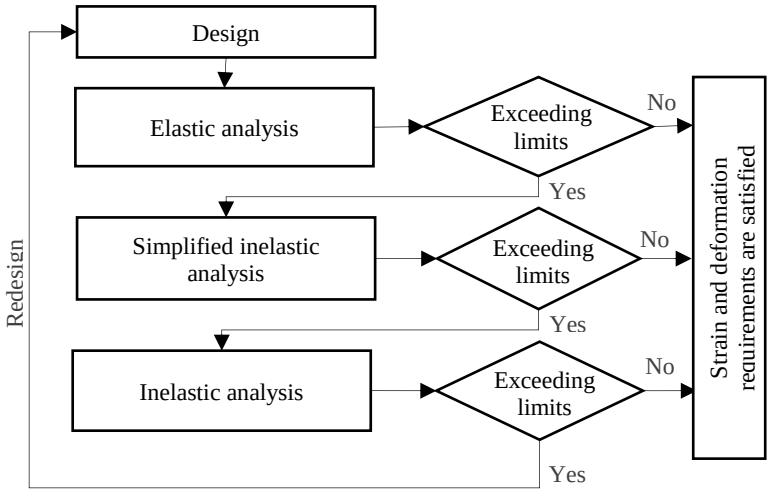

Figure 27. Flowchart of analysis procedure for evaluation of inelastic strain limits

2.8.1.3.1 Elastic analysis

The elastic analysis is typically preferred among engineers since it is the easiest, most convenient and least expensive analysis method. The method involves linearization to separate and categorize stresses to approximate the more accurate plastic and creep analysis. Further, there are tests provided in the code to ensure that strain- and deformation requirements are met. The method is appropriate to use when the combined primary and secondary stresses are below the yield strength of the material [14]. However, a downside with stress categorization is that it requires substantial knowledge and engineering judgement, especially for complex structures and three-dimensional stress fields [59]. In addition, strain- and deformation-controlled limits in Subsection NH require primary and secondary stress categories to be dealt with separately as opposed to the elastic method in ASME VIII-2. However, there are alternative tests for the elastic analysis which offer an alternative to avoid separation of primary and secondary stresses. The elastic analysis is not as accurate as a plastic or creep analysis, which more accurately predicts the materials stress-strain relationship. It is, however the most conservative criteria and considered adequate for most design applications [14].

2.8.1.3.2 Simplified inelastic analysis

The simplified inelastic analysis also uses the results from the stress categorization made with the elastic analysis. However, these are used to calculate a strain which is compared to the allowable strain limit, thus the name simplified inelastic analysis. The method is based on the concept that the core stress remains elastic when subjected to primary and secondary stresses (obtained from stress linearization). By normalizing the primary and secondary stresses, the magnitude of the elastic core of the component can be establish with a so-called Bree-diagram. The value of the elastic core can subsequently be used to calculate the resulting strain [9, 14].

2.8.1.3.3 Inelastic analysis

The inelastic analysis method does neither include comprehensive nor specific guidance in Subsection NH. This was an intentional decision, since material models for inelastic analysis are still under development, and it was considered that over-specific guidance would halt further progress in the field [9].

With an inelastic analysis, the inelastic strains and deformation due to service loads can be obtained directly from the analysis. The analysis does however require constitutive equations that describe both time-independent and time-dependent material response. There exist many formulations of such equations, however the prediction obtained from the various equations can vary significantly, as previously mentioned in Chapter 2.7.1. For predictions with an inelastic analysis to be meaningful, the equation selected to model the material's response must be evaluated according to the materials load and temperature history. This typically require a large quantity of material test data which are typically not available and material testing would be required. All the above-mentioned requirements make the method both expensive and time consuming. In addition, since it is not practical to test a material for all stages of the load and temperature history, the choice of material model and the evaluation of the results therefore requires a substantial portion of engineering judgement [9, 14].

2.8.1.4 Accumulated creep-fatigue damage evaluation

The method for evaluating accumulated creep-fatigue in ASME-NH [11] is based on superposition of the Miners rule for fatigue and the time-fraction rule for creep damage. The damage due to creep and fatigue are evaluated separately and combined as follows:

$$\sum_{j=1}^{P}\left(\frac{n}{N_d}\right)_j + \sum_{k=1}^{q}\left(\frac{\Delta t}{T_d}\right)_k = D_f + D_c = D \qquad \text{Eq. 2.44}$$

Where n/N_d is the cyclic portion of the life fraction, for which n is the number of fatigue cycles at a given strain range j, N_d is the number of allowable cycles (the fatigue life) for cycle type, j corresponding to a given strain range at the maximum temperature occurring during the cycle. The creep life fraction given by $\Delta t/T_d$ is time dependent, where Δt is the duration of the time interval, k, at a certain stress- and temperature-level and T_d is the rupture time at that same stress and maximum temperature for the time interval k. D is the total creep-fatigue damage factor [11].

This linear damage approach was chosen in the 1970s, and is consistent with the other damage assessment procedures in the ASME code. The use of Miners rule is for example used for assessing fatigue damage at lower temperatures in Subsection NB. Many methods for evaluating creep-fatigue damage was considered, however the linear fraction approach was chosen since it was straight forward and does not require as many tests as other methods. Important to mention is that the linear fraction damage summation is unconservative without the safety factors incorporated in Subsection NH [9].

Figure 28 shows the bilinear summation diagram used in the Subsection NH for creep-fatigue interaction. The intersection points for the permitted materials are also indicated in the figure. The lines in the envelope are conservative lower bound limits based on experimental data.

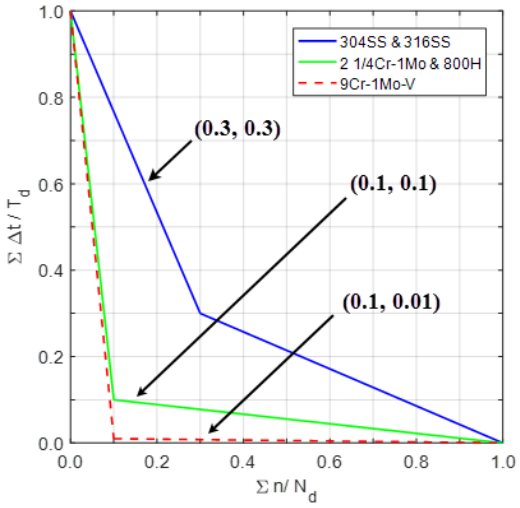

Figure 28. Creep-fatigue damage envelope re-plotted from ASME-NH [11]

2.8.1.5 Creep-fatigue analysis method

When the inelastic strain- and deformation-limits for functional- and structural integrity requirements are met the creep fatigue analysis can be carried out. The rules for cyclic loads in Subsection NH involve determining points within a cycle time for which the stress levels in a certain point of a component are at a maximum. Stresses are then evaluated against load- and strain-controlled limits for creep and fatigue, similar to the procedure explained in the previous subchapter [14].

As pointed out by Jawad and Jetter [14] a substantial amount pf calculations are required before Eq. 2.44 can be solved. Subsection NH provides two alternative approaches for solving the creep-fatigue damage equation [11]:

- Inelastic creep-fatigue analysis
- Elastic creep-fatigue analysis

Conceptually, creep-fatigue evaluation with inelastic analysis is relatively straightforward and will not be discussed further. However, the difficulties associated with inelastic analysis as mentioned above still apply [9].

2.8.1.5.1 Elastic creep-fatigue analysis

The creep-fatigue analysis in Subsection NH provides a complicated calculation procedure for creep-fatigue evaluation especially for complex load-temperature histories with many cycles. It also requires complex interpolation procedures to regenerate isochronous stress-strain curves for each temperature-time block [58].

Very briefly explained, the procedure requires a set-up of the entire load- and temperature history of a point of interest. The load and temperature history is divided into cycles, and for each cycle type, a total strain range, ε_t is computed. ε_t is used in the evaluation of the fatigue fraction term n/N_d to determine the number of allowable fatigue cycles $(N_d)_j$ for each cycle type. ε_t is also used for obtaining the corresponding stress level which is necessary for computing the creep fraction term $\Delta t/T_d$ in Eq. 2.44. The procedure requires composing a stress-time history envelope that includes all cycle types which is modified to include the transient effects of stress relaxation as illustrated in Figure 29. The period for stress relaxation is then divided into time blocks for which an average constant

stress and constant temperature are assumed and for each of these time blocks, the life fraction is computed and summed.

The general creep-fatigue procedure in Subsection NH include the following steps [11]:

- Defining the total number of hours, t_H, spent at elevated temperatures
- Define the hold temperature, T_{HT} as the metal temperature that occurs during sustained normal operation.
- Define average cycle time, $\bar{t}_j$ for each cycle type as $\bar{t}_j = t_H/n_j$, where n_j is the number of applied repetitions for cycle type j.
- Compute the total strain range ε_t and establish the corresponding stress S_j from time-independent stress-strain curves corresponding to T_{HT}
- Adjust S_j with respect to stress relaxation and the multiaxial stress state
- Construct a stress-time history envelope for the cycle type j and define transient parameters
- Superimpose all stress-time history envelopes to construct a composite stress-time history envelope that includes all cycle types
- Determine the time interval $(\Delta t)_k$ for the creep damage term. For each time interval, determine the allowable time duration need $(T_d)_k$ from the stress to rupture curves.

Not mentioned here are the numerous safety factors and engineering corrections for stress concentrations, multiaxiality etc. that are incorporated in the procedure. The code also provides alternative methods with various level of conservatism for some of the steps in the above list.

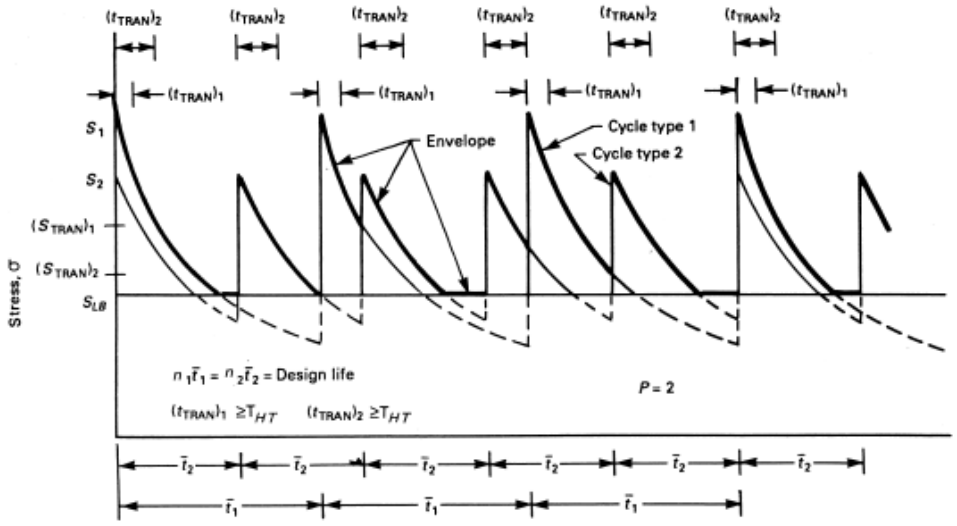

Figure 29. Stress-time history envelope for creep damage assessment [11]

In a review [58] of the rules in Subsection NH it was found that the evaluation procedures and rules are too complex to carry out for an actual reactor design with consideration for all the design transient conditions, by using hand calculations. A computerized implementation of the rules was proposed to solve the problem.

2.9 Pressure vessel design

According to the definition in ASME VIII-1 [60], pressure vessels are containers used for containment of either internal or external pressure, which may be obtained from an external source or by applying heat from a direct or indirect source.

Pressure vessels operating under high-temperature service where the effect of creep is significant can be found in chemical plants, refineries and power generation plants. One of the design issues for such pressure vessels are the variable loading conditions due to start up and shut down in combination with the effect of long time exposure at elevated temperatures. The capability of a pressure vessel shell to perform properly depends on several factors, like the stress level, material properties, operating temperature and temperature range and pressure cycles [14]. The purpose of this section is to describe stresses in pressure vessels due to the design pressure and to describe in short, some different design methodologies used in pressure vessel design.

Generally, pressure vessels can be categorized into thin-walled or thick (heavy)-walled configuration and depending on what configuration the pressure vessel has, different approaches can be used for computing the stresses. There are also several types of shape configurations for pressure vessels. However, in the following sections regarding thin- and thick-walled configurations, only stresses with respect to cylindrical shape pressure vessels will be discussed.

2.9.1 Thin-walled pressure vessel configuration

When pressure is applied to a cylinder, three principal stresses arise in the material, namely circumferential or hoop stress (σ_h), radial stress (σ_r) and longitudinal or axial stress (σ_z). The assumption made for thin-walled cylinders is that the hoop and axial stresses are constant through the wall thickness without any pressure gradients and that the radial stress can be neglected since it is considered small in comparison [48]. The hoop stress and axial stress are due to the internal pressure P_i and can for a thin walled cylinder be approximated with the following expressions:

$$\sigma_h = \frac{P_i D_i}{2t} \qquad \textit{Eq. 2.45}$$

$$\sigma_z = \frac{P_i D_i}{4t} \qquad \textit{Eq. 2.46}$$

where D_i is the internal diameter and t is the cylinder thickness. The thin-walled approximation is generally considered rather accurate when the ratio of thickness to inside radius is less than 1/10 [48].

2.9.2 Thick-walled pressure vessel configuration

For thick-walled cylinders when the ratio of the wall thickness to the inside radius becomes too large, stresses become triaxial and the biaxial assumption used for the thin-walled configuration is no longer valid. In addition, the stresses must be evaluated with respect to the radius since hoop and radial stress vary across the wall thickness as illustrated in Figure 30. Stresses for thick-walled cylinders can be described with the Lamé equations given by [48]:

$$\sigma_h(r) = A + \frac{B}{r^2} \qquad \textit{Eq. 2.47}$$

$$\sigma_r(r) = A - \frac{B}{r^2} \qquad \text{Eq. 2.48}$$

Where A and B are constants that are derived from the boundary conditions. The general case of a cylinder subjected to both internal and external pressure yields the following Lamé constants.

$$A = \frac{P_i r_i^2 - P_o r_o^2}{r_o^2 - r_i^2} \qquad \text{Eq. 2.49}$$

$$B = \frac{r_i^2 r_o^2 (P_i - P_o)}{r_o^2 - r_i^2} \qquad \text{Eq. 2.50}$$

For a cylinder with closed ends subjected to both internal and external pressure, the axial stress along the cylinder equals the Lamé constant A.

$$\sigma_z = A = \frac{P_i r_i^2 - P_o r_o^2}{\left(r_o^2 - r_i^2\right)} \qquad \text{Eq. 2.51}$$

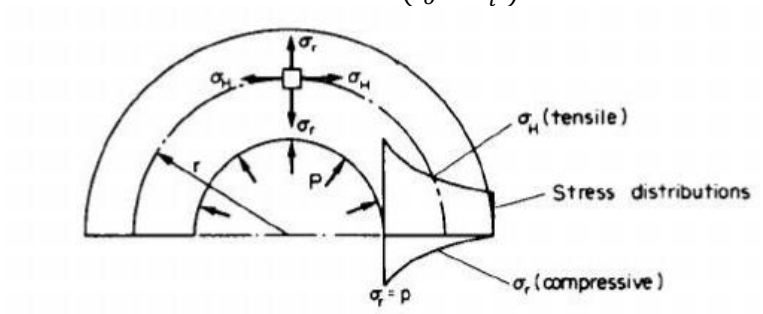

Figure 30. Stress distribution of a thick-walled cylinder subjected to internal pressure [48]

2.9.3 ASME VIII - Pressure vessel design methods

ASME BPVC is a widely used code for the design of pressure vessels and while there other pressure vessel codes, such as the European Standard EN 13445 [27] the following section only concerns the design methodologies given in ASME BPVC section VIII.

In ASME-VIII there are basically two methods for design of pressure containing components to determine the required wall thickness to withstand internal pressure and external loads. These are often referred to as Design by Rule (DBR) and Design by Analysis (DBA). Simply described, the DBR approach provide formulas to determine the required wall thickness based on design pressure, allowable stress and geometry parameters and the requirements for specific configurations are determined by several diagrams provided in the code [14].

With the DBA method given in ASME VIII-2 [59], a component is evaluated based on results obtained from numerical analysis. The DBA-requirements are based on protection against the following failure modes; plastic collapse; local failure; collapse from buckling and failure due to cyclic loading (ratcheting). The code offers linear-elastic and elastic-plastic analysis procedures for each of the above listed failure modes and provides different acceptance criteria to determine if the component is safe depending on what type of analysis is being used. The procedures for protection against buckling and failure due to cyclic loading will not be further discussed, however short descriptions of the procedures for protection against plastic collapse and local failure are given below.

For protection against plastic collapse there are three alternative analysis methods provided in the code:

1. *Elastic Stress Analysis Method* – Stresses are computed using a linear-elastic material model and classified into categories and compared to related limiting values which have been established conservatively.
2. *Limit-Load Method* – The procedure involves determining the lower bound limit load of a component. An elastic-perfectly plastic material model with small displacement theory shall be used and the concept of load and resistance factor design (LRFD) is used to establish the limit load as a safety measure against plastic collapse.
3. *Elastic-Plastic Stress Analysis Method* – In this analysis procedure a plastic collapse load is derived from an elastic-plastic analysis by using either a material model that includes hardening and softening or an elastic-perfectly plastic material model. Like the Limit-Load method, design factors are used to establish the maximum allowable load.

From the above listed analysis procedures for protection against plastic collapse the elastic stress analysis method has been the most commonly used design methodology, particularly for components at elevated temperatures [14]. However, categorization of stresses requires both experience and judgement, especially for complex geometries and particularly those with three-dimensional stress fields. Therefore nowadays, the analysis methods involving elastic-plastic material models are becoming more and more utilized. In addition, the structural evaluation made with the elastic stress analysis only approximates the protection against plastic collapse and a more accurate assessment can be obtained with method 2) and 3) by determining the limit or the plastic collapse load. Nevertheless, the elastic-plastic analysis provides the most accurate estimate for protection against plastic collapse because it provides a better estimate of the structural behaviour since the stress redistribution due to inelastic deformation and deformation characteristics of the component are considered directly in the analysis. Also, worth mentioning is that for heavy-wall configuration $(R_i/t \leq 4)$ pressure containing components, the use of elastic stress analysis with stress classification is not recommended since it can yield non-conservative results especially around discontinuities. The reason for this is that the nonlinear distribution of stress associated with heavy wall sections is not sufficiently well represented by implicit linear stress [59].

For protection against local failure both elastic and elastic plastic analysis can be used. Like in the procedure for protection against plastic collapse, the elastic-plastic method provides a more accurate estimate of protection against local failure. In the elastic analysis procedure for local failure, a triaxial stress limit given by the sum of the three linearized primary principal stresses are evaluated against a limiting criterion while the elastic-plastic analysis involves evaluating the plastic strain for all points in the component against a triaxial limiting strain [59].

3 METHOD – CREEP DAMAGE ASSESSMENT

This Chapter explains the procedure of a creep damage assessment made for a pressure vessel with the use of the nonlinear Pavlou creep damage model and the linear Life Fraction Rule. The first part evaluates how to use the nonlinear creep model for practical design applications. The evaluation is based on applicable data from variable-load creep tests and previous research. The second part presents the chosen material data for the pressure vessel and creep-rupture curves for the selected material are made and evaluated. In the last section, a Finite Element Analysis is conducted to evaluate stresses on the pressure vessel and the results from the analysis are used for remaining life assessment.

The numerical computing platform MATLAB was used for setting up calculations and creating plots that are presented in this chapter. Computer-aided engineering software ANSYS Workbench has been used for making the geometry and for the stress analysis of the pressure vessel.

3.1 Evaluation of creep models

Previous evaluations of Pavlou's nonlinear creep model had various suggestions for how to use it. In Pavlou's analysis [16] it was suggested to replace the original creep endurance limit with a fitting parameter to consider the transient behaviour of the material during variable step loading. However, in the research made by Grell [17] it was suggested to use the original parameter since the choice of a fitting parameter would limit the model to stresses below the fitting parameter. A third suggestion that has been made is to replace the Larson-Miller parameter curve with a normalized curve [18].

This section is dedicated to evaluating how to use the nonlinear model in practice and evaluate which of the above suggestions should apply when evaluating the creep life of a component.

3.1.1 Validation of the nonlinear Pavlou model

A recreation of Pavlou's analysis [16] was made to validate the script in MATLAB and to confirm Pavlou's results. To verify the nonlinear creep model Pavlou used experimental results [61] from austenitic high-temperature steel X8CrNiMoNb 16-16 and high-purity aluminium (Al 99.98). The materials were tested at a constant temperature for two-step loading up to failure. The loading conditions and test results are given in Table 6 and Table 7.

Table 6. Load conditions for variable step creep loading

Material	σ_1 (MPa)	σ_2 (MPa)	T_1 (K)	T_2 (K)
X8CrNiMoNb-16-16	150	170	973	973
Al-99.98	12	14	498	498

Table 7. Test results from two step creep test for materials [61]

X8CrNiMoNb-16-16	t_1/t_{f_1}	0.05	0.1	0.35	0.40	0.44	0.46	0.55	0.88
	t_2/t_{f_2}	0.70	0.61	0.21	0.25	0.20	0.21	0.21	0.05
Al-99.98	t_1/t_{f_1}	0.12	0.13	0.3	0.32	0.50	0.65	0.70	0.75
	t_2/t_{f_2}	0.58	0.56	0.38	0.37	0.24	0.16	0.13	0.11

According to Pavlou's model the failure criterion for a two-step loading can be written:

$$D = \left(\frac{t_1}{t_{f_1}}\right)^{\frac{T_1 \log(\sigma_2/p)}{T_2 \log(\sigma_1/p)}} + \frac{t_2}{t_{f_2}} = 1 \qquad \textit{Eq. 3.1}$$

Eq. 3.1 can be solved equation in with respect to the fitting parameter p by

$$p = 10^{\left(\frac{-log\sigma_2 + log\sigma_1 \cdot \frac{T_2 \log\left(1-\frac{t_2}{t_{f_2}}\right)}{T_2 \log\left(\frac{t_1}{t_{f_1}}\right)}}{\frac{T_2 \log\left(1-\frac{t_2}{t_{f_2}}\right)}{T_1 \log\left(\frac{t_1}{t_{f_1}}\right)} - 1}\right)} \qquad \textit{Eq. 3.2}$$

Pavlou used the first pair of test results in Table 7 together with the loading condition in Table 6 to obtain the fitting parameter p=184.916 MPa for the materials X8CrNiMoNb-16-16 and p=15.577 MPa for Al 99.98. Pavlou compared the theoretical results obtained with Eq. 3.1 with the experimental results from Table 7 by plotting the time fractions of consumed life versus the remaining life. The recreated comparison given in Figure 31 and Figure 32.

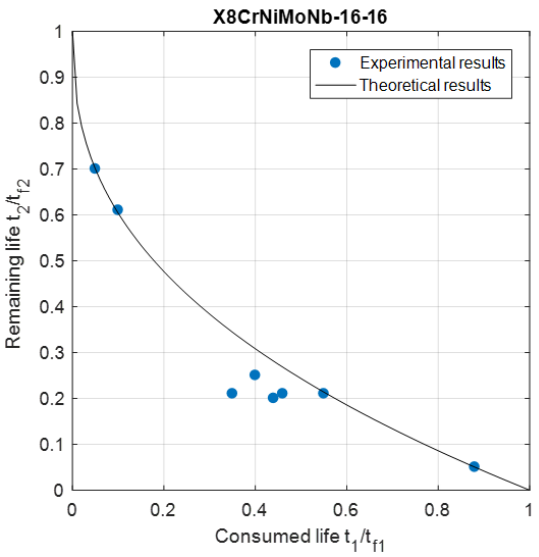

Figure 31. Remaining life t_2/t_{f2} for σ_2=170 MPa versus consumed life t_1/t_{f1} for σ_1=150 at constant temperature T=973 K for material X8CrNiMoNb-16-16 with fitting parameter p=184.916 MPa

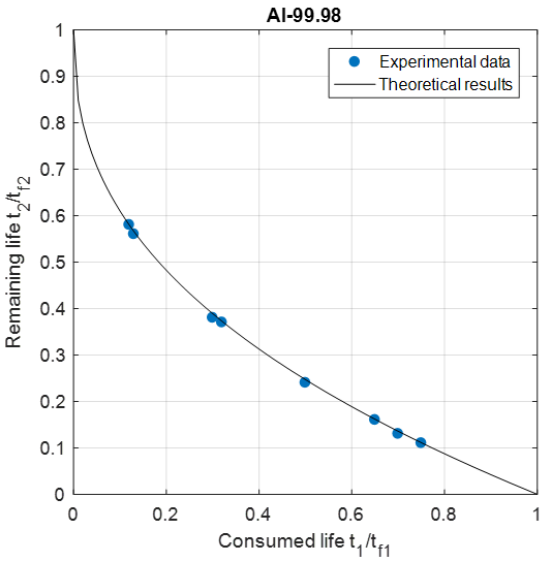

Figure 32. Remaining life t_2/t_{f2} for σ_2=14 MPa versus consumed life t_1/t_{f1} for σ_1=12 at constant temperature T=498 K for material Al-99.98 with fitting parameter p=15.577 MPa

Table 8. Fitting parameter for obtained from test results.

X8CrNiMoNb-16-16	p (MPa)	184.92	185.38	176.27	180.02	178.13	179.53	184.43	184.87
Al-99.98	p (MPa)	15.58	15.53	15.50	15.55	15.49	15.55	15.45	15.55

The fitting parameters given in Table 8 was obtained from the other sets of test results from Table 7. The difference between the largest and smallest fitting parameter was 9.11 MPa for X8CrNiMoNb-16-16 and 0.13 MPa for Al-99.98. The theoretical predictions of the remaining life fraction t_2/t_{f_2} using Eq. 3.1 was made with each of the fitting parameters for X8CrNiMoNb-16-16 (Figure 33) and for Al-99.98 (Figure 34) and compared with the experimental results. As seen from the figures below, all the fitting parameters yielded satisfactory predictions.

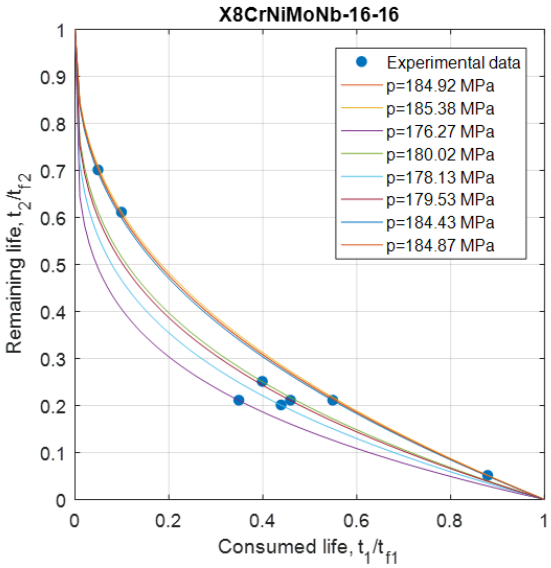

Figure 33. Remaining life t_2/t_{f2} for σ_2=170 MPa versus consumed life t_1/t_{f1} for σ_1=150 at constant temperature T=973 K for material X8CrNiMoNb-16-16 with fitting parameters from Table 8

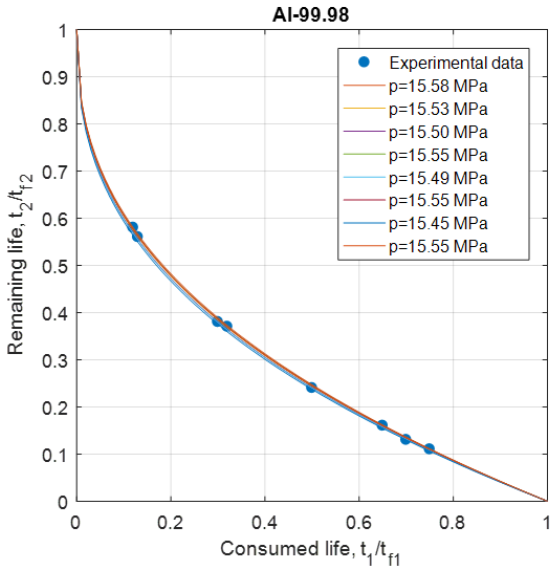

Figure 34. Remaining life t_2/t_{f2} for σ_2=14 MPa versus consumed life t_1/t_{f1} for σ_1=12 at constant temperature T=498 K for material Al-99.98 with fitting parameters from Table 8

3.1.1.1 Fitting parameter versus creep endurance limit

It has been recommended to use the creep endurance limit instead of the fitting parameter [17]. Pavlou's definition [16] of a creep endurance limit as stress low enough to cause no creep damage at all has not been frequently mentioned in creep literature. However, creep endurance or creep resistance is typically defined as a stress level needed to produce a nominal strain for instance 0.1% in a certain time [1]. Instead of regarding creep endurance as a limit for which damage will not occur regardless of temperature and load duration it can be regarded as a strain-limit criterion.

The creep resistance σ_{Rp1} is defined as a stress needed to produce 1% strain in a certain period. For austenitic steel X8CrNiMoNb-16-16 at temperature 973 K (700 °C) the creep resistance for 10 000 h is σ_{Rp1}=64 MPa and σ_{Rp1}=34 MPa for the period 100 000 h [62]. By replacing the fitting parameter in Eq. 3.1 with the creep endurance limit σ_e or as defined above, σ_{Rp1} Palou's failure criteria become:

$$D = \left(\frac{t_1}{t_{f_1}}\right)^{\frac{T_1 \log(\sigma_2/\sigma_{Rp1})}{T_2 \log(\sigma_1/\sigma_{Rp1})}} + \frac{t_2}{t_{f_2}} = 1 \qquad \textit{Eq. 3.3}$$

The theoretical results obtained with Eq. 3.3 for austenitic steel X8CrNiMoNb-16-16 was compared with the experimental results in Table 7. As clearly indicated in Figure 35 the predicted remaining life t_2/t_{f_2} did not agree well with the experimental test data.

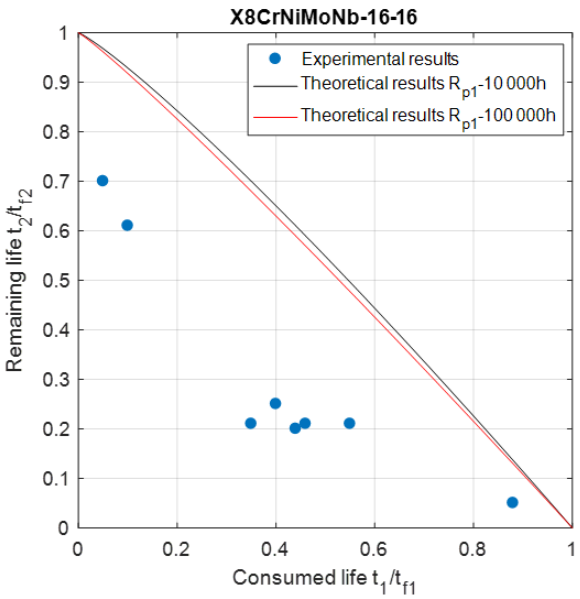

Figure 35. Remaining life t_2/t_{f2} for σ_2=170 MPa versus consumed life t_1/t_{f1} for σ_1=150 at constant temperature T=973 K for material X8-CrNiMoNb-16-16 with creep resistance σ_{Rp1}=64 MPa for 10 000 h and σ_{Rp1}=34 MPa for 100 000 h

The Pavlou model is based on the hypothesis that creep damage can be modelled as isodamage lines. that all intersect in a common point at the failure line 100% damage [16]. The failure criterion in equation Eq. 3.1 can be rearranged to the following form of relationship for a two-step loading:

$$D = 1 - \frac{t_2}{t_{f_2}} = \left(\frac{t_1}{t_{f_1}}\right)^{q_{1,2}} \qquad \textit{Eq. 3.4}$$

With the above relationship, the duration t_1 with the loading condition corresponding to the first loading step σ_1, T_1 should yield the same damage as the loading condition σ_2, T_2 does for the time duration $(1 - t_2/t_{f_2})\, t_{f_2}$ and thus should be on the same damage line. The experimentally obtained time fractions in Table 7 and rupture times given in Table 9 were used for plotting the hold time versus the stress on a log-log plot. The data points corresponding to the same damage state were connected with lines to represent the isodamage lines for the various damage states.

Table 9. Rupture time for material X8CrNiMoNb-16-16 and Al 99.98 [61]

Material	T_1 (K)	σ_1 (MPa)	t_{f_1} (h)	T_2 (K)	σ_2 (MPa)	t_{f_2} (h)
X8CrNiMoNb-16-16	973	150	447	973	170	200
Al 99.98	498	12	17	498	14	6.9

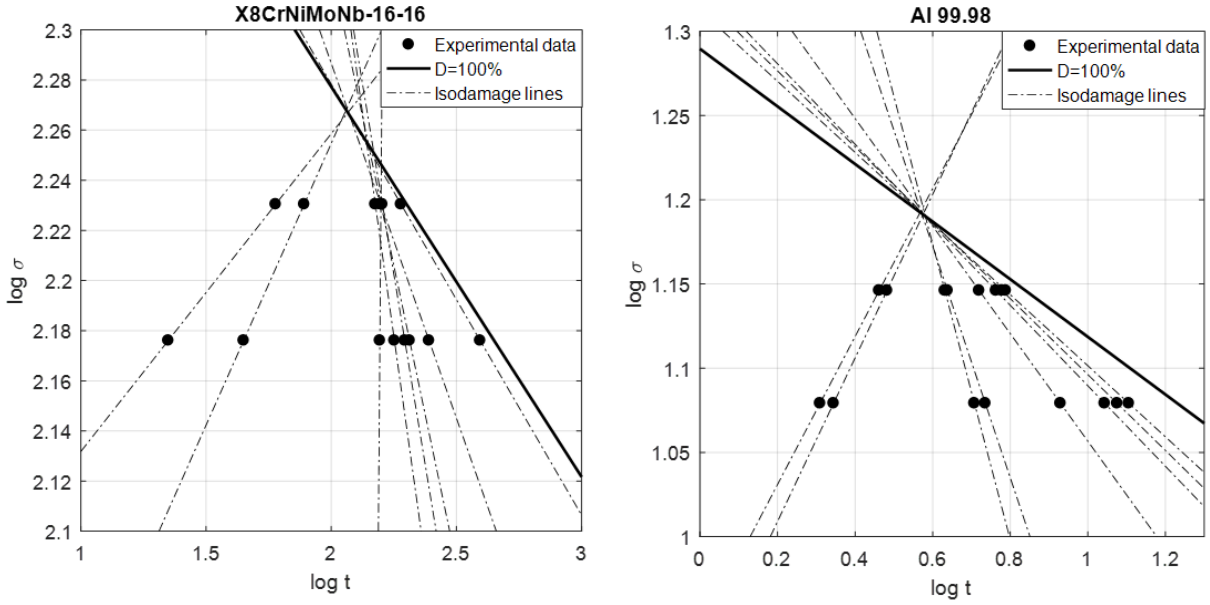

Figure 36. Isodamage lines plotted based on experimental data for material a) X-8-CrNiMoNb-16-16 at T=973 K and b) Al 99.98 at T=498 K

The plots with the isodamage lines and experimental data points are shown in Figure 36. From the figure, it is apparent that all lines intersect approximately at the same point. The intersection between the isodamage lines and the line representing the damage state 100% all corresponds to the values of the fitting parameters as given in Table 8. This indicates that the fitting parameter should be used instead of the creep endurance limit for variable step loading, as was also suggested by Pavlou [16].

3.1.2 Modified Pavlou creep model - normalized curve

The modified version [18] of the Pavlou model bases the damage equation on a rupture curve of normalized stresses versus temperature to represent the 100% damage state instead of using the rupture curve obtained Larson-Miller parameter. To account for temperature the rupture stresses are normalized with Young's modulus at the corresponding temperature.

Since ASME has an extensive collection of material data, rupture data from ASME III Subsection NH [11] for austenitic steel 304SS was used to create a similar rupture curve. Young's modulus at various temperatures for the same material was obtained from ASME section II [63] and linear interpolation and extrapolation was made to obtain values for some of the temperatures. The original rupture data is given in Figure 37 and the normalized rupture data in Figure 38. As seen from the figures, the normalized stress did not transform the data points in such a way so that they could be correlated by a straight line. The modified form of Pavlou's model may have given reasonable remaining life predictions for alloy Sn-3.5Ag-0.5Cu but it is apparent that the method might be limited to certain materials.

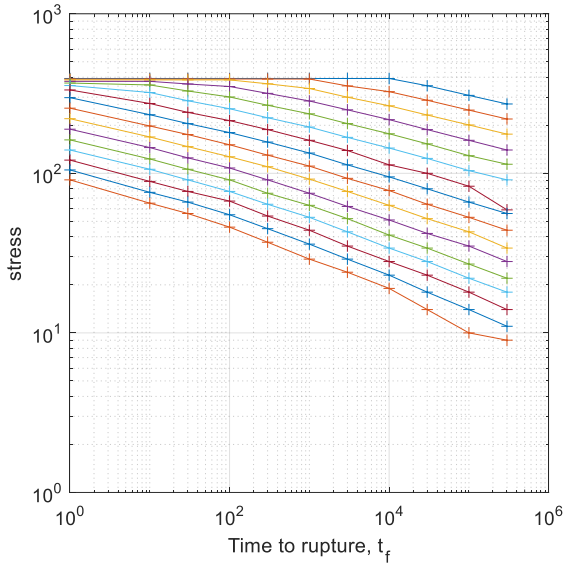

Figure 37. Stress versus rupture time for material 304SS at various temperatures

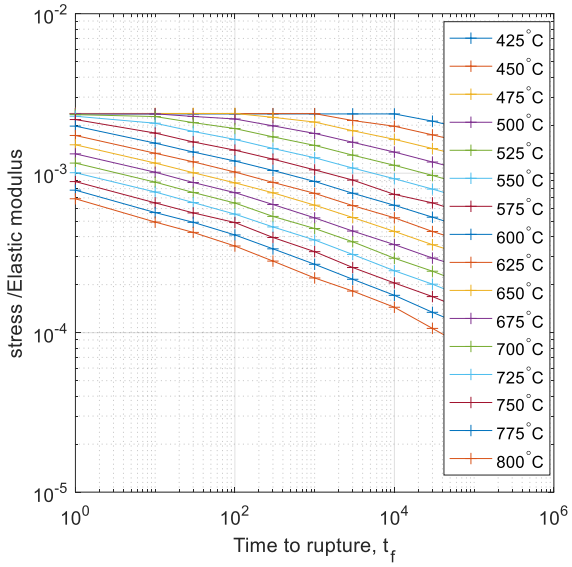

Figure 38. Normalized stress versus rupture time for material 304SS at various temperatures

3.1.3 Sequence effect on load and temperature history

The main difference between the Pavlou creep damage model and the linear time fraction rule is that the Pavlou model considers the sequence effect from both the load and the temperature history.

The behaviour of the Pavlou damage model was investigated by assuming different loading conditions for the austenitic material X8CrNiMoNb-16-16 with the same fitting parameter p=184.916 MPa as were previously obtained from the experimental data. A comparison for a two-step loading were made between using equation Eq. 3.1 and the time fraction rule which for a two-step variable loading can be written:

$$D = \frac{t_1}{t_{f_1}} + \frac{t_2}{t_{f_2}} = 1 \qquad \text{Eq. 3.5}$$

The various loading and temperature conditions were applied in low-high sequences (L-H) and for high-low sequences (H-L).

3.1.3.1 Variable step loading with constant temperature

The sequence effect due to the loading was investigated by keeping the temperature constant at 973 K while various loading conditions were applied in low-to-high loading sequence (L-H) and in high-to-low loading sequence (H-L). The load cases that were used for this are given in Table 10.

Table 10. Two stage loading data of material X8CrNiMoNb-16-16 with constant temperature T=973 K

	L-H		H-L	
	σ_1 (MPa)	σ_2 (MPa)	σ_1 (MPa)	σ_2 (MPa)
Case 1	150	170	170	150
Case 2	110	160	160	110
Case 3	110	130	130	110
Case 4	150	183	183	150
Case 5	190	200	200	190
Case 6	160	190	190	160

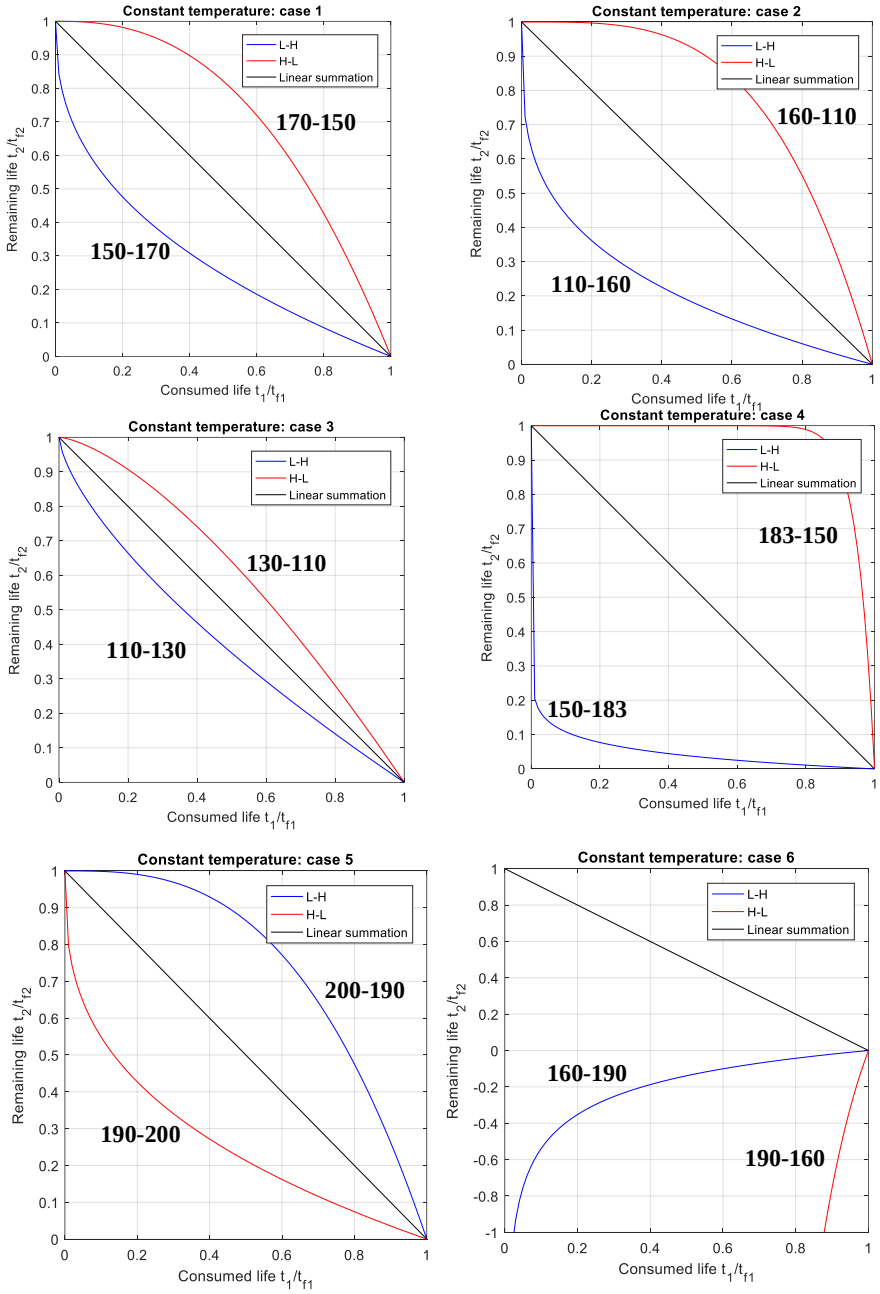

Figure 39. Nonlinear creep damage model versus linear creep damage model for variable step loading

Load case 1-6 from Table 10 are illustrated in Figure 39. To demonstrate the behaviour of the nonlinear model compared to linear summation rule the load cases were plotted in terms of time fractions. Case 1-4 showed that the linear summation (time fraction rule) is non-conservative and overestimates the remaining life for load sequence L-H while it underestimates the remaining life for the H-L sequence.

By comparing load case 2 and 3 it was apparent that with decreasing difference between σ_1 and σ_2 ($\Delta\sigma$) the difference between predictions made with the nonlinear damage model and the linear summation became smaller. This is because the exponent in Eq. 3.1 reaches unity when $\Delta\sigma$ gets closer to zero. It was pointed out in Pavlou's research [16] that for the special case of constant stress and constant temperature, the expression in Eq. 3.1 can be written as Eq. 3.5.

When both stresses σ_1 and σ_2 are larger than the fitting parameter p, as in case 5, the nonlinear model shows an opposite behaviour than to previous load cases. In this case, the remaining life for the L-H sequence become less conservative than the linear summation. Similarly, the sequence H-L indicates a lower remaining life and thus is more conservative than the time fraction rule. This phenomenon could indicate that the model is only valid for stresses below the fitting parameter.

Similar to the Subramanyan fatigue model [43, 44] and as stated in the research by Grell [17], Pavlou's model becomes unstable if the fitting parameter p lies between any of the stresses σ_1 to σ_n as for load case 6. This is due to singularity that occurs when the logarithmic argument in the exponent reaches unity. Another unstable behaviour also occurred for load case 4 which had one stress value very close to the fitting parameter.

3.1.3.2 Variable temperature steps with constant loading

The stress was held at a constant level (σ_1= σ_2) at 150 MPa to see how the nonlinear Pavlou model performed compared to the time fraction rule for various temperature sequences. The different temperature cases that were tested are given in Table 11. The various temperatures were applied in a low-to-high temperature sequence (L-H) and in high-to-low temperature sequence (H-L).

The Pavlou model has in previous research not been tested for variable temperature sequences. Due to lack of experimental data for various temperature steps, the behaviour of the nonlinear creep damage model cannot be verified for the different temperature steps. The purpose of applying various temperature steps was solely to investigate the numerical behaviour of the model.

Table 11. Two step temperature with constant stress σ=150 MPa

	L-H		H-L	
	T_1 (K)	T_2 (K)	T_1 (MPa)	T_2 (MPa)
Case 1	953	973	973	953
Case 2	873	973	973	873
Case 3	873	1073	1073	873
Case 4	773	1073	1073	773

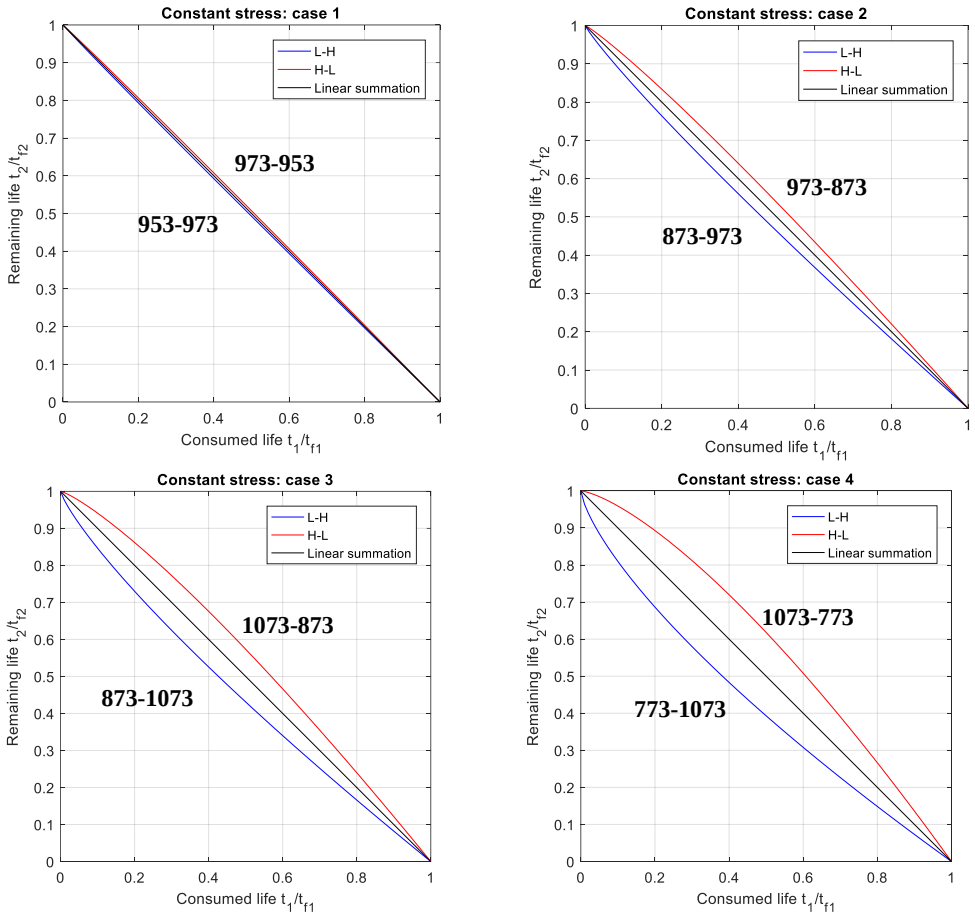

Figure 40. Nonlinear creep damage model versus linear creep damage model with constant stress σ=150 MPa and variable temperature for X8CrNiMoNb-16-16

The nonlinear damage accumulation model did not have the same restrictions for temperature ranges as it did for stresses and there is no risk of singularity since the creep model is not used for temperatures remotely close to zero degrees Kelvin (-273 °C).

What was evident from Figure 40 is that for lager temperature differences between T_1 and T_2 (ΔT) the more the nonlinear creep damage model differs from the linear summation. As for the variable stress sequence, the linear summation predicts a less conservative remaining life for the L-H temperature sequence and a more conservative value for the H-L sequence when compared to the nonlinear model.

By using various temperatures, it was seen from Pavlou's model that the variable temperature sequences did not affect the creep damage as much as variable stresses. This agrees with research by Tiara [40] where it was concluded that temperature cycling does not have as much influence on creep as temperature cycling.

3.1.4 Discussion on further use of the nonlinear creep damage model

It was previously mentioned that various recommendations have been proposed on how to use the nonlinear creep model. According to Pavlou [16] the fitting parameter should be used to consider the transient effect that occurs during cyclic loading. Grell [17] on the other hand recommended the use of the original parameter, the creep endurance limit. The two statements however are ambiguous and would yield opposite results in terms of the remaining life for the L-H/H-L load sequences.

When predictions from the Pavlou model was compared with experimental data for X8CRNiMoNb-16-16 and Al-99.98 the predictions agreed well with the test results. However, when the creep resistance replaced the fitting parameter in Eq. 3.1 the predictions did not yield accurate predictions at all. The plot of isodamage lines that were made with the experimental data is another indicator that the fitting parameter is the better choice to use for creep life prediction under variable step loading conditions. In the unsuccessful attempt that was made to normalize stress rupture data for material 304SS to replace the Larson-Miller parameter expression in the Pavlou model, it appears that the modified version of the model might be limited to certain materials.

From the above-mentioned reasons, it appears that the best way of using the Pavlou model in its original form with the use of a fitting parameter. However, as pointed out by Grell [17], this limits the model to stresses a certain level below the fitting parameter as was seen from load cases 4-6 in the previous subchapter.

None of the research that has been made on the Pavlou creep model discusses the creep-fatigue interaction and how to determine the number of allowable fatigue cycles. Nor has there been any discussions on whether it should be combined with a fatigue model or not. Due to uncertainties of the creep-fatigue interaction, further use of the model will be limited to very few fatigue cycles to reduce the effect from fatigue.

To determine the value of the fitting parameter experimental data from variable step loading is necessary. Since the fitting parameter for X8CrNiMoNb-16-16 had already been obtained, and similar data for other materials were difficult to find, the same material was used for design of the pressure vessel. There has been no comparison with experimental results for variable temperature steps with the Pavlou model in its original form. It is also uncertain if experimental data under different temperatures would have resulted in a different fitting parameter value. Due to these uncertainties, the design temperature in the analysis of remaining life should be at the same temperature as those the model has been validated for (973 K).

The following is a list of assumptions and conditions that was made for further use of the nonlinear damage model for remaining life analysis of a pressure vessel design:

- The austenitic material X8CrNiMoNb-16-16 with fitting parameter p =184.916 MPa is considered for the analysis.
- Temperature conditions for the analysis should be equal to those which the nonlinear model has been validated for.
- The design temperature for the pressure vessel is set to constant at 973 K (700 °C).
- The temperature is high and creep damage is assumed to be the predominant cause of damage
- The pressure vessel is subjected to a two-step variable loading and damage due to fatigue is negligible since fatigue damage is considered small in comparison to creep damage.

3.2 Material data

The material X8CrNiMoNb-16-16 was selected for the pressure vessel design since there were existing experimental creep data for the material from which a fitting parameter could be obtained. The material is an austenitic high-temperature and high strength steel used for elevated temperature applications. The chemical composition of the material is given in Table 12.

Table 12. Chemical composition of X8CrNiMoNb 16-16 in Wt% [62]

	C	Ni	Cr	Mn	P	S	Si	Mo	Nb	Ta
Min	0.04	15.5	15.5				0.3	1.6	10xC	
Max	0.1	17.5	17.5	1.5	0.035	0.015	0.6	2	1.2	1.2

The mechanical properties of the material X8CrNiMoNb-16-16 at room temperature (RT) and at 700 °C are given in Table 1. The properties at 700 °C were obtained by linear extrapolation of the available material data which was obtained from a material database [62]. The density change due to material expansion at elevated temperature was neglected and the material density at 700 °C was assumed to be equal to the density at RT.

Table 13. Properties of X8CrNiMoNb-16-16 at RT and at 700°C [62]

Property	Symbol	Unit	Temperature	
			RT	700 °C
Young's modulus	$\boldsymbol{E}$	GPa	198	141
Yield stress	$\boldsymbol{S_y}$	MPa	≥215	127
Ultimate strength	$\boldsymbol{S_u}$	MPa	530	313
Density	$\boldsymbol{\rho}$	kg/dm3	8	8
Coefficient of thermal expansion	$\boldsymbol{\alpha_t}$	10^-6/(°C)	N/A	18.8[1)]
Poisson's ratio	$\boldsymbol{\nu}$		0.3	0.3

1) Mean coefficient of thermal expansion between RT (20°C) and 700°C

Available material creep data [62] was used for making a Larson-Miller parameter plot for creep resistance, σ_{Rp1} and creep rupture strength, σ_{CRS} so both time-to-rupture and time-to-1% strain could be obtained for different stress levels. Data for $\sigma_{Rp1}$was included since many designs are based on a maximum allowable amount of creep strain, for example 0.1 or 1% during the expected lifetime of a component [64]. As were also previously mentioned the 1% strain limit is also typically used to avoid damage due to lack of ductility. All material data that was used are noted in Appendix A.

3.2.1.1 Accuracy of the Larson-Miller parameter plot

The Larson-Miller parameter, P_{LM} which is given in Eq. 2.2 was used to correlate the temperature and time with stress so the creep data could be described in one fit from which allowable time corresponding to a certain stress and temperature could be obtained. The fit can be optimized by changing the variable C to optimize the correlation coefficient, R^2. However, predictions should only be made within the stress range of the data [65]. Although there are other more complex creep data correlation methods which might be more accurate, the Larson-Miller parameter was chosen because of its relatively easy data correlation.

Fits, both with and without logarithmic scale on the stress axis, were tested. By changing the C-value, four fits each were selected for the creep resistance, σ_{Rp1} and the creep rupture strength, σ_{CRS} based on the R^2-value. The R^2 value can range between 0 and 1 where a value closer to 1 indicates a better

correlation between the data and the fit. The best fits were obtained with a second order polynomial fit and a Gaussian fit. Graphical representations of the obtained fits are presented in Figure 41.

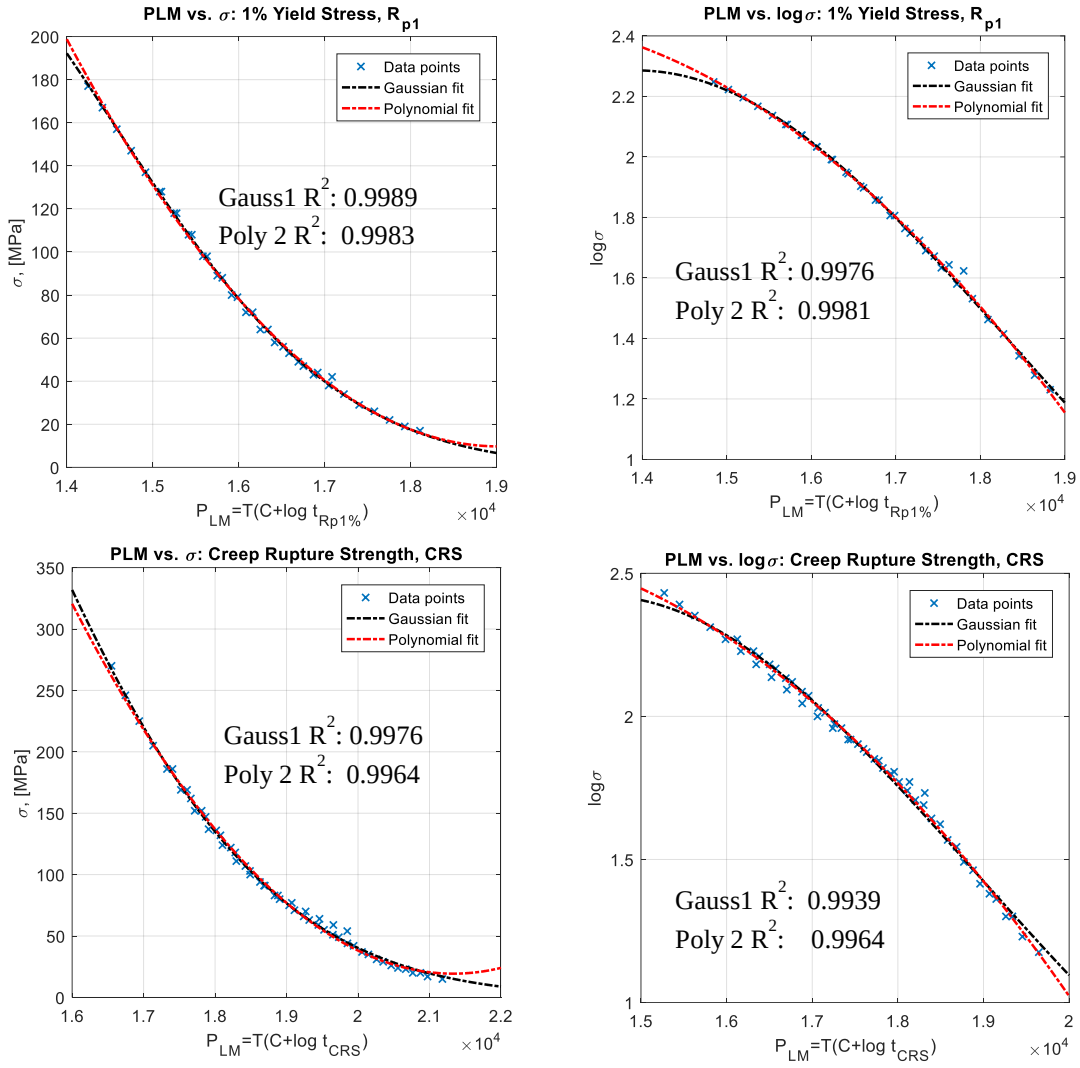

Figure 41. Larson-Miller parameter plots with Gaussian and second order polynomial fits for σ_{Rp1} and σ_{CRS}

The R^2 value alone does not necessarily guarantee if the fit is good and useful for predictions and there are other statistics which can be used for evaluating the appropriateness of the fit such as the sum of squares due to errors (SSE) and the root mean squared error (RMSE) given below [66] [67]:

$$SSE = \sum_{i=1}^{n} w_i (y_i - \hat{y}_i)^2 \qquad \text{Eq. 3.6}$$

$$RMSE = \sqrt{\frac{SSE}{n-m}} \qquad \text{Eq. 3.7}$$

Where w_i are the weights which regulates how much each response value impact the final parameter, y_i is the data points, $\hat{y}_i$ is the value from the fit and $(y_i - \hat{y}_i)$ represent the residuals. In the expression

for RMSE, n repsesent the number of data points and m is the number of parameters in the function. For SSE and RMSE a value closer to zero is an indication that the fit is useful for prediction [67]. MATLAB curve fitting application in was used for obtaining the statistical curve fitting data. The statistics results from each evaluated fit for σ_{Rp1} and σ_{CRS} are given in Table 14 and Table 15.

Table 14. Statistics of CRS-fits from MATLAB

Name	C	Fit type	SSE	R^2	$n-m$	RMSE	
Log CRS	13.9	Poly 2	0.0197	0.9964	51	0.01965	3
Log CRS	13.9	Gauss 1	0.03325	0.9939	51	0.02553	3
CRS	15.4	Poly 2	742	0.9964	51	3.814	3
CRS	15.4	Gauss 1	498.5	0.9976	51	3.126	3

Table 15. Statistics of Rp1-fits from MATLAB

Name	C	Fit type	SSE	R^2	$n-m$	RMSE	m
Log Rp1	13.4	Poly 2	0.005157	0.9981	33	0.0125	3
Log Rp1	13.4	Gauss 1	0.006412	0.9976	33	0.01394	3
Rp1	12.7	Poly 2	115.5	0.9983	33	1.871	3
Rp1	12.7	Gauss 1	73.03	0.9989	33	1.488	3

A bad fit can severely over and underestimate the allowable time duration under a certain stress and temperature. As seen from the tables, the best fits for both creep resistance and creep rupture strength was obtained with the second order polynomial fits when stresses on the ordinate were plotted with a logarithmic scale. These are highlighted in yellow and the equations for the selected fits are given by:

$$log\sigma_{Rp1} = -2.721 \cdot 10^{-8}\, P_{LM}^2 + 6.564 \cdot 10^{-4} P_{LM} - 1.495 \qquad \text{Eq. 3.8}$$

$$log\sigma_{CRS} = -2.901 \cdot 10^{-8}\, P_{LM}^2 + 7.302 \cdot 10^{-4} P_{LM} - 1.98 \qquad \text{Eq. 3.9}$$

$$P_{LM}(\sigma_{Rp1}) = T\left(logt_{f_{Rp1}} + C\right) \qquad \text{Eq. 3.10}$$

$$P_{LM}(\sigma_{CRS}) = T\left(logt_{f_{CRS}} + C\right) \qquad \text{Eq. 3.11}$$

The above equations do not display all decimal places. The equations were solved with respect to the allowable time duration for the corresponding stress and temperature condition using MATLAB where all decimal places in the fits were used. Solving without all decimal places the obtained results can differ from the ones calculated by the software.

The error between the allowable time obtained from the fits and from the data points was calculated using Eq. 3.12 to get an indication of how much the rupture-time and 1%strain-time deviated from the actual values. The time calculated from the fits, the actual time from the creep data and the error between them for some of the extremes are given in Table 16 and Table 17 respectively.

$$\%_{error} = \left| \frac{t_{f\,fit} - t_{f\,data}}{t_{f\,data}} \right| \cdot 100 \qquad \textit{Eq. 3.12}$$

Table 16. Sample points for testing the accuracy of the fitted CRS curves

Temperature $\boldsymbol{T}$ (℃)	**Stress** $\boldsymbol{\sigma_{CRS}}$	**From creep data** $\boldsymbol{t_{CRS_{data}}(h)}$	**Polynomial fit** $\boldsymbol{t_{CRS_{fit}}(h)}$	**Error** (%)
670	111	10 000	14 100	41.00
680	100	10 000	13 841	38.41
670	66	100 000	100 534	0.53
620	103	200 000	199 098	0.45

Table 17. Sample points for testing the accuracy of the fitted Rp1 curves

Temperature $\boldsymbol{T}$ (℃)	**Stress** $\boldsymbol{\sigma_{Rp1}}$	**From creep data** $\boldsymbol{t_{Rp1_{data}}(h)}$	**Polynomial fit** $\boldsymbol{t_{Rp1_{fit}}(h)}$	**Error** (%)
750	42	10 000	6 666	33.34
740	44	10 000	8 464	15.36
610	147	10 000	9990	0.10
620	88	100 000	99 923	0.08

As seen from the tables the chosen fits overestimated and underestimated the time duration for some stress and temperature combinations. However, the average error between all the data points and the corresponding values from the fits were 6.19% for the creep resistance and 13.08% for the creep rupture strength. The residual plots for the fits given in Figure 42 shows the values of the Larson-Miller parameter that produced most error.

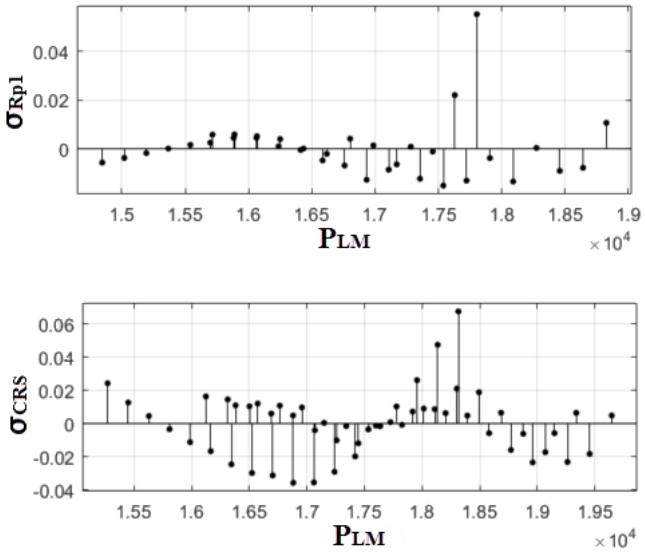

Figure 42. Residual plots for σ_{Rp1} and σ_{CRS}

3.3 Pressure vessel model for creep damage analysis

The difference in remaining life between the nonlinear creep damage model and the linear time fraction rule was evaluated by studying a pressure vessel subjected to variable pressure. The setup of pressure vessel geometry and the stress analysis was made by using ASNSYS Workbench. ANSYS DesignModeler (DM) was used for setting up the geometry and the toolbox static-structural was used for the analysis part. ANSYS DM is a part of ASNSYS Workbench and was chosen for modelling, which allows for easy updating and modification of the geometry. It also allows for geometry parameters in the analysis.

For this study, a simple generic model was considered sufficient. A two-dimensional axisymmetric model was set up for the analysis because it allows for a finer mesh and significantly reduces computation demands. The axisymmetric alternative can be used when the geometry stresses, boundary conditions and material properties are symmetric with respect to an axis. The geometry and the dimensions of the model that was used in the analysis is given in Figure 43. Due to the high-temperature and hence the low yield stress, a small diameter pressure vessel was considered since the wall stress increase as the inner diameter increase.

For the stress evaluation, both a linear-elastic and an elastic-plastic material model was used to investigate how the different analysis methods would affect the remaining life. The elastic-plastic analysis method considers both the applied loading in addition to the deformation characteristics of the pressure vessel and should therefore provide a more accurate assessment than the elastic stress analysis. Ideally, a time-dependent creep analysis should have been used to model the time-dependent material response for obtaining the most accurate results. However, that additional material data which is required for a creep analysis was non-available.

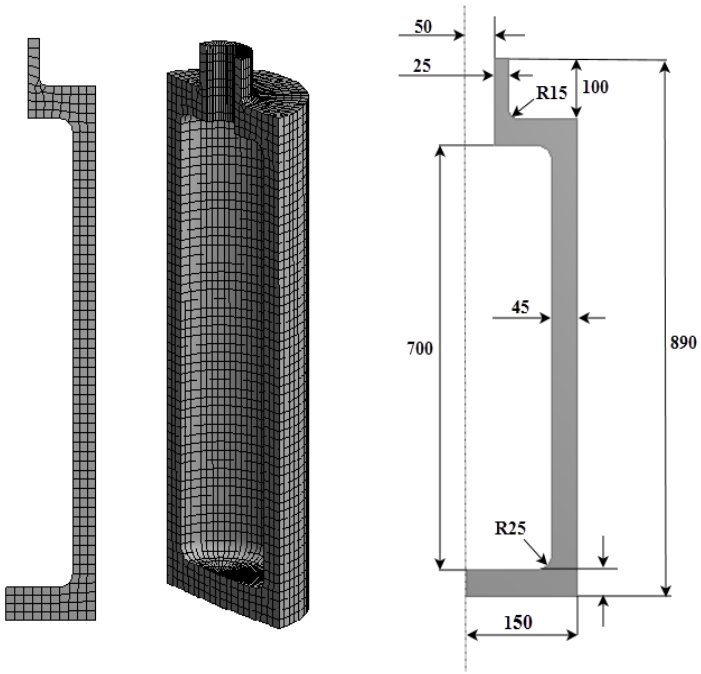

Figure 43. Axisymmetric FEA model and dimensions

3.3.1 Loading conditions

The following assumptions were made for the setup of the analysis:

- The pressure vessel is filled with gas and the weight from the medium is considered negligible
- External pressure atmospheric pressure is considered insignificant compared to internal pressure and can be neglected
- The pressure vessel is very small and the effect of gravity does not have significant effect on the structure. Gravity is therefore not considered in the analysis
- Two-step internal pressure
- The temperature has reached steady-state (700°C) and there are no temperature gradients
- The pressure vessel is free to expand and thermal stresses are non-present

Table 18 contains the loading conditions for the applied two-step loading that were used for both the linear-elastic and elastic-plastic analysis. The applied loads and boundary conditions that were applied to the axisymmetric model are given in Figure 44, where (A) is a displacement constraint at the bottom vertex that was set to zero in y-direction, (B) is the internal pressure and (C) is the nozzle end-cap pressure, $P_n = P_i A_i / A_n$, which was applied to create static equilibrium.

Table 18. Loading conditions for FEA analysis

Load		Magnitude	Magnitude
Internal pressure	P_i	8 MPa	12 MPa
End cap pressure at nozzle	P_n	-6.4 MPa	-9.6 MPa
Temperature S.S	T	700 °C	700 °C

0

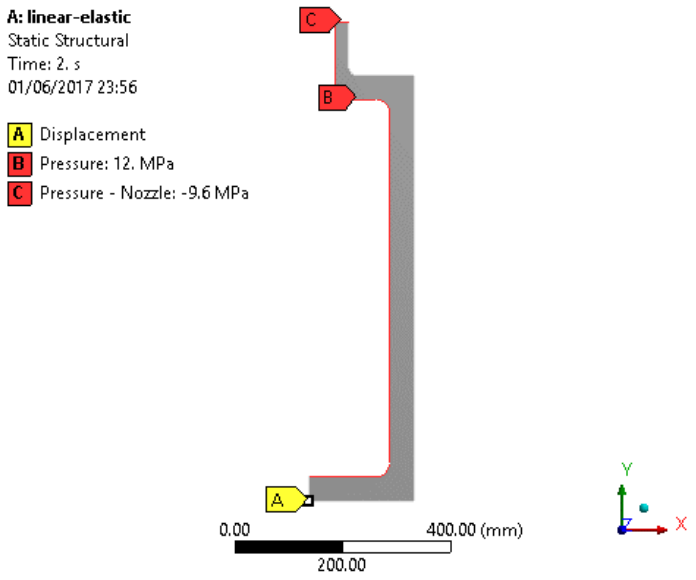

Figure 44. Applied loads and boundary conditions

3.3.2 Engineering data

For the linear-elastic analysis the material properties at 700 °C given in Table 13 were used. The same properties were also used for the elastic-plastic analysis to create a true stress-strain curve that includes temperature dependent hardening behaviour. The true-stress strain curve was made according to ASME VIII-2 Appendix 3D and has a perfect plastic behaviour beyond the limit of the true ultimate stress as can be seen in Figure 45. The true stress-strain data was used as material input to ANSYS for the elastic-plastic analysis.

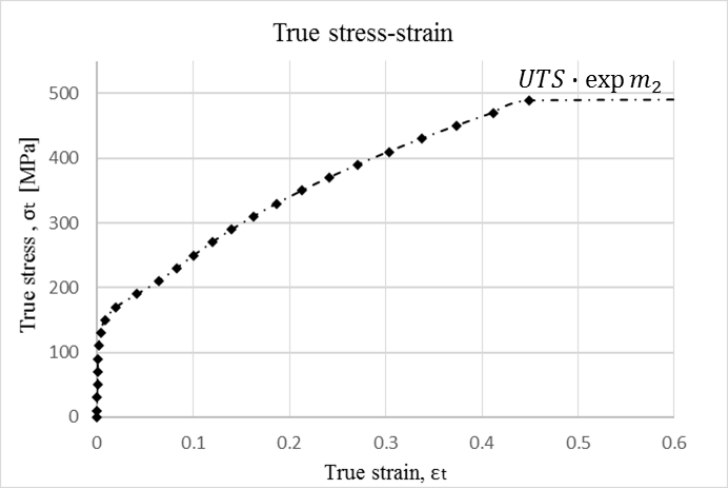

Figure 45. True stress-strain for X8CrNiMoNb-16-16 at T=700 °C

In ANSYS the multilinear kinematic hardening option were used to represent the plastic stress-strain data because it can represent both monotonic and cyclic loading. The multilinear alternative was chosen since gives a more accurate representation of the stress-strain strain relationship compared to the bilinear alternative. For the rate-independent plasticity modelling with the multilinear kinematic hardening, ANSYS uses the von Mises yield criterion to determine when yielding occurs. In the elastic-plastic analysis large deformation effects was also used to more closely approximate the structural behaviour.

3.3.3 Meshing and 2D plane elements

In finite element analysis, meshing is the process of discretising the model into a finite number of elements. The mesh represents a system of algebraic equations which are used to numerically solve the structural system. The quality of the mesh is important for the accuracy and stability of the numerical computation [53]. For 2D plane problems triangular and quadrilateral plane elements as shown in Figure 46 can be used. The 2D elements can represent both planar and axisymmetric solids [53]. Without midside nodes the elements are linear meaning linear interpolation provides the approximate field values between the nodes. When assigning midside nodes to the elements they become quadratic and quadratic interpolation assigns the approximate values. The midside node also allows the element sides to form into quadratic curves and therefore quadratic elements gives a good geometric fit to curved structure boundaries [52].

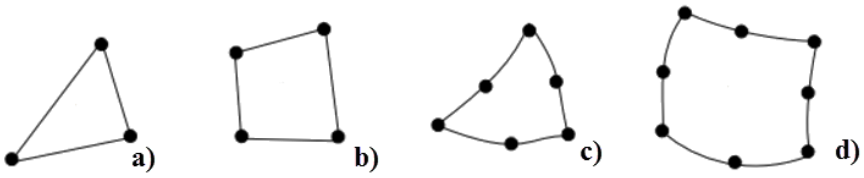

Figure 46. Element types: a) 3 node triangle b) 4 node quadrilateral c) 6 node triangle d) 8 node quadrilateral [68]

3.3.3.1 Mesh analysis and convergence test

A Quadrilateral dominant mesh with midside nodes was selected for the model because of its model flexibility and accuracy. The ANSYS Workbench mesh metric tool was used for controlling shape parameters of the elements to ensure the quality of the generated mesh. It is generally recommended to use a finer mesh to obtain stresses than for displacements because the stress and strain are obtained from derivative of the displacement gradients [52, 69].

A mesh convergence study was made with the linear-elastic material model to determine the necessary element count to describe the stresses. For the convergence test the load case with internal pressure of P_i=12 MPa was used. First the body mesh was established to determine the necessary amount of through thickness elements for the pressure vessel. The maximum von Mises stress through the nozzle and pressure vessel wall were both included in the body mesh convergence test. The locations from where maximum von Mises stresses were obtained are given in Figure 47 and the result from the test is given in Table 19.

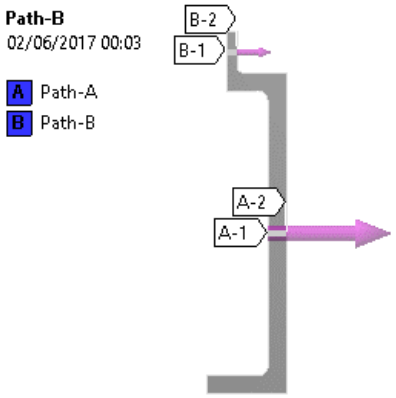

Figure 47. Through wall thickness path for nozzle and the pressure vessel wall

Table 19. Body mesh convergence test

Mesh size [mm]	Cylinder wall σ_{VM} [MPa]	Nozzle wall σ_{VM} [MPa]
25	50.976	46.258
20	50.978	47.141
15	51.225	48.739
10	51.367	49.369
5	51.428	49.698
4	51.438	49.779
3	51.446	49.887

For the body mesh, an element size of 3 mm seemed sufficient. This corresponded to eight elements through the nozzle thickness and fifteen elements through the wall thickness of the pressure vessel.

Once the body mesh had been established, mesh refinement was made at the notches where stress concentrations were present since large stress gradients require a finer mesh. The lowermost notch on the inside of the cylinder had the largest stress and was used for the mesh refinement convergence test.

Table 20. Mesh convergence for notch

Edge Mesh Size [mm]	Total no. of elements	Total no. of nodes	Lower notch σ_{VM} [MPa]
3	5509	17298	121.27
2	5669	17792	121.71
1.5	5826	18283	121.86
1	6095	19130	121.97
0.5	7088	22211	122.01
0.25	8845	27666	122.07
0.2	9660	30203	122.07

Since the body mesh elements were already small there were only slight change of notch stress as the notch elements were refined as seen in Table 20. However, the stress seemed to stabilize for an edge size of 0.5 mm which were therefore chosen for the analysis. This resulted in a total count of 7088 elements and 22211 nodes for the model.

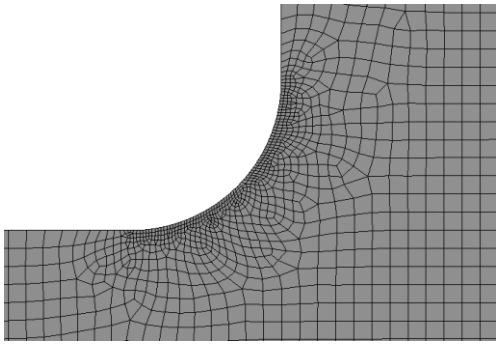

Figure 48. Mesh refinement of lower inside notch with edge mesh 0.5mm

3.3.4 Model verification

The purpose of the analysis is to obtain physical stress quantities and the simulation should represent the physics of the object being modelled. To verify the model setup and boundary conditions and to check for numerical error, the stresses from the linear-elastic numerical analysis were compared to stresses obtained with analytical calculations. Since stresses are triaxial in thick walled cylinders, Lamé equations were used to obtain the analytical solutions. The same through thickness locations in Figure 47 that was used for the mesh convergence test was also used to obtain the numerical solutions for the numerical-analytical stress comparison. The locations for the comparison were chosen to avoid the effect from stress concentrations.

The numerical and analytical comparison of through thickness hoop stress, radial stress, axial stress and von Mises stress are plotted in Figure 49. For the pressure vessel wall (path A1-A2) there was

almost no difference between the analytical and numerical solutions but for the nozzle (path B1-B2) the two methods did not give equal results because of stress concentrations too close to the path. With the result from the comparison it was assumed that the set up for the numerical model had been done correctly.

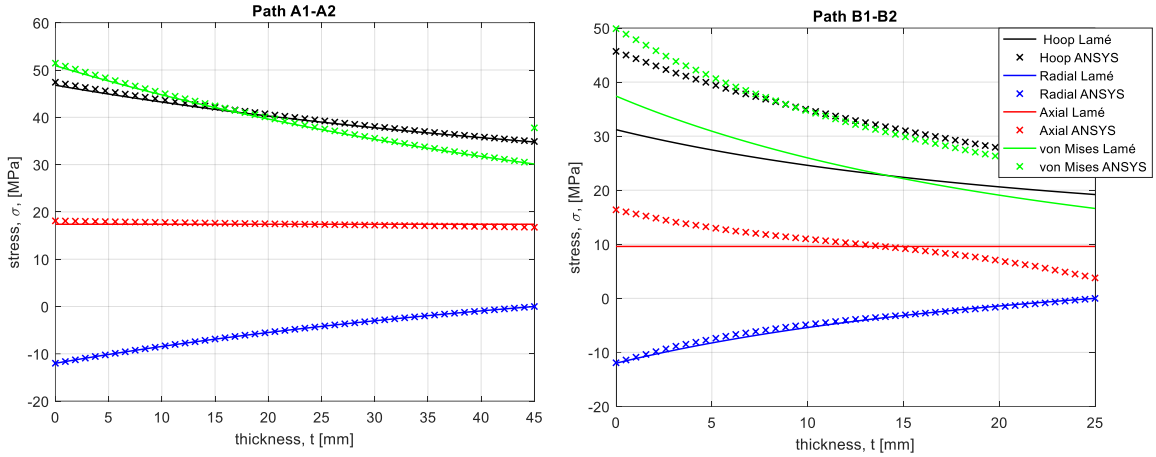

Figure 49. Comparison of ANSYS stresses and stresses calculated with Lamé equations

3.4 Protection against plastic collapse and local failure

To obtain a realistic example for the numerical studies, the pressure vessel was checked for global stability and ductility failures according to the numerical elastic-plastic analysis procedure in ASME VIII-2 [59]. It should however be mentioned that this procedure is not approved by ASME for design in the creep range when materials are governed by time-dependent properties [59] as mentioned in the Chapter 2.8.1.3.

The elastic-plastic procedure requires the use of the same true stress-strain curve as previously presented. When checking the global stability of a component there are two acceptance criteria in ASME. A global criterion, which concerns the protection against global collapse and a service criteria to check for limits such as defection that may cause operational concerns. Since no service limits had been specified for the pressure vessel only the global collapse criteria was considered.

For protection against global collapse ASME uses the concept of Load and Resistance Factor Design (LRFD) instead of determining the actual collapse load which is defined as the load that causes overall structural instability to the component. If the solution converges for the applied factored loading condition the component is considered stable. LRFD is also used to ensure that the design is safe from local failure. The maximum loading condition in Table 18 was considered for the global and local failure check. Due to the factored loads the effect of gravity could no longer be neglected and standard earth gravity 9.806.6 m/s² was considered for the dead weight of the pressure vessel. The factored loads that were used to check for global and local failure are given by Eq. 3.13 and Eq. 3.14 respectively.

$$2.4(P + P_S + D) \qquad \textit{Eq. 3.13}$$

$$1.7(P + P_S + D) \qquad \textit{Eq. 3.14}$$

Where P represents the design pressure, P_S the static head from liquid or bulk materials, which were neglected due to the previous assumption that pressure vessel is filled with gas, and D is the dead

weight of the pressure vessel. Figure 50 shows the applied loads and boundary conditions that were considered for the global and local failure check.

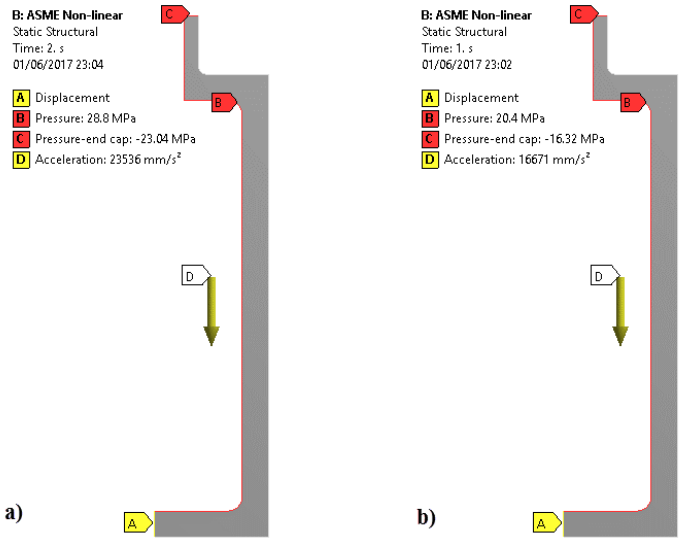

Figure 50. Applied loads and constraints for analysis of a) global collapse and b) local failure.

The solution converged in the elastic-plastic analysis under the applied factored loads in Eq. 3.13 and thus the pressure vessel was considered stable and protected against plastic collapse.

For protection against local failure all points of the component were checked with the following strain requirement

$$\varepsilon_{peq} + \varepsilon_{cf} \leq \varepsilon_L \qquad \textit{Eq. 3.15}$$

$$\varepsilon_L = \varepsilon_{Lu} \cdot exp\left[-\left(\frac{\alpha_{sl}}{1+m_2}\right)\left(\left\{\frac{\sigma_1+\sigma_2+\sigma_3}{3\sigma_{VM}}\right\}-\frac{1}{3}\right)\right] \qquad \textit{Eq. 3.16}$$

Where ε_{peq} is the equivalent plastic strain, ε_{cf} is the forming strain which is assumed to be zero and the ε_L is the triaxial limiting strain. The quantities ε_{Lu}=m_2=0.4457, α_{sl}=0.6 were obtained from ASME VIII-2 Table 5.7 [59]. With the forming strain being zero the strain requirement $\varepsilon_{peq}/\varepsilon_L \leq 1$ were evaluated for all points in the model. With the factored load from Eq. 3.14 a maximum ratio of $\varepsilon_{peq}/\varepsilon_L$=0.00747 was obtained from the analysis and the pressure vessel had fulfilled the local failure requirements.

3.5 Equivalent stresses for remaining creep life evaluation

Stresses for the creep life evaluations were obtained from both the linear-elastic and the elastic plastic stress analysis. To correlate the triaxial stress state to the uniaxial creep data both the classical equivalent stress criterions, the mixed criterion with α and β constants and Huddleston's criterion with universal constants were used. These are given in Table 21 with their corresponding material parameters. Stresses were obtained from the analysis by defining user defined equations in ANSYS.

The maximum stress occurred at the lowermost notch on the inside of the pressure vessel. This was also the point that was evaluated with the different stress criterions. The stress distribution from the different criterions obtained with the elastic analysis is given in Figure 51 and the stress distributions for the same stress criterions but obtained with the elastic-plastic analysis are given in Figure 52.

Table 21. Equivalent stresses for creep life evaluation

Stress type	**Symbol**	**Material parameter**	**Equation No.**
Von Mises	σ_{VM}	N/A	Eq. 2.14
Tresca	σ_{TR}	N/A	Eq. 2.15
Maximum principal Stress	σ_{MPS}	N/A	Eq. 2.16
Mixed criteria	σ_{eq}	α=0.8,	Eq. 2.17
Mixed criteria	σ_{eq}	α=0.9,	Eq. 2.17
Huddleston	σ_{HUD}	a=1, b=0.24 (universal constants)	Eq. 2.25

For the mixed criteria in Eq. 2.17, it was assumed that material X8CrNiMoNb 16-16 had an α value in the range of 0.8 and 0.9 and β about 0.2 to 0.1. This is typically the case for materials such as austenitic stainless steel and nickel based superalloys [1]. For Huddleston's equivalent stress the universal constants for a and b for austenitic stainless steel were used. In addition to the above mentioned equivalent stress criterions the mixed criterion proposed by the Russian research institute CKTI and the principal facet stress were also previously mentioned in Chapter 2.6. These were however not considered for the analysis since the mixed CKTI criterion requires the Norton exponent which has not been obtained for the selected material and the Principal facet stress cannot be used directly in engineering calculations without normalization.

The stresses obtained from the linear-elastic and elastic-plastic analysis are given in Table 22 and Table 23 respectively. The corresponding monotonic stress creep-rupture time t_{CRS} and the time-to-1% strain t_{Rp1} are also given in the tables. These were obtained from the polynomial Larson-Miller parameter fits given in Eq. 3.8 and Eq. 3.9 (chapter 3.2.1.1).

Table 22. Stress types from linear-elastic analysis from internal pressure P=12 MPa

Stress type	Stress value [MPa]	Allowable time $t_{f_{CRS}}$ [h]	Allowable time $t_{f_{Rp1}}$ [h]
Von Mises, σ_{VM}	122.01	2665	669
Tresca, σ_{TR}	138.22	1567	347
Maximum principal Stress, σ_{MPS}	126.24	2311	562
Mixed criteria, σ_{eq}, α=0.8	122.84	2591	646
Mixed criteria, σ_{eq}, α=0.9	122.43	2627	657
Huddleston, σ_{HUD}	125.76	2349	573

Table 23. Stress types from linear elastic-analysis with internal pressure P=8 MPa

Stress type	Stress value [MPa]	Allowable time $t_{f_{CRS}}$ [h]	Allowable time $t_{f_{Rp1}}$ [h]
Von Mises, σ_{VM}	81.34	12690	4289
Tresca, σ_{TR}	92.147	8035	2511
Maximum principal Stress, σ_{MPS}	84.162	11220	3715
Mixed criteria, σ_{eq}, α=0.8	81.896	12383	4169
Mixed criteria, σ_{eq}, α=0.9	81.618	12536	4229
Huddleston, σ_{HUD}	83.843	11376	3776

Table 24. Stress types from elastic-plastic analysis with internal pressure P=12 MPa

Stress type	Stress value [MPa]	Allowable time $t_{f_{CRS}}$ [h]	Allowable time $t_{f_{Rp1}}$ [h]
Von Mises, σ_{VM}	114.25	3487	927
Tresca, σ_{TR}	130.00	2042	482
Maximum principal Stress, σ_{MPS}	119.47	2907	743
Mixed criteria, σ_{eq}, α=0.8	115.00	3396	898
Mixed criteria, σ_{eq}, α=0.9	114.62	3442	913
Huddleston, σ_{HUD}	117.94	3065	793

Table 25. Stress types from elastic-plastic analysis with internal pressure P=8 MPa

Stress type	Stress value [MPa]	Allowable time $t_{f_{CRS}}$ [h]	Allowable time $t_{f_{Rp1}}$ [h]
Von Mises, σ_{VM}	81.281	12724	4302
Tresca, σ_{TR}	92.082	8057	2519
Maximum principal Stress, σ_{MPS}	84.098	11251	3727
Mixed criteria, σ_{eq}, α=0.8	81.836	12416	4182
Mixed criteria, σ_{eq}, α=0.9	81.559	12568	4241
Huddleston, σ_{HUD}	83.782	11406	3787

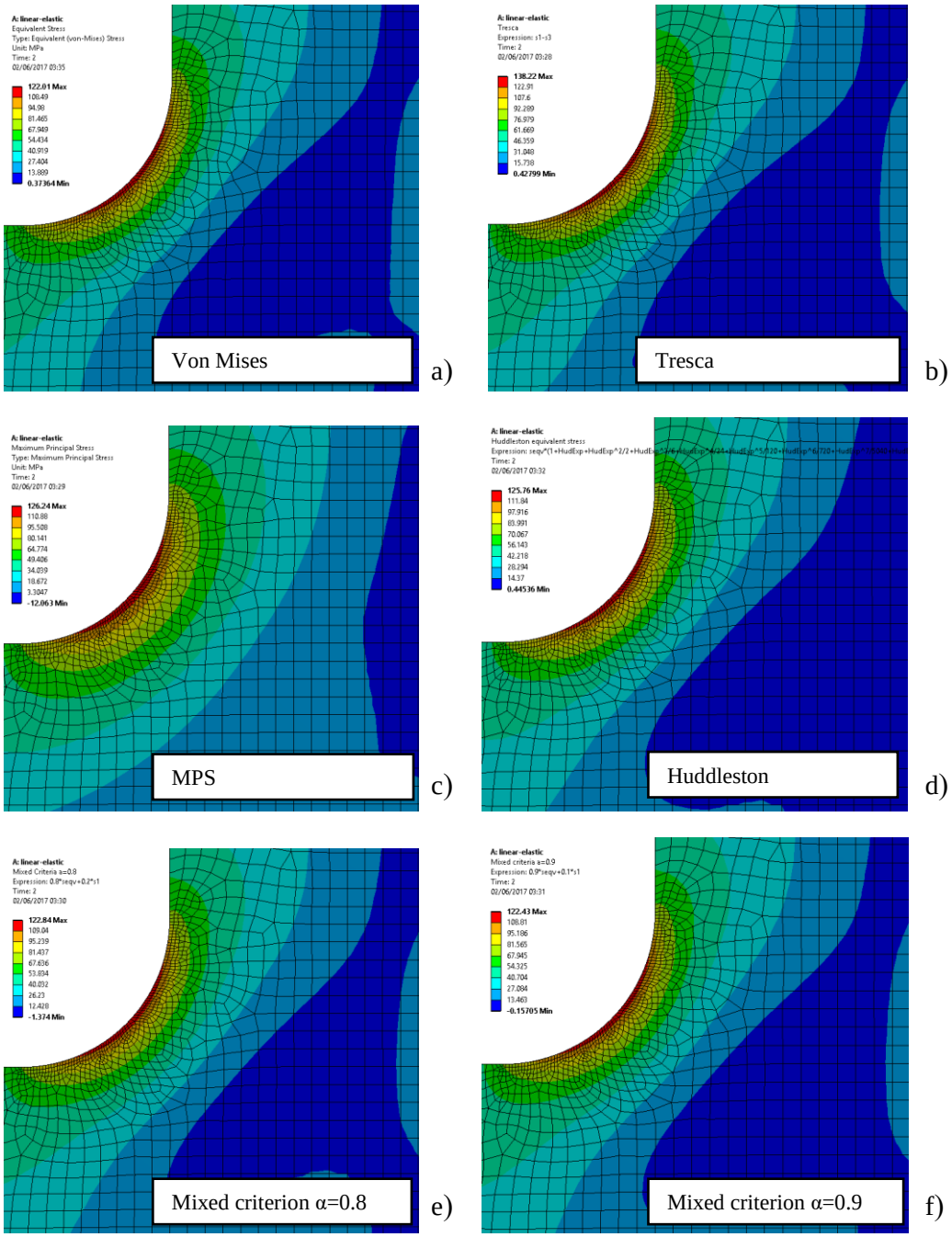

Figure 51. Stress distribution at the notch obtained with linear-elastic analysis with internal pressure P=12 MPa for a) von Mises b) Tresca c) Maximum principal stress d) Huddleston's stress e) Mixed criteria with α=0.8 and f) Mixed criteria with α=0.9

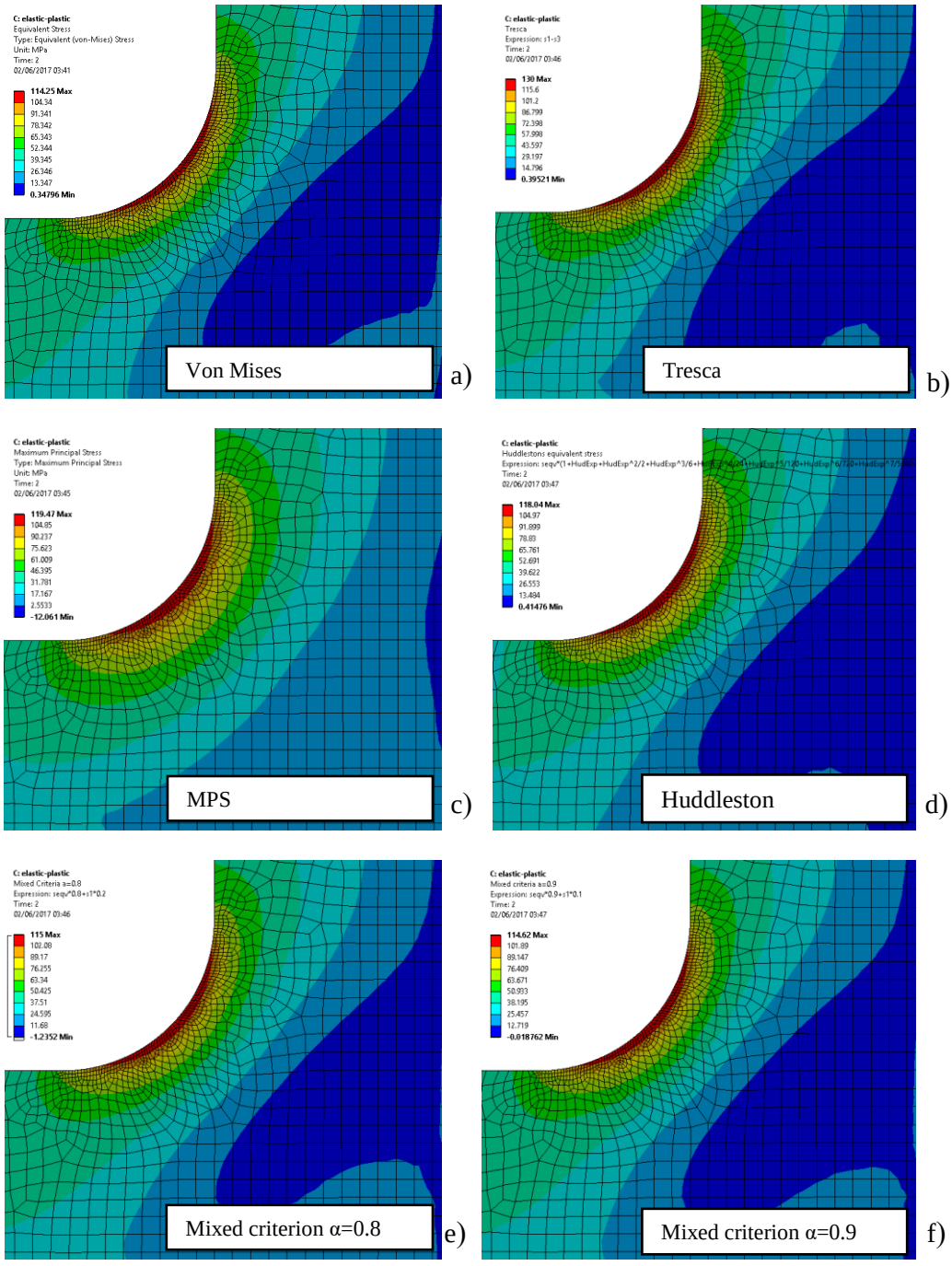

Figure 52. Stress distribution at the notch obtained with elastic-plastic analysis with internal pressure P=12 MPa for a) von Mises b) Tresca c) Maximum principal stress d) Huddleston's stress e) Mixed criteria with α=0.8 and f) Mixed criteria with α=0.9

Almost all stress criteria gave similar stress magnitudes. The maximum von Mises and maximum principal stress at the notch had similar maximum values, therefore the mixed criteria with both α=0.8 and α=0.9 were almost equal. Huddleston stress criteria, which is considered a modified version of von Mises gave stress values of slightly higher magnitude than von Mises. Had it been compressive strength it would most likely had given a lower stress since it predicts higher damage for tensile than compressive stresses. The Tresca criterion which is known to be more conservative than von Mises criteria distinguished itself from the others and gave higher stress. For the lower pressure P_i=8 MPa the difference between the stresses obtained from the linear-elastic and elastic-plastic material model were trivial because no plastic strain was present. However, for the higher loading step P_i=12 MPa the stresses from the elastic-plastic material model were lower than for the linear-elastic model since plasticity and strain hardening was considered. The linear-elastic model assumes stress and strain are proportional up to the materials yield point and therefore predicts higher stresses.

For the remaining life predictions, it was assumed that the time fraction at the first time-step, t_1/t_{1_f} were 0.3 for both the low-to-high and high-to low load sequences. The remaining life t_2 were calculated with the following equations for the Pavlou model and the time fraction rule:

$$t_{2_P} = \left(1 - \left(\frac{t_1}{t_{f_1}}\right)^{\frac{T_1 \log(\sigma_2/p)}{T_2 \log(\sigma_1/p)}}\right) t_{f_2} \qquad \textit{Eq. 3.17}$$

$$t_{2_{TFR}} = \left(1 - \frac{t_1}{t_{f_1}}\right) t_{f_2} \qquad \textit{Eq. 3.18}$$

The percental difference in remaining life between the two models was calculates by:

$$\Delta t_2\% = \frac{t_{2_P} - t_{2_{TFR}}}{t_{2_P}} \cdot 100\% \qquad \textit{Eq. 3.19}$$

4 RESULT

The following results for the predicted remaining life t_2 were computed with Eq. 3.17 for the nonlinear Pavlou creep damage model t_{2P} and with Eq. 3.18 for the time fraction rule $t_{2_{TFR}}$. Both the time difference Δt_2 and percental difference between the models are also given in the in the results.

4.1 Remaining creep rupture life of pressure vessel

Table 26. Remaining creep rupture life from linear-elastic analysis for L-H type of loading

Stress type	$\Delta\sigma$ [MPa]	Remaining Creep Rupture life, $t_{2_{CRS}}$		$\Delta t_{2_{CRS}}$ [h]	$\Delta t_{2_{CRS}}$%
		Nonlinear Pavlou model [h]	Time fraction rule [h]		
Von Mises, σ_{VM}	40.7	1216	1865	-649	-53.4
Tresca, σ_{TR}	46.1	619	1097	-477	-77.1
Maximum principal Stress, σ_{MPS}	42.1	1022	1618	-596	-58.3
Mixed criteria, σ_{eq}, α=0.8	40.9	1176	1814	-638	-54.3
Mixed criteria, σ_{eq}, α=0.9	40.8	1196	1839	-644	-53.8
Huddleston, σ_{HUD}	41.9	1043	1644	-601	-57.7

Table 27. Remaining creep rupture life from linear-elastic analysis for H-L type of loading

Stress type	$\Delta\sigma$ [MPa]	Remaining Creep Rupture life, $t_{2_{CRS}}$		$\Delta t_{2_{CRS}}$ [h]	$\Delta t_{2_{CRS}}$%
		Nonlinear Pavlou model [h]	Time fraction rule [h]		
Von Mises, σ_{VM}	40.7	11514	8883	2630	22.8
Tresca, σ_{TR}	46.1	7585	5625	1960	25.8
Maximum principal Stress, σ_{MPS}	42.1	10283	7854	2429	23.6
Mixed criteria, σ_{eq}, α=0.8	40.9	11257	8668	2589	23.0
Mixed criteria, σ_{eq}, α=0.9	40.8	11385	8775	2610	22.9
Huddleston, σ_{HUD}	41.9	10414	7963	2451	23.5

Table 28. Remaining creep rupture life from plastic analysis for L-H type of loading

Stress type	$\Delta\sigma$ [MPa]	Remaining Creep Rupture life, $t_{2_{CRS}}$		$\Delta t_{2_{CRS}}$ [h]	$\Delta t_{2_{CRS}}$%
		Nonlinear Pavlou model [h]	Time fraction rule [h]		
Von Mises, σ_{VM}	33.0	1765	2441	-676	-38.3
Tresca, σ_{TR}	37.9	931	1429	-499	-53.6
Maximum principal Stress, σ_{MPS}	35.4	1416	2035	-619	-43.7
Mixed criteria, σ_{eq}, α=0.8	33.2	1712	2377	-665	-38.8
Mixed criteria, σ_{eq}, α=0.9	33.1	1739	2409	-671	-38.6
Huddleston, σ_{HUD}	34.2	1518	2145	-627	-41.3

Table 29. Remaining creep rupture life from plastic analysis for H-L type of loading

Stress type	$\Delta\sigma$ [MPa]	Remaining Creep Rupture life, $t_{2_{CRS}}$		$\Delta t_{2_{CRS}}$ [h]	$\Delta t_{2_{CRS}}$%
		Nonlinear Pavlou model [h]	Time fraction rule [h]		
Von Mises, σ_{VM}	33.0	11094	8906	2188	19.7
Tresca, σ_{TR}	37.9	7313	5640	1673	22.9
Maximum principal Stress, σ_{MPS}	35.4	9969	7876	2093	21.0
Mixed criteria, σ_{eq}, α=0.8	33.2	10844	8691	2152	19.8
Mixed criteria, σ_{eq}, α=0.9	33.1	10967	8798	2170	19.8
Huddleston, σ_{HUD}	34.2	10036	7984	2052	20.4

4.2 Remaining life to 1% strain of pressure vessel

Table 30. Remaining life until 1% strain from linear-elastic analysis for L-H type of loading

Stress type	$\Delta\sigma$ [MPa]	Remaining Creep Rupture life, $t_{2_{Rp1}}$		$\Delta t_{2_{Rp1}}$ [h]	$\Delta t_{2_{Rp1}}$%
		Nonlinear Pavlou model [h]	Time fraction rule [h]		
Von Mises, σ_{VM}	40.7	305	468	-163	-53.4
Tresca, σ_{TR}	46.1	137	243	-106	-77.1
Maximum principal Stress, σ_{MPS}	42.1	248	393	-145	-58.3
Mixed criteria, σ_{eq}, α=0.8	40.9	293	452	-159	-54.3
Mixed criteria, σ_{eq}, α=0.9	40.8	299	460	-161	-53.8
Huddleston, σ_{HUD}	41.9	254	401	-147	-57.7

Table 31. Remaining life until 1% strain from linear-elastic analysis for H-L type of loading

Stress type	$\Delta\sigma$ [MPa]	Remaining Creep Rupture life, $t_{2_{Rp1}}$		$\Delta t_{2_{Rp1}}$ [h]	$\Delta t_{2_{Rp1}}$%
		Nonlinear Pavlou model [h]	Time fraction rule [h]		
Von Mises, σ_{VM}	40.7	3892	3003	889	22.8
Tresca, σ_{TR}	46.1	2370	1758	612	25.8
Maximum principal Stress, σ_{MPS}	42.1	3405	2601	804	23.6
Mixed criteria, σ_{eq}, α=0.8	40.9	3790	2918	871	23.0
Mixed criteria, σ_{eq}, α=0.9	40.8	3840	2960	880	22.9
Huddleston, σ_{HUD}	41.9	3456	2643	813	23.5

Table 32. Remaining life until 1% strain from elastic-plastic analysis for L-H type of loading

Stress type	$\Delta\sigma$ [MPa]	Remaining Creep life, $t_{2_{Rp1}}$		$\Delta t_{2_{Rp1}}$ [h]	$\Delta t_{2_{Rp1}}$%
		Nonlinear Pavlou model [h]	Time fraction rule [h]		
Von Mises, σ_{VM}	33.0	309	464	-154	-49.8
Tresca, σ_{TR}	37.9	220	337	-118	-53.6
Maximum principal Stress, σ_{MPS}	35.4	362	520	-158	-43.7
Mixed criteria, σ_{eq}, α=0.8	33.2	453	629	-176	-38.8
Mixed criteria, σ_{eq}, α=0.9	33.1	461	639	-178	-38.6
Huddleston, σ_{HUD}	34.2	393	555	-162	-41.3

Table 33. Remaining life until 1% strain from elastic-plastic analysis for H-L type of loading

Stress type	$\Delta\sigma$ [MPa]	Remaining Creep life, $t_{2_{Rp1}}$		$\Delta t_{2_{Rp1}}$ [h]	$\Delta t_{2_{Rp1}}$%
		Nonlinear Pavlou model [h]	Time fraction rule [h]		
Von Mises, σ_{VM}	33.0	3752	3012	740	19.7
Tresca, σ_{TR}	37.9	2286	1763	523	22.9
MPS	35.4	3302	2609	693	21.0
Mixed criteria, σ_{eq}, α=0.8	33.2	3652	2927	725	19.8
Mixed criteria, σ_{eq}, α=0.9	33.1	3701	2969	732	19.8
Huddleston, σ_{HUD}	34.2	3332	2651	681	20.4

5 DISCUSSION

The remaining life predictions obtained with the two damage models gave very different results. The nonlinear Pavlou damage model predicted shorter remaining life for the second load step t_2 for low-to-high loading sequences and longer remaining life for the high-to-low loading sequences when compared to the life fraction rule.

The percental differences $\Delta t_{2_{CRS}}\%$ and $\Delta t_{2_{Rp1}}\%$ for the rupture life and for the remaining life to 1% strain were equal for the same stresses, which shows that the allowable time $t_{f_{CRS}}$ and $t_{f_{Rp1}}$ for the corresponding stress and temperature level has no effect on the discrepancies between the remaining life predictions of the two models. The difference between the predictions were solely dependent on the stress difference between the first and second load step $\Delta\sigma$ and the larger difference in stress, the larger the difference between the two models remaining life predictions. At most, the time faction rule predicted a remaining life that was 77.1% longer compared to the prediction made with nonlinear model. Due to the short allowable time $t_{f_{CRS}}$ and $t_{f_{Rp1}}$, this difference did not seem very significant in terms of hours. However, the time difference from the predictions would seem much more significant for longer allowable time durations.

The allowable time $t_{f_{CRS}}$ and $t_{f_{Rp1}}$ corresponding to the various stresses at temperature at 700 °C were obtained from fitted curves made from data points for creep rupture strength (σ_{CRS}) and 1% Yield stress (σ_{Rp1}). The average error between the fitted curves and the actual data was 13.08% for the creep rupture strength and 6.19% for the creep resistance. Although this error manifests itself for the remaining life it does not affect the percental difference between the predictions of the two models, since that was only dependent on the stress difference between the load steps.

The short rupture life of the pressure vessel was due to the high-temperature and stresses. No significant loss of ductility due to long-term operation at elevated temperature is therefore to be expected and a ductile rupture behaviour can be assumed. Since the von Mises stress is the controlling parameter for ductile ruptures, the von Mises stress criterion, Huddleston criterion which can be considered a modified form of the Mises, or one of the mixed criterions most likely is the best to correlate the multiaxial rupture to the uniaxial rupture data.

The strain hardening response in the elastic-plastic analysis caused lower stresses than for the corresponding linear-elastic analysis for the loading step with internal pressure P_i=12 MPa. Strain hardening also occur in transient creep and the elastic-plastic analysis may have more resemblance to an actual creep analysis out of the two material models that were used, since it considers plasticity. However, since none of the used material models incorporates time in the analysis, none of them can therefore predict actual stress and strain distribution in the creep range since they are time dependent. For stress concentrations, like the ones present in the considered notch, time dependent stress relaxation and stress redistribution would occur, which can only be taken into consideration with a time-dependent material model. Unfortunately, no such analysis could be made since no experimental creep data (which is necessary for obtaining temperature dependent constants for the material model) were applicable for the selected pressure vessel material. Even if the essential material constants could have been obtained to describe the material response for this creep analysis, the model still would have been needed to be validated, both for the material and loading history to provide useful predictions, since various material models give very different predictions even for the same loading history. Most likely this would have required additional creep tests.

Potential notch weakening or notch strengthening behaviour could not be obtained for the material and has therefore not been considered for the remaining life of the pressure vessel.

To use a creep damage model for design requires a certain degree of conservatism to be included in the life assessment. The time fraction rule is known to be unconservative without the corrections used in guidelines and codes. More useful information could have been gained by comparing the nonlinear model to for instance ASME-NH which is known to be conservative. This could have given an indication on how much adjustment in form of engineering corrections that may be necessary for the nonlinear model to always provide conservative predictions. Such a correction could for example have been to make an adjustment of the fitting parameter. A comparison with ASME-NH was however not possible to make in this study since the nonlinear model requires variable step-load experimental data to obtain the fitting parameter. Such data were unfortunately not available for any of the permitted ASME-NH materials.

Another aspect of the ASME-NH procedure to consider for the nonlinear creep damage assessment is use of the elastic analysis procedure to approximate the time-dependent stress and strain distributions. Such an elastic procedure would make the nonlinear model more convenient to use in design applications because the abovementioned difficulties associated with inelastic time-dependent analysis would be avoided.

The need of necessary material data has been mentioned many times throughout this study. Other more sophisticated models than the time fraction rule has previously been proposed for predicting creep damage but none of them has yet gained universal acceptance like the time fraction rule. One reason for this is the additional material creep data that is necessary to obtain material specific constants for the creep models. Most creep and rupture data are obtained from constant load and constant temperature creep tests and it is typically undesirable to use creep models that require additional material testing since this entails extra costs in addition to being time consuming. The fitting parameter in the Pavlou model seems to be a crucial factor to obtain accurate predictions. The disadvantage of the fitting parameter is however that it can only be obtained from variable stepped-load creep tests which is not a standard creep testing procedure.

For the nonlinear model, there have been various opinions whether to use the fitting parameter or the creep endurance limit and it was pointed out by Grell that a fitting parameter would limit the model to design stresses below the fitted value. Although this is true it may not be an issue when the nonlinear model is used for practical applications. As for the material used in this study the fitting parameter was significantly larger than the yield stress and stresses of that magnitude would limit the service life of the pressure vessel significantly. Although there are elevated temperature components that are designed for short time service, many components are also designed for longer service and for those, stresses must be kept in the lower range and the fitting parameter would then not be a limiting factor.

In the present study, two tests have indicated that the fitting parameter should be used instead of the creep endurance limit for the nonlinear creep damage model. When the creep resistance for 1% strain within 10 000 and 100 000 hours was used as a creep endurance limit for the material X8CrNiMoNb-16-16 the predicted results deviated grossly from the experimental data. Secondly, the isodamage lines which were plotted by using the stepped-load experimental data for X8CrNiMoNb-16-16 and Al-99.98 showed that the isodamage lines intersected the rupture curve (damage state 100%) at the value of the fitting parameter. This confirmed Pavlou's hypothesis of isodamage lines all intersecting the rupture curve at a common point. However, for the Pavlou creep damage model to be more convenient for design applications, a simpler way of establishing the fitting parameter than having to

perform variable step-load creep tests might be necessary. Perhaps further understanding of the physical meaning behind the fitting parameter could be useful for finding alternative ways for it to be determined. Another important aspect of the fitting parameter that deserves more attention, is its sensitivity to temperature change. No such sensitivity studies have yet been made. If it does not change significantly for various temperatures, the same fitting parameter could possibly also be used under variable temperature conditions.

So far, the nonlinear creep model has only been tested for few load cycles under conditions where creep damage is predominant. Whether the nonlinear model considers creep-fatigue interaction or to what degree fatigue damage is accounted for requires further analysis and testing for any conclusions to be made. A bilinear creep-fatigue interaction diagram is used to combine the linear summation of creep and fatigue damage but since the Pavlou model is nonlinear such a diagram cannot be used if the creep model were to be combined with a fatigue model. A different damage criteria for creep-fatigue would then have to be determined.

The understanding of the creep phenomenon has increased significantly over the years. However, there are still uncertainties in creep life assessments due to difficulty of generalizing the creep response for various materials and load histories. Therefore, a creep analysis to determine stress and strain distribution may not always lead to accurate predictions. The elastic analysis in in ASME-NH is typically considered more convenient than inelastic methods for approximating stress and strain distribution and therefore many times it is the preferred method amongst engineers. A similar elastic approach to determine the stress distribution could therefore be beneficial also for the Pavlou creep damage model. Approximations and generalizations used in life prediction should also include a certain level of conservatism to account for uncertainties. This certainly is the case in ASME-NH which have included several load- and strain-limits checks to ensure safe designs. For the Pavlou method to be used in elevated temperature design applications similar safety measures must be considered.

To summarize, confirmed by experimental data in Pavlou's research [16] and re-demonstrated here, the Pavlou model has accurately predicted creep rupture life for both Al-99.98 and X8CrNiMoNb-16-16. It has also in other research given more accurate predictions than the time fraction rule, both in its modified and original form, by considering the sequence from the load history in the life assessment. The remaining life calculations with the nonlinear model are also almost as simple to perform as for the life fraction method which seems to be a crucial factor for a method to gain acceptance in engineering applications of elevated temperature components. However, further testing and validation for other materials and load histories are necessary before it can be applied for life prediction of elevated temperature components.

6 CONCLUSION

In this thesis, the nonlinear cumulative Pavlou creep damage model has been studied and compared to the linear time fraction rule. The comparison of two models was made by studying the creep life of a pressure vessel subjected to two-step variable loading at different load sequences. The following observations listed below are conclusions of the present work

1. The isodamage lines plotted in Figure 36 using the stepped-load experimental data from other research showed that the isodamage lines all intersected with the rupture curve (D=100%) at the value of the fitting parameter. This indicates that Pavlou's hypothesis of isodamage lines all intersecting at a common point is correct. It also suggests that the fitting parameter should be used instead of the creep endurance limit in the nonlinear creep damage model.
2. Stress cycling cause larger deviation than temperature cycling between the time fraction rule and the Pavlou damage model. The percental difference in remaining life between the two models are only dependent on the stress difference between the loading steps σ_1 and σ_2 and/or the temperature difference ΔT
3. Pavlou's creep damage model predicts a longer remaining life for the high-low load sequence and predicts a more conservative remaining life for the low-high load sequence compared to predictions with the fraction rule.

6.1 Recommendations for further work

Further knowledge of how the model works is required for further use of the nonlinear model in design applications of high-temperature components. The following list contains suggestions of areas for further work which could help to gain a better understanding of the nonlinear model.

1. **Investigate if there are alternative ways to obtain the fitting parameter.**
   Further understanding of the physical meaning behind the fitting parameter could lead to a more simple way to obtain it, without the use of experimental creep data from variable step loading. This could make the Pavlou creep damage model more convenient to use in design applications since most available experimental material creep data are obtained from constant load and temperature test.
2. **Study the temperature dependence of the fitting parameter.**
   For the nonlinear creep damage model to be used for predicting creep life under variable temperatures, the fitting parameter cannot be too sensitive to temperature change. This can be determined by obtaining the fitting parameter from variable step-loading creep tests performed at various temperatures. The significance a potential change of the fitting parameter might have on the remaining life predictions should also be considered.
3. **Studying the effect of creep-fatigue interaction**
   Better understanding on how the nonlinear damage model considers creep-fatigue interaction is necessary, especially when multiple load cycles are considered in the life assessment. Further studies with the Pavlou creep damage model for multiple load cycles should therefore be investigated.
4. **Investigate how to incorporate safety factors in the nonlinear damage assessment**
   Evaluate the nonlinear Pavlou creep model against current standards used for elevated temperature design (e.g. ASME-NH). This could give an indication of how much adjustment in form of engineering corrections that may be necessary for the nonlinear model to always provide conservative predictions.

5. **Study possibility for improvement of the cumulative nonlinear creep damage model**
   Briefly mentioned in Chapter 2.5 is the more recent one-parameter nonlinear fatigue damage accumulation model proposed by Rege and Pavlou [45] published in the International Journal of Fatigue in 2017. In their work, they suggest that the fatigue isodamage lines can be replaced with nonlinear isodamage curves. An investigation whether a similar approach can be used for the Pavlou creep damage model could potentially lead to an improvement of the creep life assessment.

7 APPENDICES

APPENDIX A	Material data for X8CrNiMoNb 16-16 10 pages
APPENDIX B	Calculation sheets from MATLAB and Excel 39 pages
APPENDIX C	Remaining Life calculations 3 pages

8 REFERENCES

[1] R. K. Penny and D. L. Marriott, *Design for creep*, 2nd ed. ed. London: Chapman & Hall, 1995.

[2] E. N. da C. Andrade, "On the Viscous Flow in Metals, and Allied Phenomena," *Proceedings of the Royal Society of London. Series A,* vol. 84, no. 567, pp. 1-12, 1910.

[3] F. Abe, T. U. Kern, and R. Viswanathan, *Creep-Resistant Steels* (Woodhead Publishing Series in Metals and Surface Engineering). Cambridge, England Woodhead Publishing Limited 2008.

[4] L. F. Coffin and R. M. Goldhoff, "Predictive Testing in Elevated Temperature Fatigue and Creep: Status and Problems," *ASTM Special Technical Publication,* pp. 22-74, 1972.

[5] A. E. Johnson, J. Henderson, and B. Khan, *Complex-stress Creep Relaxation and Fracture of Metallic Alloys*. Edinburgh: H.M.S.O. , 1962.

[6] B. J. Cane, "Creep Damage Accumulation and Fracture under Multiaxial Stresses," in *Proc. Advances in Fracture Research (Fracture 81)*, Cannes, France 1981, vol. 3: Pergamon Press.

[7] B. J. Cane and R. J. Browne, "Representative stresses for creep deformation and failure of pressurised tubes and pipes," *International Journal of Pressure Vessels and Piping,* vol. 10, no. 2, pp. 119-128, 1982/03/01 1982.

[8] D. J. Gooch and I. M. How, *Techniques for Multiaxial Creep Testing*. London: Elsevier Applied Science, 1986.

[9] R. I. Jetter, "Subsection NH-Class 1 Components in Elevated Temperature Service " in *Companion Guide to the ASME Boiler and Pressure Vessel Code*, vol. Vol. 1, K. R. Rao, Ed. 4th ed. Three Park Avenue, New York, NY: ASME Press, 2012.

[10] E. L. Robinson, "Effect of temperature variation on the creep strength of steels," *Trans. ASME,* vol. 60, no. 74, p. 1952, 1938.

[11] *ASME: Boiler & Pressure Vessel Code, Section III, Division 1, Subsection NH - Class 1 Components in Elevated Temperature Service*, 2015.

[12] *R5: Assessment procedure for the high temperature response of structures*, 2003.

[13] *Design and Construction Rules for Mechanical Components of FBR Nuclear Islands*, 2002.

[14] M. H. Jawad and R. I. Jetter, *Design and analysis of boiler and pressure vessel components in the creep range*. New York: ASME Press, 2009.

[15] R. Viswanathan, *Damage mechanisms and life assessment of high-temperature components*. Metals Park, Ohio: ASM International, 1989.

[16] D. G. Pavlou, "Creep life prediction under stepwise constant uniaxial stress and temperature conditions," *Engineering Structures,* vol. 23, no. 6, pp. 656-662, 2001.

[17] W. A. Grell, G. H. Niggeler, M. E. Groskreutz, and P. J. Laz, "Evaluation of creep damage accumulation models: Considerations of stepped testing and highly stressed volume," *Fatigue & Fracture of Engineering Materials & Structures,* vol. 30, no. 8, pp. 689-697, 2007.

[18] C.-K. Lin and H.-Y. Teng, "Creep properties of Sn-3.5Ag-0.5Cu lead-free solder under step-loading," *Journal of Materials Science: Materials in Electronics,* journal article vol. 17, no. 8, pp. 577-586, 2006.

[19] H. E. Boyer, *Atlas of creep and stress-rupture curves*. Metals Park, Ohio: ASM International, 1988.

[20] J. R. Davis and A. S. M. International Handbook Committee, *ASM specialty handbook: Heat-resistant materials*. Materials Park, Ohio: ASM International, 1997.

[21] J. Betten, *Creep mechanics*, 3rd ed. ed. Berlin: Springer, 2008.

[22] J. R. Davis and A. S. M. I. H. Committee, *ASM Metals handbook: 8 Mechanical testing and evaluation*, 10th ed. ed. Materials Park, OH: ASM International, 2000.

[23] G. A. Antaki, *Fitness-for-service and integrity of piping, vessels, and tanks : ASME code simplified* (McGraw-Hill mechanical engineering). New York: McGraw-Hill, 2005.

[24] F. C. Campbell, *Elements of Metallurgy and Engineering Alloys*. Materials Park: A S M International, 2008.

[25] (27.05.2017). *Deformation-Mechanism Maps: The Plasticity and Creep of Metals and Ceramics*. Available: http://engineering.dartmouth.edu/defmech/
[26] W. Gan, P. Zhang, R. H. Wagoner, and G. S. Daehn, "Effect of load redistribution in transient plastic flow," *Metallurgical and Materials Transactions A,* journal article vol. 37, no. 7, pp. 2097-2106, 2006.
[27] J. L. Zeman, F. Rauscher, and S. Schindler, *Pressure Vessel Design : The Direct Route* (Advances in Structural Integrity). Burlington: Elsevier Science, 2006.
[28] E. P. Esztergar, "Creep-Fatigue Interaction and Cumulative Damage Evaluations for Type 304 Stainless Steel: Hold-Time Fatigue Test Program and Review of Multiaxial Fatigue " Oak Ridge National Laboratory Oak Ridge, TennesseeORNL-4757 1972, Available: https://www.iaea.org/inis/collection/NCLCollectionStore/_Public/04/038/4038440.pdf.
[29] F. H. Norton, *The creep of steel at high temperatures*. London: McGraw-Hill book company, inc., 1929.
[30] R. W. Bailey, "The Utilization of Creep Test Data in Engineering Design," *Proceedings of the Institute of Mechanical Engineers,* vol. 131, pp. 131-349, 1935.
[31] B. Geddes, H. Leon, and X. Huang, *Superalloys: Alloying and Performance*. ASM International, 2010.
[32] S. Zhang, T. Wakai, and M. Sakane, "Creep rupture life and damage evaluation under multiaxial stress state for type 304 stainless steel," *Materials Science and Engineering: A,* vol. 510–511, pp. 110-114, 2009.
[33] S. Mukai, T. Takada, M. Sakane, M. Ohnami, and T. Tsurui, "Development of multiaxial creep testing machine using cruciform specimen," *Zairyo/Journal of the Society of Materials Science, Japan,* Article vol. 45, no. 5, pp. 559-565, 1996.
[34] A. Makinde, L. Thibodeau, and K. Neale, "Development of an apparatus for biaxial testing using cruciform specimens," *Experimental Mechanics,* vol. 32, no. 2, pp. 138-144, 1992.
[35] D. R. Hayhurst, "A biaxial-tension creep-rupture testing machine," *The Journal of Strain Analysis for Engineering Design* vol. 8, no. 2, pp. 119-123, 1973/04/01 1973.
[36] D. R. Hayhurst and I. D. Felce, "Creep rupture under triaxial tension," in *Proceedings of the International Union of Theoretical and Applied Mechanics, Symposium on Mechanics of Damage and Fatigue*, Israel Institute of Technology and at Tel Aviv University, 1985.
[37] F. R. Larson and J. Miller, "A time-temperature relationship for rupture and creep stresses," *Trans. ASME,* vol. 174, p. 765−775, 1952.
[38] A. Palmgren, "Durability of Ball Bearings," *ZDVI,* vol. 68, no. 14, 1924.
[39] M. A. Miner, "Cumulative damage in fatigue," *J. Appl. Mech.,* vol. 12, no. 3, pp. A159-A164, 1945.
[40] S. Tiara, "Lifetime of Structures Subjected to Varying Load and Temperature," in *Creep in Structures: Colloquium Held at Stanford University, California July 11–15, 1960*, N. J. Hoff, Ed. Berlin: Springer Verlag 1962, pp. 96-124.
[41] L. Bertini and E. Manfredi, "Nuclear science and technology: Study of damage approaches for life assessment in the creep-fatigue range " European Comission Luxembourg 1995.
[42] R. D. Campbell, "Creep/Fatigue Interaction Correlation for 304 Stainless Steel Subjected to Strain-Controlled Cycling With Hold Times at Peak Strain," *Journal of Engineering for Industry,* vol. 93, no. 4, pp. 887-892, 1971.
[43] S. Subramanyan, "A Cumulative Damage Rule Based on the Knee Point of the S-N Curve," *Journal of Engineering Materials and Technology,* vol. 98, no. 4, pp. 316-321, 1976.
[44] A. Fatemi and L. Yang, "Cumulative fatigue damage and life prediction theories: a survey of the state of the art for homogeneous materials," *International Journal of Fatigue,* vol. 20, no. 1, pp. 9-34, 1998.
[45] K. Rege and D. G. Pavlou, "A one-parameter nonlinear fatigue damage accumulation model," *International Journal of Fatigue,* vol. 98, pp. 234-246, 2017.
[46] R. L. Huddleston, "An Improved Multiaxial Creep-Rupture Strength Criterion," *Journal of Pressure Vessel technology,* vol. 107, pp. 421-429, Nov 1985 1985.

[47] A. P. Boresi and R. J. Schmidt, *Advanced mechanics of materials*, 6th ed. ed. New York: Wiley, 2003, pp. 8-15, 104-141.
[48] E. J. Hearn, *Mechanics of Materials 1: An Introduction to the Mechanics of Elastic and Plastic Deformation of Solids and Structural Material*, 3rd ed. Oxford: Butterworth-Heinemann, 1997, pp. 401-429, 198-253.
[49] H.-K. Kim, F. A. Mohamed, and J. C. Earthman, "High-temperature rupture of microstructurally unstable 304 stainless steel under uniaxial and triaxial stress states," *Metallurgical Transactions A,* journal article vol. 22, no. 11, p. 2629, 1991.
[50] R. L. Huddleston, "Assessment of an Improved Multiaxial Strength Theory Based on Creep-Rupture Data for Type 316 Stainless Steel," *Journal of Pressure Vessel Technology,* vol. 115, no. 2, pp. 177-184, May 1993 1993.
[51] R. L. Huddleston, "Assessment of an Improved Multiaxial Strength Theory Based on Creep-Rupture Data for Inconel 600," in *American Society of Mechanical Engineers (ASME) pressure vessel and piping conference*, Denver, CO, 1993: Trans ASME.
[52] R. D. Cook, D. S. Malkus, M. E. Plesha, and R. J. Witt, *Concepts and applications of finite element analysis*, 4th ed. ed. New York: Wiley, 2002.
[53] ANSYS, "User's guide ", 17.0 Academic ed: ANSYS.
[54] R. C. Hibbeler, *Mechanics of materials*, 8th ed. ed. Upper Saddle River, N.J: Pearson Prentice Hall, 2010.
[55] R. Li, Y. Zhang, and L.-W. Tong, "Numerical study of the cyclic load behavior of AISI 316L stainless steel shear links for seismic fuse device," *Frontiers of Structural and Civil Engineering,* journal article vol. 8, no. 4, pp. 414-426, 2014.
[56] D. L. May, A. P. Gordon, and D. S. Segletes, "The Application of the Norton-Bailey Law for Creep Prediction Through Power Law Regression," in *Turbine Technical Conference and Exposition*, San Antonio, Texas, USA, 2013, no. 55263, p. V07AT26A005, Volume 7A: Structures and Dynamics: Proceedings of ASME Turbo Expo 2013.
[57] *ASME: Boiler & Pressure Vessel Code, Section III, Division 1, Subsection NB - Class 1 Components*, 2015.
[58] G.-H. Koo and J.-H. Lee, "Development of an ASME-NH program for nuclear component design at elevated temperatures," *International Journal of Pressure Vessels and Piping,* vol. 85, no. 6, pp. 385-393, 2008.
[59] *ASME: Boiler & Pressure Vessel Code, Section VIII, Division 2 - Rules for construction of pressure vessels: Alternative rules*, 978-0-7918-6996-3, 2015.
[60] *ASME: Boiler & Pressure Vessel Code, Section VIII, Division 1 - Rules for construction of pressure vessels*, 2015.
[61] S. Pantelakis, "Kriechverhalten metallischer Werkstoffe bei zeitveränderlicher Spannung," Aachen, 1983.
[62] Key to Metals AG. Total Materia - The world's most comprehensive materials database [Online]. Available: http://www.totalmateria.com/
[63] *ASME: Boiler & Pressure Vessel Code, Section II-Materials, Part D-Properties (Metric)*, 2015.
[64] A. J. McEvily, *Metal Failures - Mechanisms, Analysis, Prevention*, 2 ed. Hoboken, NJ, USA: Hoboken, NJ, USA: John Wiley & Sons, Inc., 2013.
[65] S. A. Chavez, D. L. Kelly, R. J. Witt, and D. P. Stirn, "Comparison of stress-based and strain-based creep failure criteria for severe accident analysis," *Nuclear Engineering and Design,* vol. 155, no. 3, pp. 603-622, 1995/05/01 1995.
[66] A. Zielesny and SpringerLink, *From Curve Fitting to Machine Learning* (Intelligent Systems Reference Library, 18). Berlin: Springer Berlin Heidelberg, 2011.
[67] The MathWorks Inc. (28/04/2017). *Curve Fitting Toolbox: User's Guide (R2017a)*. Available: https://se.mathworks.com/help/pdf_doc/curvefit/curvefit.pdf
[68] (29.05.2016). *Element Types*. Available: http://osupdocs.forestry.oregonstate.edu/index.php/Element_Types

[69] D. L. Logan, K. K. Chaudhry, and P. Singh, *A first course in the finite element method*, 4th ed., SI ed. ed. Stamford, Conn: Cengage Learning, 2011.

This page intentionally left blank

APPENDIX A – Material data for X8CrNiMoNb 16-16

Material designation:	X8CrNiMoNb 16-16
Standard / Country:	Germany/DIN
Subgroup:	DIN 17460 (1992) High temperature austenitic steel plate and sheet, cold and hot rolled strip, bars and forgings – Technical Delivery conditions; replaced by: DIN EN 10028-7:2000; DIN EN 10222-5:2000; DIN EN 10302:2002

Mechanical properties

Property	Symbol	Value	Unit	Note
Bars, forgings, plates, sheets strips; Solution annealed; (long.)				
Yield stress	$R_{p0.2}$	≥ 215	MPa	
Tensile stress	R_m	530-690	MPa	
Elongation	A	≥ 35	%	
Impact	Kv/ku	≥ 36	J	ISO-V
Bars, forgings, plates, sheets strips; Solution annealed; (trans.)				
Yield stress	$R_{p0.2}$	≥ 215	MPa	
Tensile stress	R_m	530-690	MPa	
Elongation	A	≥ 22	%	
Impact	Kv/ku	≥ 45	J	ISO-V

Typical physical properties

Property	Symbol	Value	Unit
Density	ρ	7.86	Kg/dm^3
Modulus of elasticity	E	190-210	GPa
Poisson's coefficient	ν	0.27-0.30	

High-temperature material properties

Property	T(°C)	Value	Unit
Modulus of elasticity, E	20	198	GPa
	100	192	GPa
	200	183	GPa
	300	175	GPa
	400	167	GPa
	500	159	GPa
	600	150	GPa
	700	141*	GPa
Mean coefficient of thermal expansion between 20 (°C) and	100	16.3	10^{-6}/(°C)
	200	16.9	10^{-6}/(°C)
	300	17.3	10^{-6}/(°C)
	400	17.8	10^{-6}/(°C)
	500	18.2	10^{-6}/(°C)
	600	18.5	10^{-6}/(°C)
	700	18.8*	10^-6/(°C)
Yield stress, $R_{p0.2}$	20	215	MPa
	100	195	MPa
	200	177	MPa
	300	157	MPa
	400	147	MPa
	500	137	MPa
	550	137	MPa
	600	132	MPa
	700	127*	MPa
Thermal conductivity	20	16	W/m·°C
Specific thermal capacity	20	450	J/kg·°C
Specific electrical resistivity	20	0.7	Ω mm^2/m
Density	20	8	Kg/dm^3

* Material property at 700 ° C obtained by linear interpolation

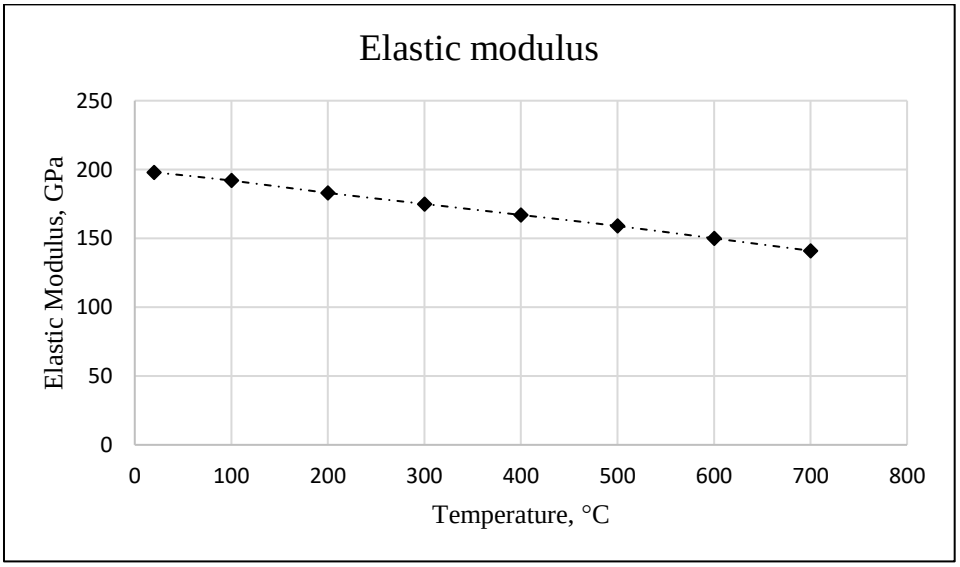

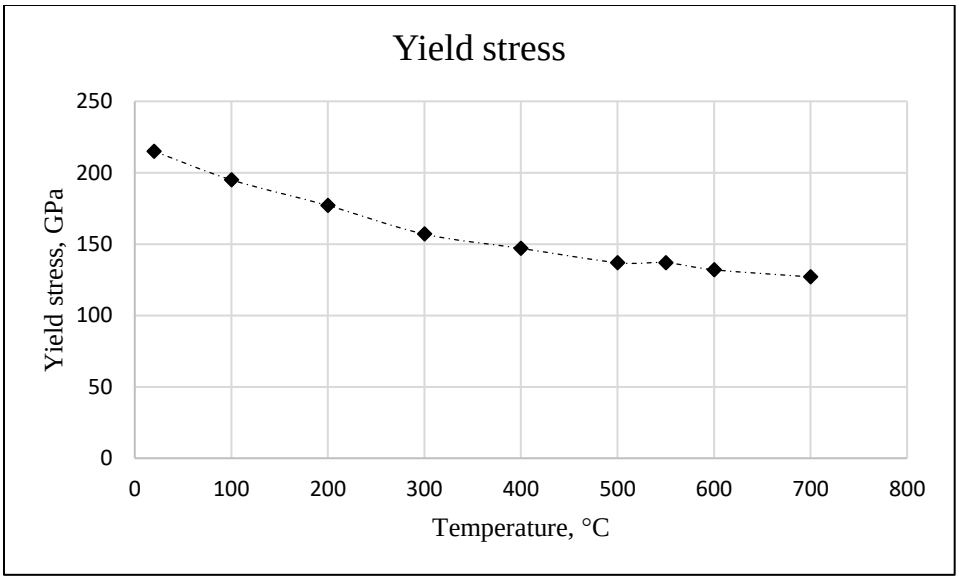
Yield stress
Yield stress, GPa
250
200
150
100
50
0
0
100
200
300
400
500
600
700
800
Temperature, °C

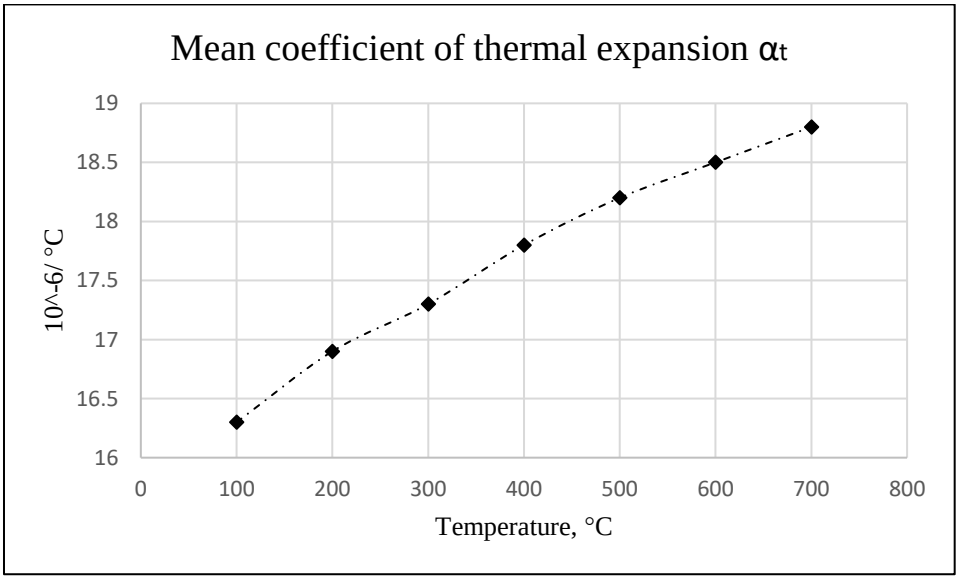
Mean coefficient of thermal expansion αt
10^-6/ °C
19
18.5
18
17.5
17
16.5
16
0
100
200
300
400
500
600
700
800
Temperature, °C

Creep properties

Material designation: X8CrNiMoNb-16-16
Standard / Country: Germany/DIN
Subgroup: DIN EN 10088-1 (2014) Stainless steels – Part 1: List of stainless steels
Austenitic creep resisting steels with Mo

Temperature (°C)	1% Yield Stress Rp1 (MPa)	Creep Rupture Strength CRS (MPa)	Temperature (°C)	1% Yield Stress Rp1 (MPa)	Creep Rupture Strength CRS (MPa)
10000 h			**200000 h**		
580	177	270	580	-	162
590	167	246	590	-	147
600	157	225	600	-	132
610	147	205	610	-	118
620	137	186	620	-	103
630	128	169	630	-	91
640	118	152	640	-	80
650	108	137	650	-	71
660	98	124	660	-	63
670	89	111	670	-	55
680	80	100	680	-	49
690	72	91	690	-	42
700	64	83	700	-	35
710	58	77	710	-	29
720	53	70	720	-	24
730	47	64	730	-	20
740	44	59	740	-	17
750	42	54	750	-	15
100000 h					
580	128	186			
590	118	169			
600	108	152			
610	98	136			
620	88	122			
630	79	107			
640	72	94			
650	64	83			
660	56	75			
670	49	66			
680	43	59			
690	38	51			
700	34	44			
710	29	37			
720	26	31			
730	22	26			
740	19	23			
750	17	20			

Error from chosen polynomial fits (Larson-Miller parameter)

	log σ_{CRS} Polynomial fit				log σRp1% Polynomial fit			
T [°C]	σ_{CRS} [MPa]	t [h]	$t_{CRS\ fit}$ [h]	error %	$\sigma_{Rp1\%}$[MPa]	t [h]	$t_{CRS\ fit}$ [h]	error %
580	270	10000	6.47E+03	35.307	177	10000	1.11E+04	10.644
590	246	10000	8.13E+03	18.720	167	10000	1.06E+04	6.487
600	225	10000	9.33E+03	6.707	157	10000	1.03E+04	2.838
610	205	10000	1.05E+04	4.692	147	10000	9.99E+03	0.095
620	186	10000	1.16E+04	15.581	137	10000	9.79E+03	2.125
630	169	10000	1.22E+04	22.293	128	10000	9.28E+03	7.220
640	152	10000	1.32E+04	32.259	118	10000	9.31E+03	6.911
650	137	10000	1.38E+04	37.610	108	10000	9.50E+03	5.018
660	124	10000	1.37E+04	37.370	98	10000	9.89E+03	1.059
670	111	10000	1.41E+04	41.002	89	10000	1.01E+04	0.531
680	100	10000	1.38E+04	38.405	80	10000	1.05E+04	4.837
690	91	10000	1.29E+04	28.935	72	10000	1.07E+04	6.690
700	83	10000	1.18E+04	17.995	64	10000	1.12E+04	12.052
710	77	10000	1.01E+04	0.998	58	10000	1.08E+04	7.614
720	70	10000	9.23E+03	7.672	53	10000	9.93E+03	0.653
730	64	10000	8.23E+03	17.704	47	10000	1.01E+04	0.901
740	59	10000	7.11E+03	28.863	44	10000	8.46E+03	15.364
750	54	10000	6.27E+03	37.295	42	10000	6.67E+03	33.340
580	186	100000	8.04E+04	19.633	128	100000	9.67E+04	3.329
590	169	100000	8.34E+04	16.637	118	100000	9.44E+04	5.587
600	152	100000	8.85E+04	11.487	108	100000	9.39E+04	6.081
610	136	100000	9.35E+04	6.477	98	100000	9.55E+04	4.451
620	122	100000	9.50E+04	4.998	88	100000	9.99E+04	0.077
630	107	100000	1.04E+05	3.930	79	100000	1.02E+05	2.180
640	94	100000	1.10E+05	9.737	72	100000	9.60E+04	3.970
650	83	100000	1.11E+05	10.985	64	100000	9.87E+04	1.253
660	75	100000	1.01E+05	1.298	56	100000	1.06E+05	5.857
670	66	100000	1.01E+05	0.534	49	100000	1.11E+05	11.005
680	59	100000	9.32E+04	6.766	43	100000	1.13E+05	13.045
690	51	100000	9.54E+04	4.564	38	100000	1.11E+05	10.695
700	44	100000	9.67E+04	3.348	34	100000	1.03E+05	2.911
710	37	100000	1.04E+05	3.934	29	100000	1.10E+05	10.097
720	31	100000	1.11E+05	10.733	26	100000	9.98E+04	0.224
730	26	100000	1.16E+05	15.555	22	100000	1.06E+05	6.184
740	23	100000	1.03E+05	3.489	19	100000	1.05E+05	5.090
750	20	100000	9.63E+04	3.681	17	100000	9.37E+04	6.322
580	162	200000	1.75E+05	12.728	-	200000	-	-
590	147	200000	1.74E+05	13.162	-	200000	-	-
600	132	200000	1.78E+05	11.209	-	200000	-	-
610	118	200000	1.81E+05	9.604	-	200000	-	-
620	103	200000	1.99E+05	0.451	-	200000	-	-
630	91	200000	2.03E+05	1.355	-	200000	-	-
640	80	200000	2.06E+05	3.024	-	200000	-	-
650	71	200000	1.98E+05	0.774	-	200000	-	-
660	63	200000	1.89E+05	5.674	-	200000	-	-
670	55	200000	1.87E+05	6.471	-	200000	-	-
680	49	200000	1.71E+05	14.366	-	200000	-	-
690	42	200000	1.75E+05	12.423	-	200000	-	-
700	35	200000	1.91E+05	4.316	-	200000	-	-
710	29	200000	2.08E+05	3.988	-	200000	-	-
720	24	200000	2.22E+05	11.122	-	200000	-	-
730	20	200000	2.29E+05	14.596	-	200000	-	-
740	17	200000	2.22E+05	10.944	-	200000	-	-
750	15	200000	1.95E+05	2.672	-	200000	-	-
			Average error	13.075			Average error	6.187
			Max error	41.002			Max error	33.340
			Min error	0.451			Min error	0.077

True Stress strain curve

Ture stress-strain curve according to ASME VIII Division 2 Annex 3-D
Material: X8CrNiMoNb-1-16
Temperature: 700 °C

Yield strength at temperature	σ_{ys}	127	MPa
Ultimate strength temperature	σ_{uts}	313	MPa
True ultimate tensile stress	$\sigma_{uts,t}$	488.7690519	MPa
Young's modulus at temperature	E_y	141000	MPa
Engineering offset strain	ε_{ys}	0.002	-
Stress-strain curve fitting parameter	ε_p	0.00002	-
Yield-tensile ratio	R	0.405750799	-
Curve fitting exponent	m_1	0.196342433	-
Curve fitting exponent	m_2	0.445686901	-
Material parameter	K	0.292700721	-
Curve fitting constant for the elastic region	A_1	431.200226	MPa
Curve fitting constant for the plastic region	A_2	700.6909187	MPa

True stress	**True strain**	**True stress strain curve fitting parameter**	**True plastic strain in the macrostrain region**	**True plastic strain in the micro strain region**	**True strain in the micro region**	**True strain in the macro region**
σ_t	ε_t (σ_t)	H (σ_t)	ε_2 (σ_t)	ε_1 (σ_t)	γ_1 (σ_t)	γ_2 (σ_t)
0	0	-6.66549	0	0	0	0
10	7.093E-05	-6.29813	7.23E-05	4.72E-09	4.72E-09	2.45E-10
20	0.000142	-5.93076	0.000342	1.61E-07	1.61E-07	2.42E-09
30	0.0002141	-5.5634	0.00085	1.27E-06	1.27E-06	1.25E-08
40	0.0002892	-5.19604	0.001622	5.5E-06	5.5E-06	4.97E-08
50	0.0003719	-4.82868	0.002676	1.72E-05	1.72E-05	1.71E-07
60	0.0004695	-4.46132	0.004028	4.34E-05	4.34E-05	5.37E-07
70	0.0005932	-4.09396	0.005693	9.52E-05	9.52E-05	1.58E-06
80	0.0007596	-3.7266	0.007681	0.000188	0.000188	4.45E-06
90	0.0009923	-3.35924	0.010005	0.000342	0.000342	1.21E-05
100	0.001325	-2.99188	0.012673	0.000585	0.000584	3.18E-05
110	0.0018085	-2.62451	0.015694	0.000951	0.000946	8.2E-05
113.1	0.0020003	-2.51063	0.016704	0.001096	0.001089	0.000109
120	0.0025234	-2.25715	0.019078	0.001482	0.001466	0.000207
130	0.0036094	-1.88979	0.022831	0.002228	0.002178	0.00051
140	0.0053193	-1.52243	0.026961	0.003249	0.003101	0.001225
150	0.0081057	-1.15507	0.031475	0.004617	0.0042	0.002842
160	0.0126859	-0.78771	0.03638	0.006414	0.005314	0.006237
170	0.0198692	-0.42035	0.041681	0.008734	0.006101	0.012562
180	0.0298662	-0.05299	0.047384	0.011685	0.006152	0.022438
190	0.0415898	0.314375	0.053495	0.015389	0.005352	0.03489
200	0.0532843	0.681737	0.06002	0.019984	0.00407	0.047796
210	0.0639357	1.049098	0.066964	0.025621	0.0028	0.059647
220	0.0735654	1.416459	0.074331	0.032471	0.001804	0.070201
230	0.082622	1.78382	0.082127	0.040721	0.001118	0.079873
240	0.0915273	2.151181	0.090356	0.050578	0.000676	0.08915
250	0.1005593	2.518542	0.099023	0.062267	0.000402	0.098385

260	0.1098768	2.885904	0.108132	0.076034	0.000236	0.107797
270	0.1195647	3.253265	0.117688	0.092148	0.000137	0.117512
280	0.1296676	3.620626	0.127694	0.110899	7.94E-05	0.127602
290	0.140209	3.987987	0.138154	0.132601	4.55E-05	0.138107
300	0.1512021	4.355348	0.149073	0.157593	2.6E-05	0.149048
310	0.1626547	4.72271	0.160454	0.186236	1.47E-05	0.160441
320	0.1745723	5.090071	0.172301	0.218922	8.3E-06	0.172294
330	0.1869592	5.457432	0.184618	0.256068	4.66E-06	0.184614
340	0.1998193	5.824793	0.197407	0.298117	2.6E-06	0.197405
350	0.2131561	6.192154	0.210673	0.345546	1.45E-06	0.210672
360	0.2269728	6.559515	0.224419	0.398857	8E-07	0.224419
370	0.2412729	6.926877	0.238649	0.458587	4.41E-07	0.238648
380	0.2560594	7.294238	0.253364	0.525303	2.43E-07	0.253364
390	0.2713356	7.661599	0.26857	0.599606	1.33E-07	0.26857
400	0.2871046	8.02896	0.284268	0.68213	7.24E-08	0.284268
410	0.3033694	8.396321	0.300462	0.773544	3.94E-08	0.300462
420	0.320133	8.763683	0.317154	0.874555	2.14E-08	0.317154
430	0.3373983	9.131044	0.334349	0.985904	1.16E-08	0.334349
440	0.3551682	9.498405	0.352048	1.108372	6.23E-09	0.352048
450	0.3734455	9.865766	0.370254	1.242779	3.35E-09	0.370254
460	0.3922331	10.23313	0.388971	1.389983	1.8E-09	0.388971
470	0.4115337	10.60049	0.4082	1.550885	9.62E-10	0.4082
480	0.4313499	10.96785	0.427946	1.726427	5.14E-10	0.427946
488.76905	0.4491533	11.28999	0.445687	1.893184	2.96E-10	0.445687

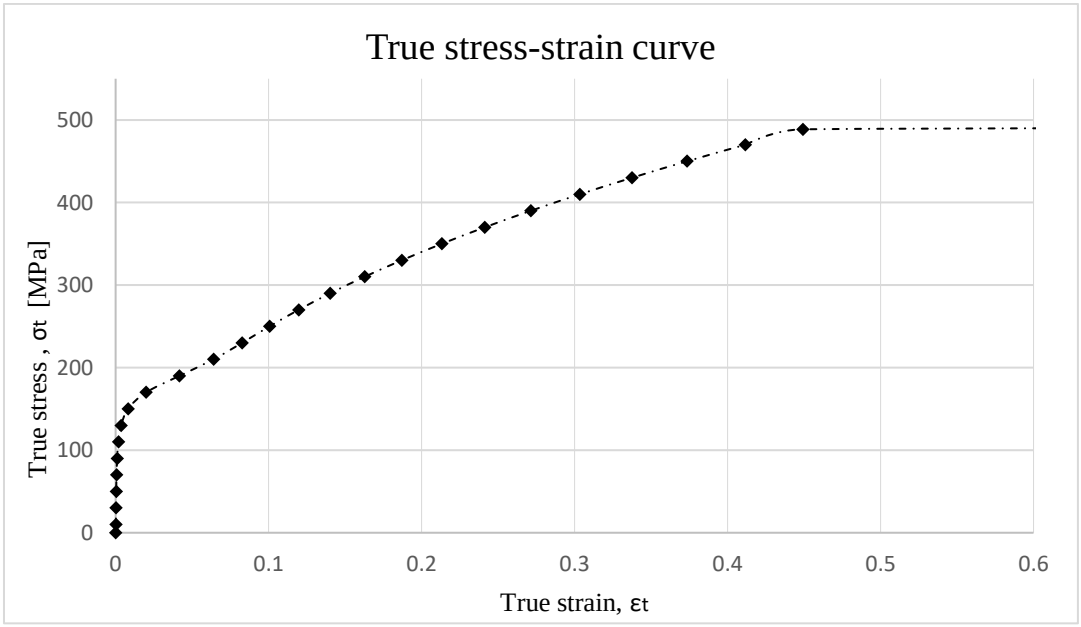

Calculation of true stress-strain curve according to ASME VIII Division 2: Annex 3-D

Material: X8CrNiMoNb-16-16
Temperature: 700 °C

Yield strength at temperature: $\sigma_{ys} := 127\ MPa$

Ultimate strength temperature: $\sigma_{uts} := 313\ MPa$

Young's modulus at temperature: $E_y := 141000\ MPa$

Engineering offset strain: $\varepsilon_{ys} := 0.002$

Stress-strain curve fitting parameter: $\varepsilon_p := 2 \cdot 10^{-5}$

Yield-tensile ratio: $R := \frac{\sigma_{ys}}{\sigma_{uts}} = 0.406$

Material parameter: $K := 1.5 \cdot R^{1.5} - 0.5 \cdot R^{2.5} - R^{3.5} = 0.293$

Curve fitting exponent: $m_1 := \frac{\ln(R) + \langle \varepsilon_p - \varepsilon_{ys} \rangle}{\ln\left(\frac{\ln\langle 1+\varepsilon_p \rangle}{\ln\langle 1+\varepsilon_{ys} \rangle}\right)} = 0.196$

Curve fitting exponent: $m_2 := 0.75 \cdot (1 - R) = 0.446$

Curve fitting constant for the elastic region: $A_1 := \frac{\sigma_{ys} \cdot \langle 1+\varepsilon_{ys} \rangle}{\langle \ln\langle 1+\varepsilon_{ys} \rangle \rangle^{m_1}} = 431.2\ MPa$

Curve fitting constant for the plastic region: $A_2 := \frac{\sigma_{uts} \cdot e^{m_2}}{m_2^{m_2}} = 700.691\ MPa$

True ultimate tensile stress: $\sigma_{uts\_t} := \sigma_{uts} \cdot e^{m_2} = 488.769\ MPa$

True stress: $\sigma_t := 0\ MPa, 10\ MPa .. \sigma_{uts\_t}$

Stress-strain curve fitting parameter: $H\langle \sigma_t \rangle := 2 \cdot \frac{\langle \sigma_t - \langle \sigma_{ys} + K \cdot \langle \sigma_{uts} - \sigma_{ys} \rangle \rangle \rangle}{K \cdot \langle \sigma_{uts} - \sigma_{ys} \rangle}$

True plastic strain in the micro strain region:

$$\varepsilon_1(\sigma_t) := \left(\frac{\sigma_t}{A_1}\right)^{\frac{1}{m_1}}$$

True plastic strain in the macrostrain region:

$$\varepsilon_2(\sigma_t) := \left(\frac{\sigma_t}{A_2}\right)^{\frac{1}{m_2}}$$

True strain in the micro region:

$$\gamma_1(\sigma_t) := \frac{\varepsilon_1(\sigma_t)}{2} \cdot (1.0 - \tanh(H(\sigma_t)))$$

True strain in the macro region:

$$\gamma_2(\sigma_t) := \frac{\varepsilon_2(\sigma_t)}{2} \cdot (1.0 + \tanh(H(\sigma_t)))$$

Total true strain:

$$\varepsilon_t(\sigma_t) := \frac{\sigma_t}{E_y} + \gamma_1(\sigma_t) + \gamma_2(\sigma_t)$$

True stress-strain curve

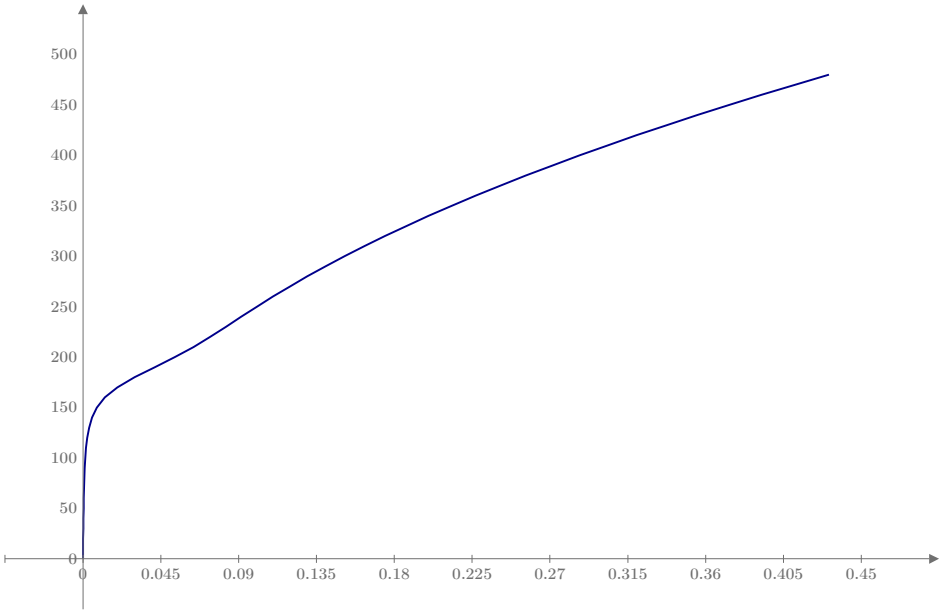

APPENDIX B – MATLAB Code

```
%=========================================================================
% Pavlou creep damage accumulation model - X8CrNiMoNb-16-16
%=========================================================================
close all;
clear all;

sigma=[150 170];          % Stress, sigma in [MPa]
T=[973 973];              % Temperature T in [K]

% Experimental test data X8CrNiMoNb-16-16
t_r1_test=[0.05 0.10 0.35 0.40 0.44 0.46 0.55 0.88];
t_r2_test=[0.70 0.61 0.21 0.25 0.20 0.21 0.21 0.05];

t_r1=[0:0.01:1];          % time to creep failure ratio t1/tf1


% Fitting parameter
p=10^((-log10(sigma(2))+log10(sigma(1))*T(2)*log10(1-
t_r2_test(1))/(T(1)*log10(t_r1_test(1))))/(log10(1-t_r2_test(1))/
log10(t_r1_test(1))-1))

for k=1:101
  for i=1:1

  % exponent
   q(i)=T(i)*log10(sigma(i+1)/p)/(T(i+1)*log10(sigma(i)/p));

  % remaining life=1-consumed life
    t_r2(k)=1-t_r1(k)^q(i);

  end

end

% plot of remaining life vs. consumed life

figure(1)
hold on
box on
axis square
grid on
scatter(t_r1_test,t_r2_test,'filled')
plot(t_r1,t_r2, 'k')
hold off
axis([0 1 0 1])
title('X8CrNiMoNb-16-16')
xlabel('Consumed life t_1/t_f_1')
ylabel('Remaining life t_2/t_f_2 ')
legend('test results','theoretical results')
```

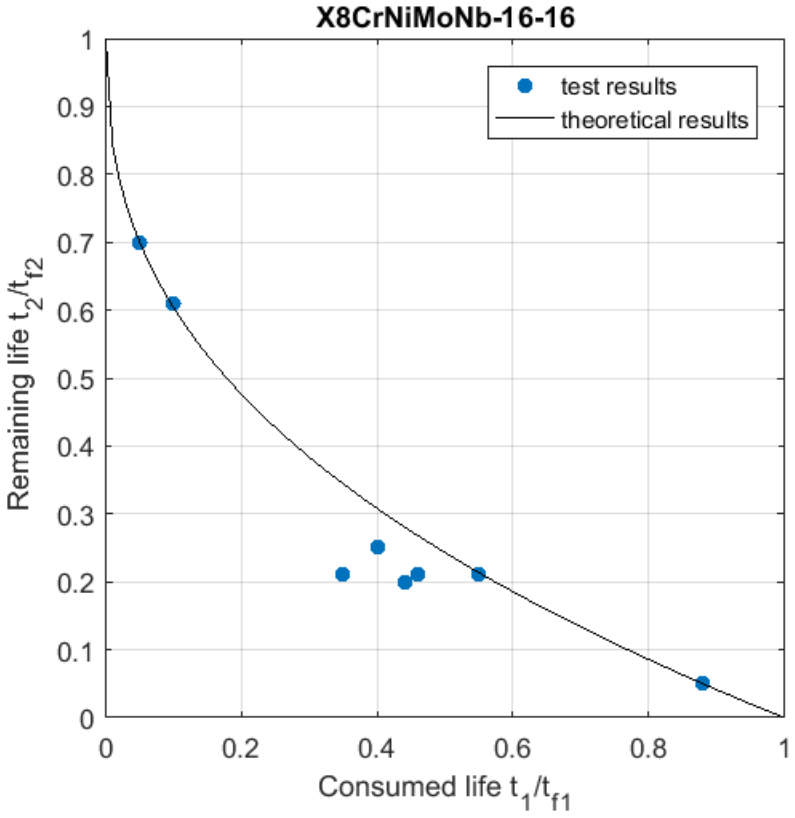

Published with MATLAB® R2016b

```
%=========================================================================
%Pavlou creep damage accumulation model - Al-99.98
%=========================================================================
close all;
clear all;

sigma=[12 14];   % Stress, sigma in [MPa]
T=[489 489];     % Temperature T in [K]

% Experimental test data Al-99.98
t_r1_test=[0.12 0.13 0.30 0.32 0.50 0.65 0.70 0.75];
t_r2_test=[0.58 0.56 0.38 0.37 0.24 0.16 0.13 0.11 ];

t_r1=[0:0.01:1];  % time to creep failure ratio t1/tf1

% Solving for fitting parameter
p=10^((-log10(sigma(2))+log10(sigma(1))*T(2)*log10(1-
t_r2_test(1))/(T(1)*log10(t_r1_test(1))))/(log10(1-t_r2_test(1))/
log10(t_r1_test(1))-1))

for k=1:101
for i=1:1

   % exponent
     q(i)=T(i)*log10(sigma(i+1)/p(1))/(T(i+1)*log10(sigma(i)/p(1)));

    % remaining life
     t_r2(k)=1-t_r1(k)^q(i);

    end
end

% plot of remaining life vs. consumed life
figure(1)
hold on
box on
axis square
grid on
scatter(t_r1_test,t_r2_test,'filled')
plot(t_r1,t_r2, 'k')
hold off
axis([0 1 0 1])
title('Al-99.98')
xlabel('Consumed life t_1/t_f_1')
ylabel('Remaining life t_2/t_f_2')
legend('test results','theoretical results')
```

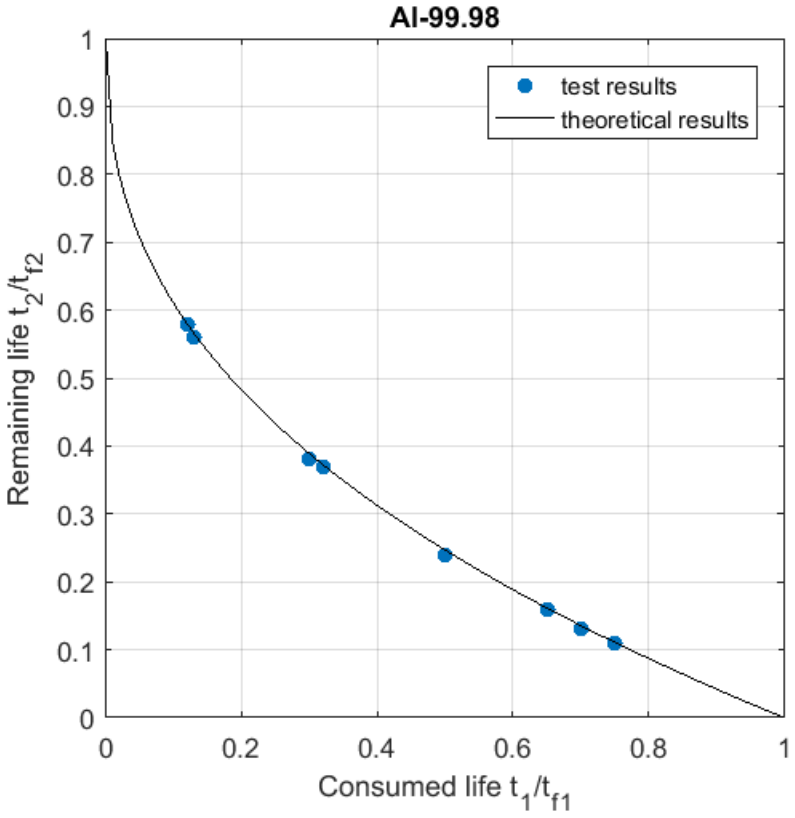

Published with MATLAB® R2016b

```
% Fitting parameters, p  steel - X-8-CrNiMoNb-16-16
%=========================================================================
close all;
clear all;

sigma=[150 170];                                        % Stress, sigma
 in [MPa]
T=[973 973];                                            % Temperature T
 in [K]
q=[];                                                   % exponent

t_r1_test=[0.05 0.10 0.35 0.40 0.44 0.46 0.55 0.88];  % test results %
 X-8-CrNiMoNb-16-16
t_r2_test=[0.70 0.61 0.21 0.25 0.20 0.21 0.21 0.05];  % test results %
 X-8-CrNiMoNb-16-16

t_r1=[0:0.01:1];                                        % time to creep
 failure ratio t1/tf1
t_r2=[];                                                % time to creep
 failure ratio t2/tf2


for m=1:8
p(m)=10^((-log10(sigma(2))+log10(sigma(1))*T(2)*log10(1-
t_r2_test(m))/(T(1)*log10(t_r1_test(m))))/(log10(1-t_r2_test(m))/
log10(t_r1_test(m))-1))
end
```

Published with MATLAB® R2016b

```
%=========================================================================
% Fitting parameters, p  Aluminium 99.98
%=========================================================================
close all;
clear all;

sigma=[12 14];                                          % Stress, sigma
 in [MPa]
T=[489 489];                                            % Temperature T
 in [K]
q=[];                                                   % exponent

t_r1_test=[0.12 0.13 0.30 0.32 0.50 0.65 0.70 0.75];  % test results %
 Alu
t_r2_test=[0.58 0.56 0.38 0.37 0.24 0.16 0.13 0.11 ];  % test results
 % Alu

t_r1=[0:0.01:1];                                        % time to creep
 failure ratio t1/tf1
t_r2=[];                                                % time to creep
 failure ratio

% Fitting parameter
for m=1:8
p(m)=10^((-log10(sigma(2))+log10(sigma(1))*T(2)*log10(1-
t_r2_test(m))/(T(1)*log10(t_r1_test(m))))/(log10(1-t_r2_test(m))/
log10(t_r1_test(m))-1))
end
```

Published with MATLAB® R2016b

```
%=========================================================================
% Pavlou model - p,sensitivity analysis
% Material: X-8-CrNiMoNb-16-16
%=========================================================================
close all;
clear all;

sigma=[150 170]; % Stress, sigma in [MPa]
T=[973 973];     % Temperature T in [K]

% Experimental test data X8CrNiMoNb-16-16
t_r1_test=[0.05 0.10 0.35 0.40 0.44 0.46 0.55 0.88];
t_r2_test=[0.70 0.61 0.21 0.25 0.20 0.21 0.21 0.05];

t_r1=[0:0.01:1]; % time to creep failure ratio t1/t_f1

% Fitting parameter

p=[184.9160 185.3775 176.2740  180.0220  178.1304  179.5320  184.4309
 184.8744]


for k=1:101
  for i=1:1
  % exponent
   q1(i)=T(i+1)*log10(sigma(i+1)/p(1))/(T(i+1)*log10(sigma(i)/p(1)));
   q2(i)=T(i+1)*log10(sigma(i+1)/p(2))/(T(i+1)*log10(sigma(i)/p(2)));
   q3(i)=T(i+1)*log10(sigma(i+1)/p(3))/(T(i+1)*log10(sigma(i)/p(3)));
   q4(i)=T(i+1)*log10(sigma(i+1)/p(4))/(T(i+1)*log10(sigma(i)/p(4)));
   q5(i)=T(i+1)*log10(sigma(i+1)/p(5))/(T(i+1)*log10(sigma(i)/p(5)));
   q6(i)=T(i+1)*log10(sigma(i+1)/p(6))/(T(i+1)*log10(sigma(i)/p(6)));
   q7(i)=T(i+1)*log10(sigma(i+1)/p(7))/(T(i+1)*log10(sigma(i)/p(7)));
   q8(i)=T(i+1)*log10(sigma(i+1)/p(8))/(T(i+1)*log10(sigma(i)/p(8)));

   t_r21(k)=1-t_r1(k)^q1(i);
   t_r22(k)=1-t_r1(k)^q2(i);
   t_r23(k)=1-t_r1(k)^q3(i);
   t_r24(k)=1-t_r1(k)^q4(i);
   t_r25(k)=1-t_r1(k)^q5(i);
   t_r26(k)=1-t_r1(k)^q6(i);
   t_r27(k)=1-t_r1(k)^q7(i);
   t_r28(k)=1-t_r1(k)^q8(i);
   end

end

% plot of remaining life vs. consumed life

figure(1)
hold on
grid on
box on
```

```
axis square
scatter(t_r1_test,t_r2_test,'filled')
plot(t_r1,t_r21,t_r1, t_r22,t_r1, t_r23,t_r1, t_r24,t_r1, t_r25,t_r1,
 t_r26, t_r1, t_r27, t_r1, t_r28)
hold off
axis([0 1 0 1])
title('X8CrNiMoNb-16-16')
xlabel('Consumed life, t_1/t_f_1')
ylabel('Remaining life, t_2/t_f_2')
legend('Experimental data','p=184.92 MPa','p=185.38 MPa','p=176.27
 MPa','p=180.02 MPa','p=178.13 MPa','p=179.53 MPa','p=184.43
 MPa','p=184.87 MPa')
```

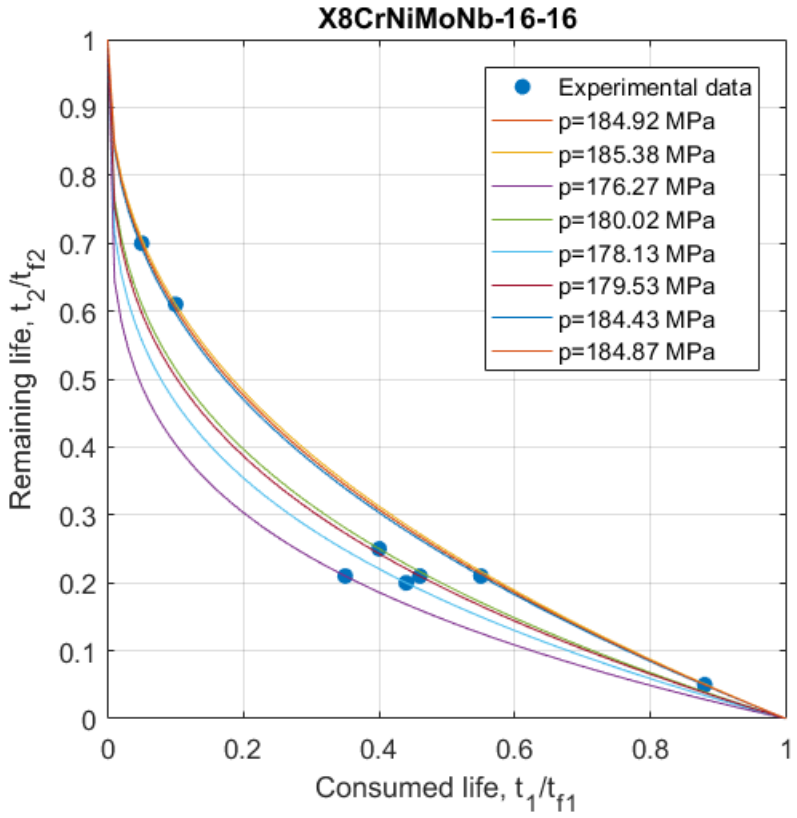

Published with MATLAB® R2016b

```
%=========================================================================
% Pavlou model - p,sensitivity analysis
% Material: Aluminium
%=========================================================================
close all;
clear all;

sigma=[12 14];  % Stress, sigma in [MPa]
T=[489 489];    % Temperature T in [K]


% Experimental test data Al-99.98
t_r1_test=[0.12 0.13 0.30 0.32 0.50 0.65 0.70 0.75];
t_r2_test=[0.58 0.56 0.38 0.37 0.24 0.16 0.13 0.11];

t_r1=[0:0.01:1];   % time to creep failure ratio t1/t_f1


% Fitting parameter
p=[15.5771 15.5313 15.4958 15.5522 15.4884 15.5470 15.4529 15.5493]


for k=1:101
  for i=1:1
  % exponent
   q1(i)=T(i+1)*log10(sigma(i+1)/p(1))/(T(i+1)*log10(sigma(i)/p(1)));
   q2(i)=T(i+1)*log10(sigma(i+1)/p(2))/(T(i+1)*log10(sigma(i)/p(2)));
   q3(i)=T(i+1)*log10(sigma(i+1)/p(3))/(T(i+1)*log10(sigma(i)/p(3)));
   q4(i)=T(i+1)*log10(sigma(i+1)/p(4))/(T(i+1)*log10(sigma(i)/p(4)));
   q5(i)=T(i+1)*log10(sigma(i+1)/p(5))/(T(i+1)*log10(sigma(i)/p(5)));
   q6(i)=T(i+1)*log10(sigma(i+1)/p(6))/(T(i+1)*log10(sigma(i)/p(6)));
   q7(i)=T(i+1)*log10(sigma(i+1)/p(7))/(T(i+1)*log10(sigma(i)/p(7)));
   q8(i)=T(i+1)*log10(sigma(i+1)/p(8))/(T(i+1)*log10(sigma(i)/p(8)));

   t_r21(k)=1-t_r1(k)^q1(i);
   t_r22(k)=1-t_r1(k)^q2(i);
   t_r23(k)=1-t_r1(k)^q3(i);
   t_r24(k)=1-t_r1(k)^q4(i);
   t_r25(k)=1-t_r1(k)^q5(i);
   t_r26(k)=1-t_r1(k)^q6(i);
   t_r27(k)=1-t_r1(k)^q7(i);
   t_r28(k)=1-t_r1(k)^q8(i);
   end

end

% plot of remaining life vs. consumed life

figure(1)
hold on
grid on
box on
```

```
axis square
scatter(t_r1_test,t_r2_test,'filled')
plot(t_r1,t_r21,t_r1, t_r22,t_r1, t_r23,t_r1, t_r24,t_r1, t_r25,t_r1,
 t_r26, t_r1, t_r27, t_r1, t_r28)
hold off
axis([0 1 0 1])
title('Al-99.98')
xlabel('Consumed life, t_1/t_f_1')
ylabel('Remaining life, t_2/t_f_2')
legend('Experimental data','p=15.58 MPa','p=15.53 MPa','p=15.50
 MPa','p=15.55 MPa','p=15.49 MPa','p=15.55 MPa','p=15.45 MPa','p=15.55
 MPa')
```

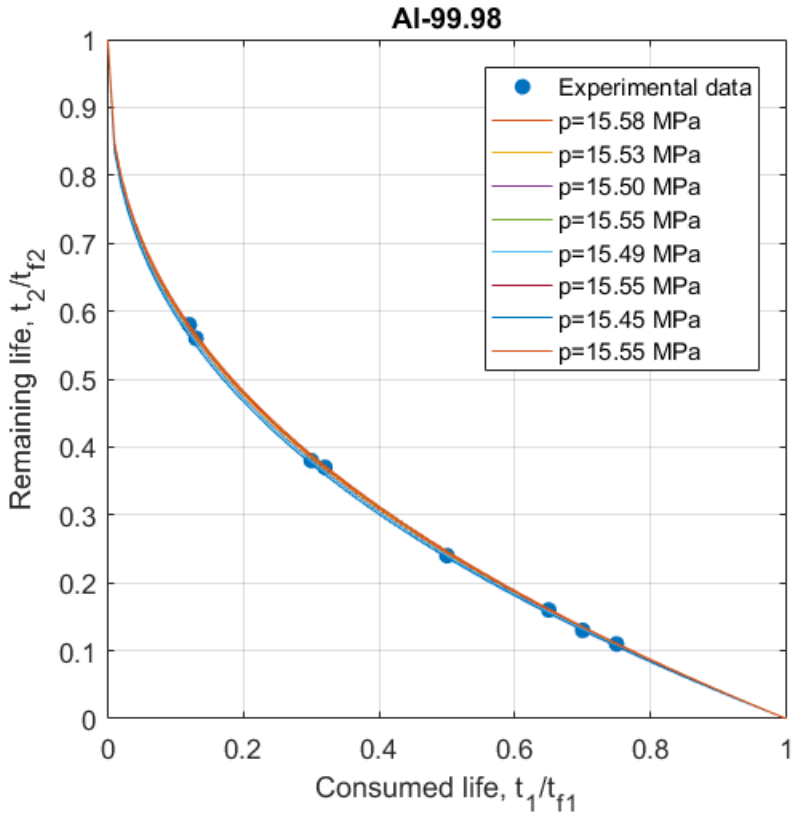

Published with MATLAB® R2016b

```
%=========================================================================
% Isodamage lines: X8CrNiMoNb-16-16
%=========================================================================
close all; clear all;

steel_tf1=447    % time-to-rupture (h)
steel_tf2=200    % time-to-rupture (h)


S1=ones(1,9)*log10(150)  % stress step 1
S2=ones(1,9)*log10(170)  % stress step 2

S11=ones(1,8)*log10(150)  % stress step 1 (for scatter plot)
S22=ones(1,8)*log10(170)  % stress step 2 (for scatter plot)

% lifetime ratios Experimental data X8CrNiMoNb-16-16
tr1_test=[0.05 0.10 0.35 0.40 0.44 0.46 0.55 0.88 1];
tr2_test=[0.70 0.61 0.21 0.25 0.20 0.21 0.21 0.05 0];

tr11_test=[0.05 0.10 0.35 0.40 0.44 0.46 0.55 0.88];  % (for scatter
 plot)
tr22_test=[0.70 0.61 0.21 0.25 0.20 0.21 0.21 0.05];  % (for scatter
 plot)

D1=tr1_test    % damage due to stress 1
D2=1-tr2_test  % 1-damage due to stress 2 = damage due to stress 1
 (D2=D1)

D11=tr11_test    %(for scatter plot)
D22=1-tr22_test  %(for scatter plot)

% time to cause damage D1=D2
t1=log10(D1*steel_tf1)
t2=log10(D2*steel_tf2)

t11=log10(D11*steel_tf1) %(for scatter plot)
t22=log10(D22*steel_tf2) %(for scatter plot)

% Constants for isodamage lines
[m1, b1]=str_lin(t1(1), S1(1), t2(1), S2(1))
[m2, b2]=str_lin(t1(2), S1(2), t2(2), S2(2))
[m3, b3]=str_lin(t1(3), S1(3), t2(3), S2(3))
[m4, b4]=str_lin(t1(4), S1(4), t2(4), S2(4))
[m5, b5]=str_lin(t1(5), S1(5), t2(5), S2(5))
[m6, b6]=str_lin(t1(6), S1(6), t2(6), S2(6))
[m7, b7]=str_lin(t1(7), S1(7), t2(7), S2(7))
[m8, b8]=str_lin(t1(8), S1(8), t2(8), S2(8))
[m9, b9]=str_lin(t1(9), S1(9), t2(9), S2(9))

x=[0:0.01:4]

% Isodamage lines
```

```
y1=m1*x+b1
y2=m2*x+b2
y3=m3*x+b3
y4=m4*x+b4
y5=m5*x+b5
y6=m6*x+b6
y7=m7*x+b7
y8=m8*x+b8
y9=m9*x+b9

figure(1)
axis([1 3 2.1 2.3])
axis square
box on
grid on
hold on
p(11)=scatter(t11,S11,'o k', 'filled')
p(12)=scatter(t22,S22,'o k','filled')
p(1)=plot(x,y1,'-.k')
p(2)=plot(x,y2,'-.k')
p(3)=plot(x,y3,'-.k')
p(4)=plot(x,y4,'-.k')
p(5)=plot(x,y5,'-.k')
p(6)=plot(x,y6,'-.k')
p(7)=plot(x,y7,'-.k')
p(8)=plot(x,y8,'-.k')
p(9)=plot(x,y9,'k')
set(p(9),'LineWidth',1.5);
legend(p([11 9  7 ]),'Data points','D=100%', 'Isodamage lines')
title('X8CrNiMoNb-16-16')
xlabel('log t')
ylabel('log \sigma')
hold off
```

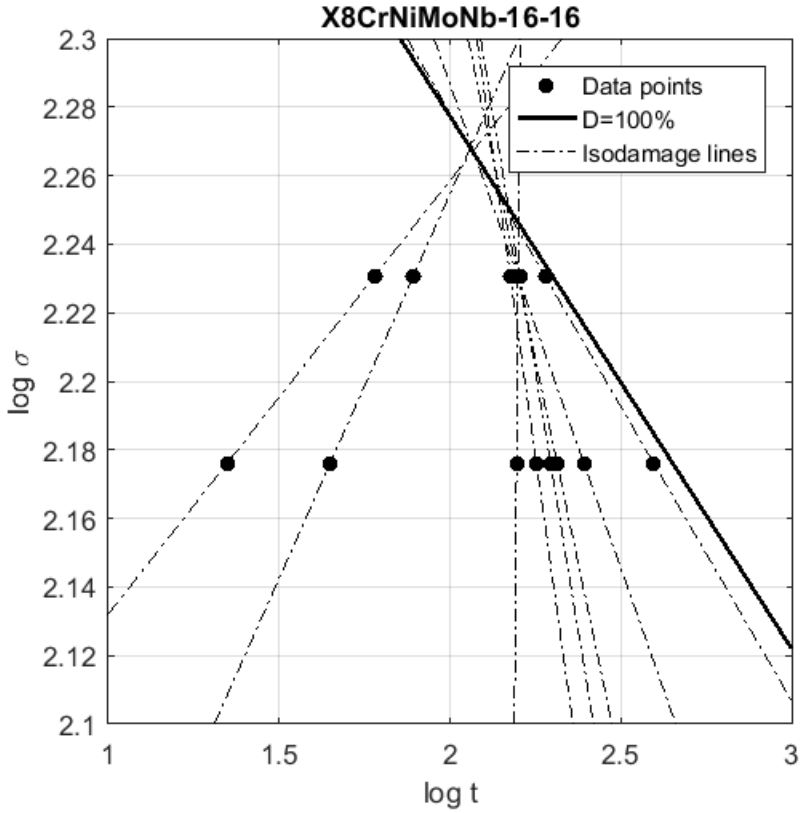

Published with MATLAB® R2016b

```
%=========================================================================
% Isodamage lines: Al 99.98
%=========================================================================
close all; clear all;

al_tf1=17     % time-to-rupture (h)
al_tf2=6.9    % time-to-rupture (h)


S1=ones(1,9)*log10(12)  % stress step 1
S2=ones(1,9)*log10(14)  % stress step 2

S11=ones(1,8)*log10(12)  % stress step 1 (for scatter plot)
S22=ones(1,8)*log10(14)  % stress step 2 (for scatter plot)

% lifetime ratios lifetime ratios Experimental data Alu-99.98
tr1_test=[0.12 0.13 0.30 0.32 0.50 0.65 0.70 0.75 1];
tr2_test=[0.58 0.56 0.38 0.37 0.24 0.16 0.13 0.11 0];

tr11_test=[0.12 0.13 0.30 0.32 0.50 0.65 0.70 0.75];  %(for scatter
 plot)
tr22_test=[0.58 0.56 0.38 0.37 0.24 0.16 0.13 0.11];  %(for scatter
 plot)

D1=tr1_test    % damage due to stress 1
D2=1-tr2_test  % 1-damage due to stress 2 = damage due to stress 1
 (D2=D1)

D11=tr11_test    %(for scatter plot)
D22=1-tr22_test  %(for scatter plot)

% time to cause damage D1=D2
t1=log10(D1*al_tf1)
t2=log10(D2*al_tf2)

t11=log10(D11*al_tf1) %(for scatter plot)
t22=log10(D22*al_tf2) %(for scatter plot)

% Constants for isodamage lines
[m1, b1]=str_lin(t1(1), S1(1), t2(1), S2(1))
[m2, b2]=str_lin(t1(2), S1(2), t2(2), S2(2))
[m3, b3]=str_lin(t1(3), S1(3), t2(3), S2(3))
[m4, b4]=str_lin(t1(4), S1(4), t2(4), S2(4))
[m5, b5]=str_lin(t1(5), S1(5), t2(5), S2(5))
[m6, b6]=str_lin(t1(6), S1(6), t2(6), S2(6))
[m7, b7]=str_lin(t1(7), S1(7), t2(7), S2(7))
[m8, b8]=str_lin(t1(8), S1(8), t2(8), S2(8))
[m9, b9]=str_lin(t1(9), S1(9), t2(9), S2(9))

x=[0:0.01:4]

% Isodamage lines
```

```
y1=m1*x+b1
y2=m2*x+b2
y3=m3*x+b3
y4=m4*x+b4
y5=m5*x+b5
y6=m6*x+b6
y7=m7*x+b7
y8=m8*x+b8
y9=m9*x+b9

figure(1)
axis([0 1.3 1 1.3])
axis square
box on
grid on
hold on
p(11)=scatter(t11,S11,'o k', 'filled')
p(12)=scatter(t22,S22,'o k','filled')
p(1)=plot(x,y1,'-.k')
p(2)=plot(x,y2,'-.k')
p(3)=plot(x,y3,'-.k')
p(4)=plot(x,y4,'-.k')
p(5)=plot(x,y5,'-.k')
p(6)=plot(x,y6,'-.k')
p(7)=plot(x,y7,'-.k')
p(8)=plot(x,y8,'-.k')
p(9)=plot(x,y9,'k')
set(p(9),'LineWidth',1.5);
legend(p([11 9  7 ]),'Data points','D=100%', 'Isodamage lines')
title('Al 99.98')
xlabel('log t')
ylabel('log \sigma')
hold off
```

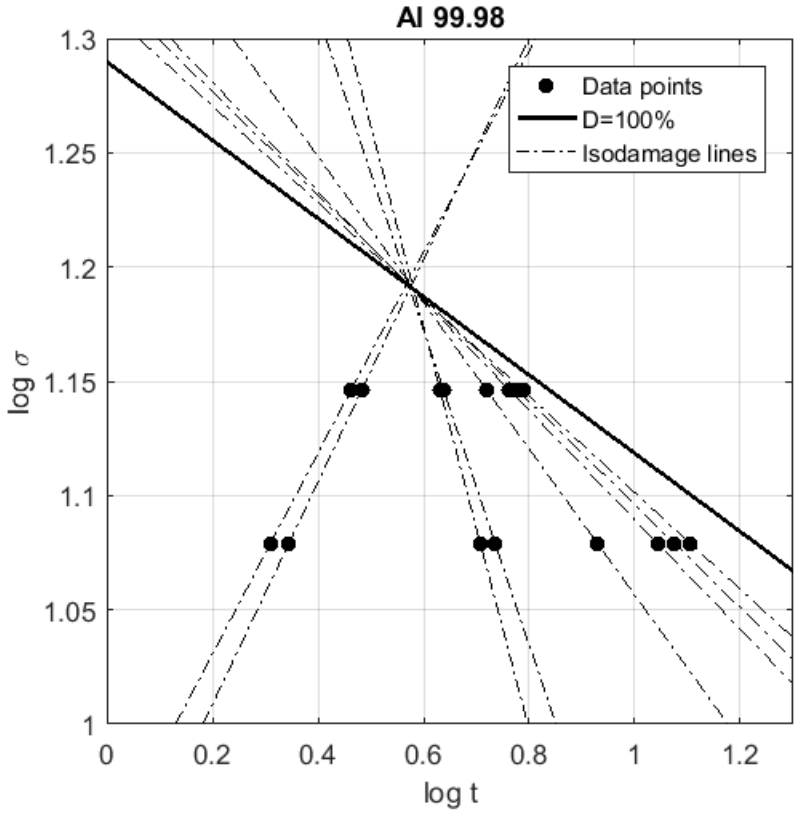

Published with MATLAB® R2016b

```
%=========================================================================
% Gauss vs polynomial fit
% Creep Data: creep rupture strength (CRS) X8CrNiMoNb 16-16
%=========================================================================
close all; clear all;

load CRS_X8CrNiMoNb1616.dat

T_C=CRS_X8CrNiMoNb1616(:,1);        % Temperature in Celcius
S_CRS=CRS_X8CrNiMoNb1616(:,2);      % Creep Rupture Strength
 CRS (MPa))
t=CRS_X8CrNiMoNb1616(:,3);          % CRS time in hours
T_K=T_C+273.15;                     % Temperature in Kelvin

C=15.4;                             % Larson-Miller constant
PLM=T_K.*(C+log10(t));              % Larson-Miller parameter


% Creep conditions
T=750+273.15                        % Temperature in Kelvin
S=15                                % Stress in MPa

% Fitted curves

% Gaussian fit

f=fit(PLM,S_CRS,'gauss1');          % Gaussian fit function
c=coeffvalues(f);
a=c(1); b=c(2); c=c(3);             % Coefficients of Gauss function

syms plm
plm=double(solve(a*exp(-((plm-b)/c)^2)==S, plm) );
plm(2);
t_CRS=10^(plm(2)/T-C);

% Polynomial fit

fp=fit(PLM,S_CRS,'poly2');          % Polynomial fit function
cp=coeffvalues(fp);
p1=cp(1); p2=cp(2); p3=cp(3);       % Coefficients of polynomial
 function

syms plm_p
plm_p=double(solve(p1*plm_p^2 + p2*plm_p + p3==S, plm_p) );
plm_p(1);
t_CRS_p=10^(plm_p(1)/T-C);


figure (1)
box on
grid on
axis square
```

```
hold on
h1=scatter(PLM,S_CRS, 'x');
h2=plot(f,'-.k');
h3=plot(fp,'-.r');
set(h1,'LineWidth',1);
set(h2,'LineWidth',1.5);
set(h3,'LineWidth',1.5);
xlabel('P_L_M=T(C+log t_C_R_S)')
ylabel('\sigma, [MPa]')
legend('Data points','Gaussian fit','Polynomial fit');
title('PLM vs. \sigma: Creep Rupture Strength, CRS')
```

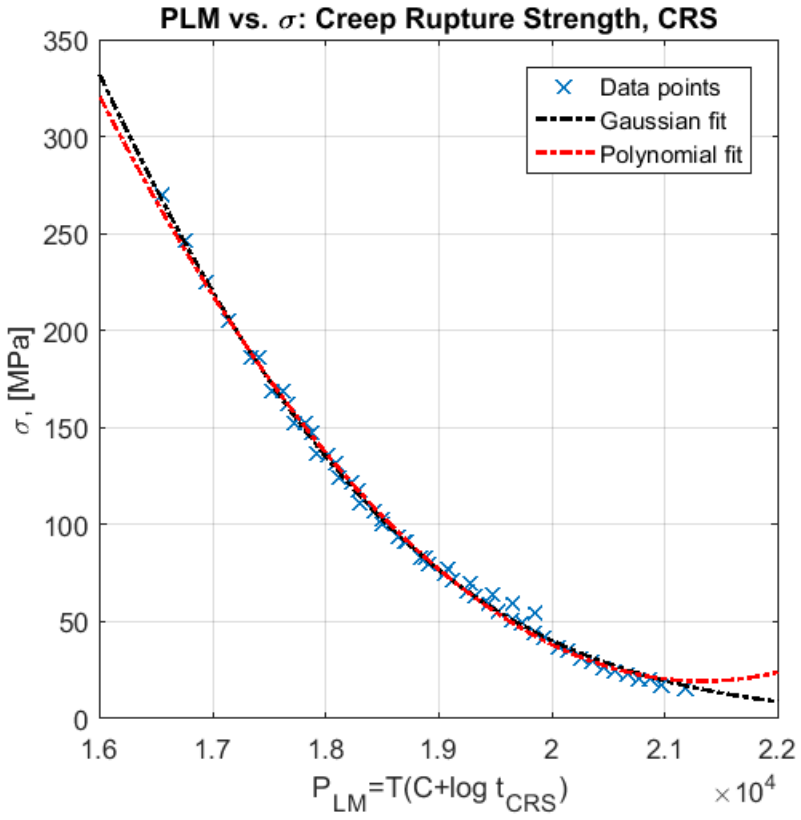

Published with MATLAB® R2016b

```
%=========================================================================
% Gauss vs polynomial fit (log stress)
% Creep Data: creep rupture strength (CRS) X8CrNiMoNb 16-16
%=========================================================================
close all; clear all;
load CRS_X8CrNiMoNb1616.dat

T_C=CRS_X8CrNiMoNb1616(:,1);            % Temperature in Celcius
S_CRS=log10(CRS_X8CrNiMoNb1616(:,2));   % Creep Rupture Strength
 CRS (MPa))
t=CRS_X8CrNiMoNb1616(:,3);              % CRS time in hours
T_K=T_C+273.15;                         % Temperature in Kelvin

C=13.9;                                 % Larson-Miller constant
PLM=T_K.*(C+log10(t));                  % Larson-Miller parameter


% Creep conditions
T=650+273.15                            % Temperature in Kelvin
S=170;                                  % Stress in MPa

% Fitted curves

% Gaussian fit

f=fit(PLM,S_CRS,'gauss1');              % Gaussian fit function
c=coeffvalues(f);
a=c(1); b=c(2); c=c(3);                 % Coefficients of Gauss
 function

syms plm
plm=double(solve(a*exp(-((plm-b)/c)^2)==log10(S), plm) );
plm(2);
t_CRS=10^(plm(2)/T-C);

% Polynomial fit

fp=fit(PLM,S_CRS,'poly2');          % Polynomial fit function
cp=coeffvalues(fp);
p1=cp(1); p2=cp(2); p3=cp(3);       % Coefficients of polynomial
 function

syms plm_p
plm_p=double(solve(p1*plm_p^2 + p2*plm_p + p3==log10(S), plm_p) );
plm_p(2);
t_CRS_p=10^(plm_p(2)/T-C);


figure (1)
box on
grid on
axis square
```

```
hold on
h1=scatter(PLM,S_CRS, 'x');
h2=plot(f,'-.k');
h3=plot(fp,'-.r');
xlabel('P_L_M=T(C+log t_C_R_S)')
ylabel('log\sigma')
set(h1,'LineWidth',1);
set(h2,'LineWidth',1.5);
set(h3,'LineWidth',1.5);
legend('Data points','Gaussian fit','Polynomial fit');
title('PLM vs. log\sigma: Creep Rupture Strength, CRS')
```

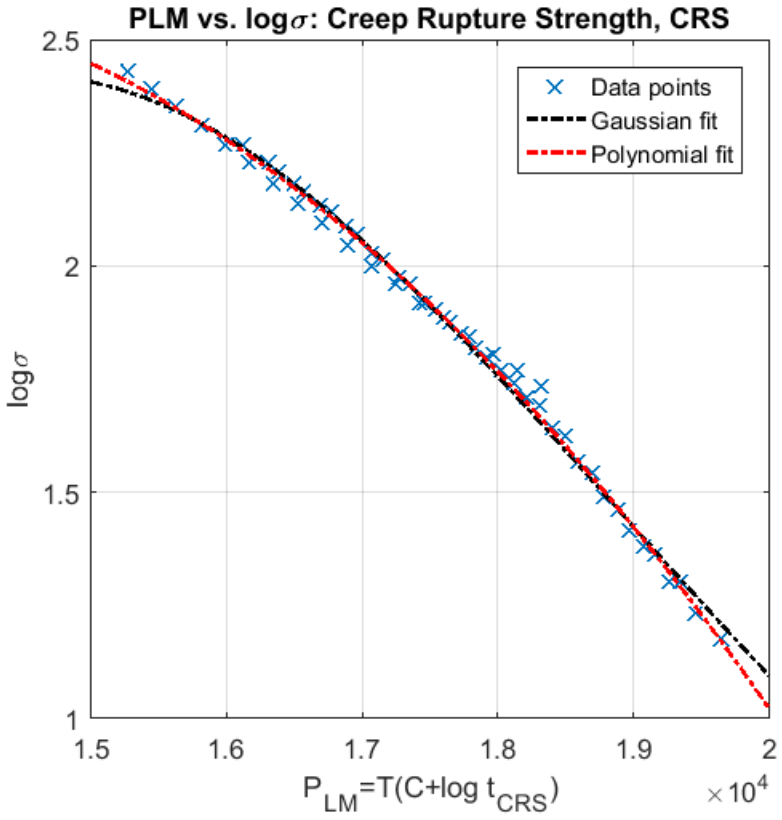

Published with MATLAB® R2016b

```
%=========================================================================
% Gauss vs polynomial fit
% Creep Data: creep resistance (Rp1) X8CrNiMoNb 16-16
%=========================================================================
close all; clear all;

load Rp1_X8CrNiMoNb1616.dat

T_C=Rp1_X8CrNiMoNb1616(:,1);        % Temperature in Celcius
S_Rp1=Rp1_X8CrNiMoNb1616(:,2);      % 1% Yield Stress Rp1 (MPa)
t=Rp1_X8CrNiMoNb1616(:,3);          % Rp1% time in hours
T_K=T_C+273.15;                     % Temperature in Kelvin

C=12.7;                             % Larson-Miller constant
PLM=T_K.*(C+log10(t));              % Larson-Miller parameter


% Creep conditions
T=750+273.15;                       % Temperature in Kelvin
S=17;                               % Stress in MPa

% Fitted curves

% Gaussian fit

f=fit(PLM,S_Rp1,'gauss1');           % Gaussian fit function
c=coeffvalues(f);
a=c(1); b=c(2); c=c(3);              % Coefficients of Gauss function

syms plm
plm=double(solve(a*exp(-((plm-b)/c)^2)==S, plm) );
plm(2);
t_Rp1=10^(plm(2)/T-C)

% Polynomial fit

fp=fit(PLM,S_Rp1,'poly2');         % Polynomial fit function
cp=coeffvalues(fp);
p1=cp(1); p2=cp(2); p3=cp(3);      % Coefficients of polynomial
 function

syms plm_p
plm_p=double(solve(p1*plm_p^2 + p2*plm_p + p3==S, plm_p) );
plm_p(1)
t_Rp1_p=10^(plm_p(1)/T-C)


figure (1)
box on
grid on
axis square
hold on
```

```
h1=scatter(PLM,S_Rp1, 'x');
h2=plot(f,'-.k');
h3=plot(fp,'-.r');
xlabel('P_L_M=T(C+log t_R_p_1_%)')
ylabel('\sigma, [MPa]')
set(h1,'LineWidth',1);
set(h2,'LineWidth',1.5);
set(h3,'LineWidth',1.5);
legend('Data points','Gaussian fit','Polynomial fit');
title('PLM vs. \sigma: 1% Yield Stress, R_p_1')

figure (2)
hold on
w1=plot(fp, PLM, S_Rp1,'Residuals')
w2=plot(f, PLM, S_Rp1,'Residuals')
```

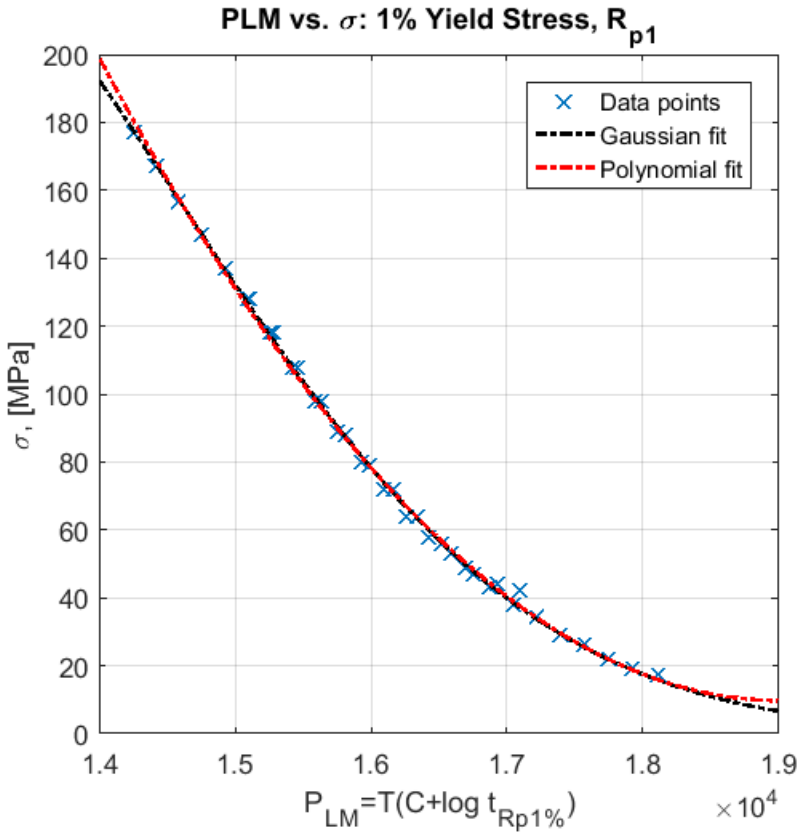

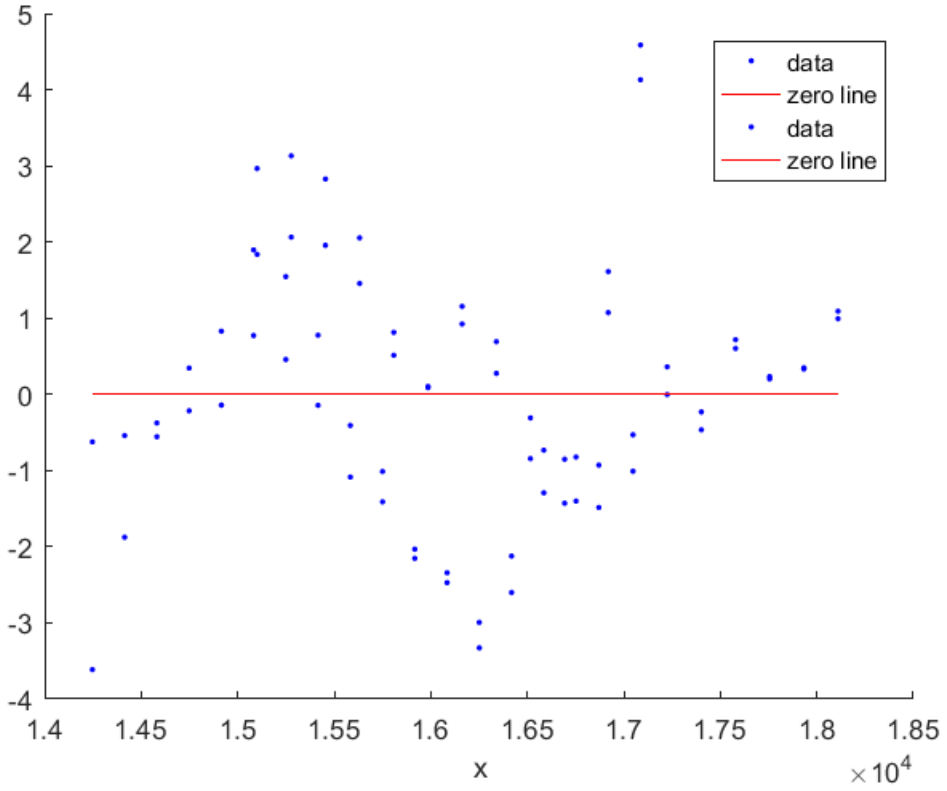

Published with MATLAB® R2016b

```
%=========================================================================
% Gauss vs polynomial fit (log stress)
% Creep Data: creep resistance (Rp1) X8CrNiMoNb 16-16
%=========================================================================
close all; clear all;

load Rp1_X8CrNiMoNb1616.dat

T_C=Rp1_X8CrNiMoNb1616(:,1);            % Temperature in Celcius
S_Rp1=log10(Rp1_X8CrNiMoNb1616(:,2));   % 1% Yield Stress Rp1 (MPa)
t=Rp1_X8CrNiMoNb1616(:,3);              % Rp1% time in hours
T_K=T_C+273.15;                         % Temperature in Kelvin

C=13.4;                                 % Larson-Miller constant
PLM=T_K.*(C+log10(t));                  % Larson-Miller parameter


% Creep conditions
T=700+273.15;                           % Temperature in Kelvin
S=152.51;                               % Stress in MPa

% Fitted curves

% Gaussian fit

f=fit(PLM,S_Rp1,'gauss1');              % Gaussian fit function
c=coeffvalues(f);
a=c(1); b=c(2); c=c(3);                 % Coefficients of Gauss
 function

syms plm
plm=double(solve(a*exp(-((plm-b)/c)^2)==log10(S), plm) );
plm(2);
t_Rp1=10^(plm(2)/T-C)

% Polynomial fit

fp=fit(PLM,S_Rp1,'poly2');          % Polynomial fit function
cp=coeffvalues(fp);
p1=cp(1); p2=cp(2); p3=cp(3);       % Coefficients of polynomial
 function

syms plm_p
plm_p=double(solve(p1*plm_p^2 + p2*plm_p + p3==log10(S), plm_p) );
plm_p(2)
t_Rp1_p=10^(plm_p(2)/T-C)


figure (1)
box on
grid on
axis square
```

```
hold on
h1=scatter(PLM,S_Rp1, 'x');
h2=plot(f,'-.k');
h3=plot(fp,'-.r');
xlabel('P_L_M=T(C+log t_R_p_1_%)')
ylabel('log\sigma')
set(h1,'LineWidth',1);
set(h2,'LineWidth',1.5);
set(h3,'LineWidth',1.5);
legend('Data points','Gaussian fit','Polynomial fit');
title('PLM vs. log\sigma: 1% Yield Stress, R_p_1')
```

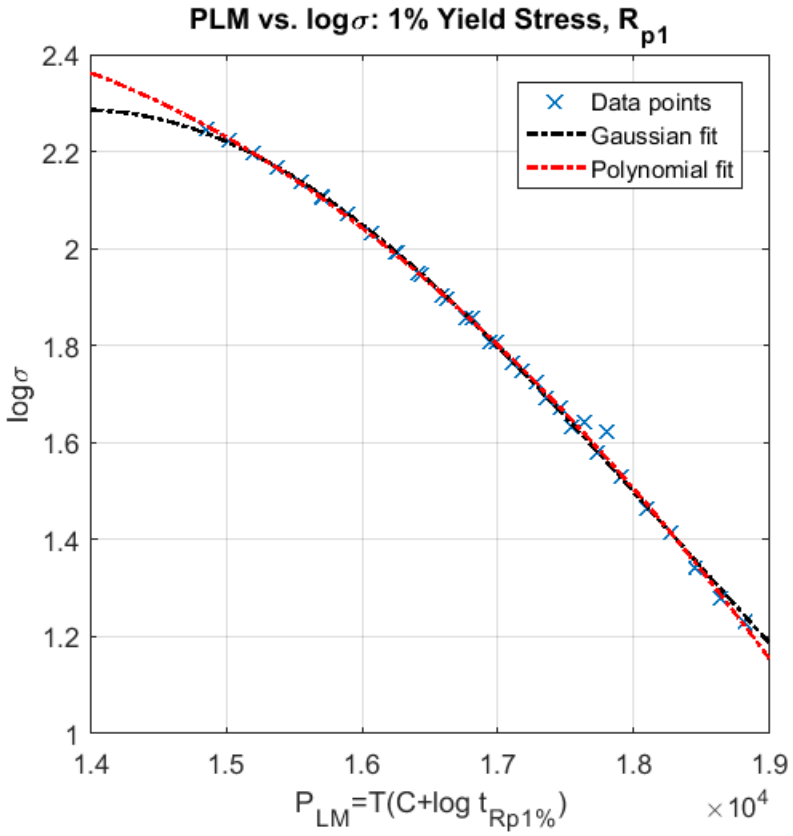

Published with MATLAB® R2016b

```
%=========================================================================
% Larson-Miller parameter fit for creep resistance 1% strain (Rp1)
% Creep Data: Rp1 X8CrNiMoNb 16-16
%=========================================================================
close all; clear all;

load Rp1_X8CrNiMoNb1616.dat

T_C=Rp1_X8CrNiMoNb1616(:,1);           % Temperature in Celcius
S_Rp1=log10(Rp1_X8CrNiMoNb1616(:,2));  % 1% Yield Stress Rp1 (MPa)
t=Rp1_X8CrNiMoNb1616(:,3);             % Rp1% time in hours
T_K=T_C+273.15;                        % Temperature in Kelvin

C=13.4;                                % Larson-Miller constant
PLM=T_K.*(C+log10(t));                 % Larson-Miller parameter


% Creep conditions
T=700+273.15;                          % Temperature in Kelvin
S=83.782;                              % Stress in MPa

% Fitted curves


% Polynomial fit

f=fit(PLM,S_Rp1,'poly2');              % Polynomial fit function
c=coeffvalues(f);
p1=c(1); p2=c(2); p3=c(3);             % Coefficients for polynomial
 function

syms plm
plm=double(solve(p1*plm^2 + p2*plm + p3==log10(S), plm) );
plm(2)
t_Rp1=10^(plm(2)/T-C)


figure (1)
box on
grid on
axis square
hold on
h1=scatter(PLM,S_Rp1, 'x');
h2=plot(f,'-.r');
xlabel('P_L_M=T(C+log t_R_p_1_%)')
ylabel('log\sigma')
set(h1,'LineWidth',1);
set(h2,'LineWidth',1.5);
legend('Data points','Polynomial fit');
title('PLM vs. log\sigma: 1% Yield Stress, R_p_1')
```

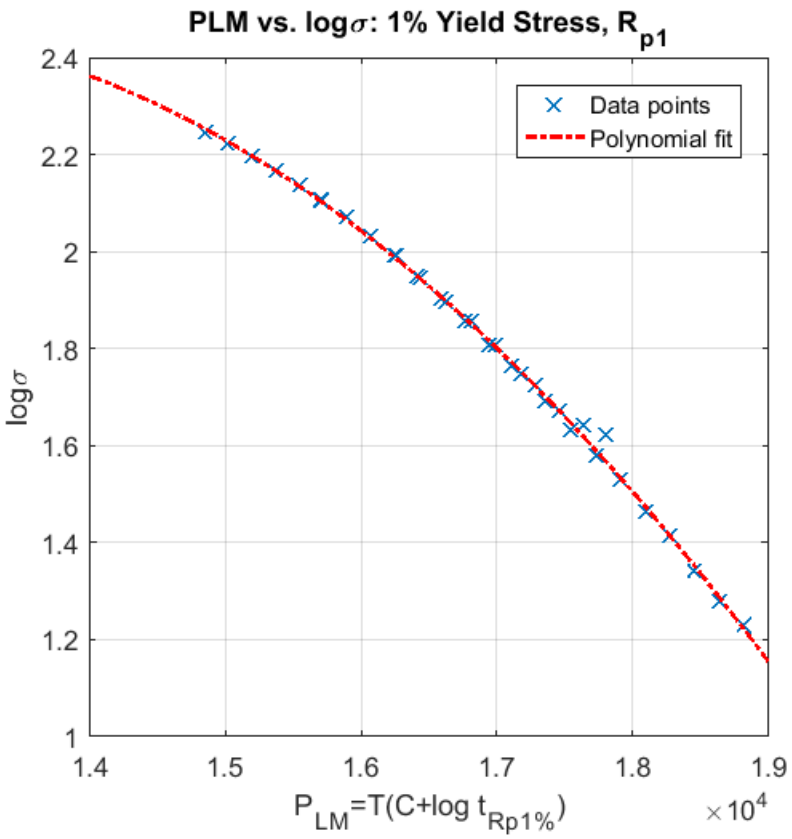

Published with MATLAB® R2016b

```
%=========================================================================
% Larson-Miller parameter fit for creep rupture strength (CRS)
% Creep Data: CRS X8CrNiMoNb 16-16
%=========================================================================
close all; clear all;
load CRS_X8CrNiMoNb1616.dat

T_C=CRS_X8CrNiMoNb1616(:,1);          % Temperature in Celcius
S_CRS=log10(CRS_X8CrNiMoNb1616(:,2)); % Creep Rupture Strength
 CRS (MPa))
t=CRS_X8CrNiMoNb1616(:,3);            % CRS time in hours
T_K=T_C+273.15;                       % Temperature in Kelvin

C=13.9;                               % Larson-Miller constant
PLM=T_K.*(C+log10(t));                % Larson-Miller parameter


% Creep conditions
T=700+273.15;                         % Temperature in Kelvin
S=184;                                % Stress in MPa

% Polynomial fit

f=fit(PLM,S_CRS,'poly2');            % Polynomial fit function
c=coeffvalues(f);
p1=c(1); p2=c(2); p3=c(3);           % Coefficients for polynomial
 function

syms plm
plm=double(solve(p1*plm^2 + p2*plm + p3==log10(S), plm) );
plm(2);
t_CRS=10^(plm(2)/T-C);


figure (1)
box on
grid on
axis square
hold on
h1=scatter(PLM,S_CRS, 'x');
h2=plot(f,'-.r');
xlabel('P_L_M=T(C+log t_C_R_S)')
ylabel('log\sigma')
set(h1,'LineWidth',1);
set(h2,'LineWidth',1.5);
legend('Data points','Polynomial fit');
title('PLM vs. log\sigma: Creep Rupture Strength, CRS')
```

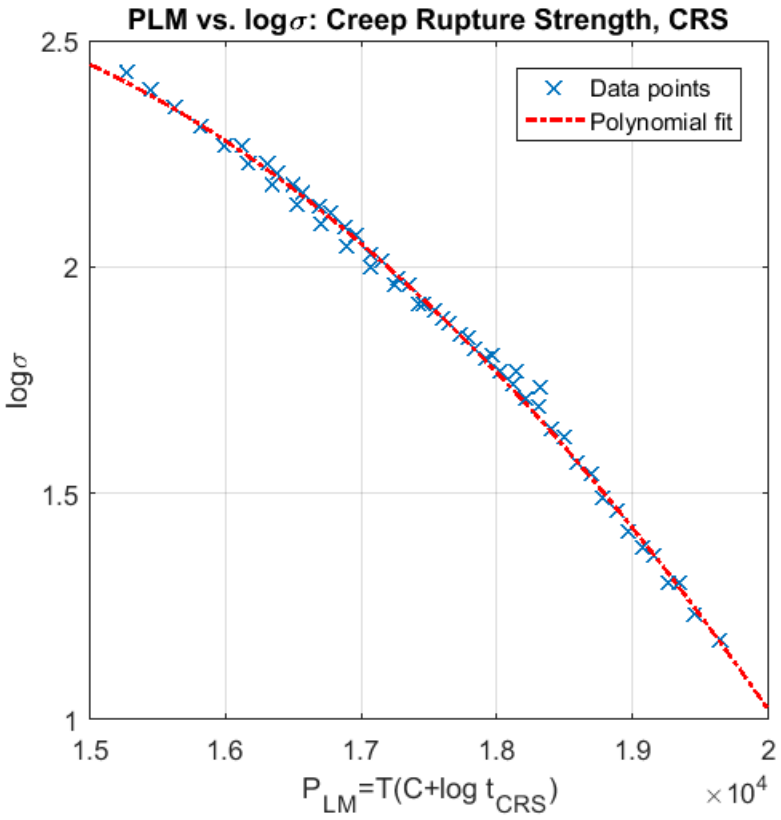

Published with MATLAB® R2016b

```
%=========================================================================
% Modified Pavlou model: Stress-rupture curve vs. Normalised curve
% Material: ASME - NH 304SS
%=========================================================================
close all; clear all;

% Temperature in celcius
T=[-200 -125 -75 25 100 150 200 250 300 350 400 450 500 550 600 650
 700];

% E(T) in MPa
E=[209 204 201 195 189 186 183 179 176 172 169 165 160 156 151 146
 140]*10^3;

% Interpolation and extrapolation of Elastic Modulus
figure(1)
 hold on
 axis square
 box on
 grid on
 hold on
 axis([-300 800 0 250*10^3])
 scatter(T,E,'filled')
 plot(T, E, '-.b')
 coeffs = polyfit(T, E(1:17), 2);
 Tfit = linspace(T(1), E(end), 140);
 Efit = polyval(coeffs, Tfit);
 hold on;
 plot(Tfit, Efit, 'r-.');
 grid on;
 ax = gca;
 ax.XAxisLocation = 'origin';
 ax.YAxisLocation = 'origin';
 xlabel('Temperature, ^{\circ}C')
 ylabel('Moduli of Elasticity, E [MPa]')

% Get value for E(T) from interpolation and extrapolation
Efit425=interp1(T,E,425,'linear');
Efit450=interp1(T,E,450,'linear');
Efit475=interp1(T,E,475,'linear');
Efit500=interp1(T,E,500,'linear');
Efit525=interp1(T,E,525,'linear');
Efit550=interp1(T,E,550,'linear');
Efit575=interp1(T,E,575,'linear');
Efit600=interp1(T,E,600,'linear');
Efit625=interp1(T,E,625,'linear');
Efit650=interp1(T,E,650,'linear');
Efit675=interp1(T,E,675,'linear');
Efit700=interp1(T,E,700,'linear');
Efit725 = polyval(coeffs, 725);
Efit750 = polyval(coeffs, 750);
Efit775 = polyval(coeffs, 775);
```

```
Efit800 = polyval(coeffs, 800);

% Rupture stresses at temperature T
S=[393 390 385 377 368 355 333 298 256 220 189 162 140 121 105 91;
   393 390 385 377 358 321 274 233 198 169 145 123 106 89 76 65;
   393 390 385 363 328 285 241 205 175 147 125 106 91 77 66 56;
   393 390 385 350 301 254 214 180 151 127 108 91 77 67 55 46;
   393 390 364 317 267 223 188 157 130 110 91 75 64 54 45 37;
   393 390 340 284 236 195 161 134 111 92 75 63 53 44 36 29;
   393 353 300 250 205 168 139 113 93 77 62 52 43 35 29 24;
   393 325 265 217 177 144 113 95 78 63 51 41 34 28 23 19;
   354 287 232 188 153 124 100 80 64 52 42 34 28 23 18 14;
   308 249 201 161 129 104 83 66 53 43 35 27 22 18 14 10;
   272 219 176 140 114 91 59 56 44 34 28 22 18 14 11 9];

% Normalized stresses S/E(T)
S_norm1=S(:,1)/Efit425;
S_norm2=S(:,2)/Efit450;
S_norm3=S(:,3)/Efit475;
S_norm4=S(:,4)/Efit500;
S_norm5=S(:,5)/Efit525;
S_norm6=S(:,6)/Efit550;
S_norm7=S(:,7)/Efit575;
S_norm8=S(:,8)/Efit600;
S_norm9=S(:,9)/Efit625;
S_norm10=S(:,10)/Efit650;
S_norm11=S(:,11)/Efit675;
S_norm12=S(:,12)/Efit700;
S_norm13=S(:,13)/Efit725;
S_norm14=S(:,14)/Efit750;
S_norm15=S(:,15)/Efit775;
S_norm16=S(:,16)/Efit800;

% tf=rupture time
tf=[1;10;30;100;300;1000;3000;10000;30000;100000;300000];

% Normalized Rupture curve
figure(2)
box on
axis square
grid on
hold on
loglog(tf,S_norm1,'+-')
loglog(tf,S_norm2,'+-')
loglog(tf,S_norm3,'+-')
loglog(tf,S_norm4,'+-')
loglog(tf,S_norm5,'+-')
loglog(tf,S_norm6,'+-')
loglog(tf,S_norm7,'+-')
loglog(tf,S_norm8,'+-')
loglog(tf,S_norm9,'+-')
loglog(tf,S_norm10,'+-')
loglog(tf,S_norm11,'+-')
loglog(tf,S_norm12,'+-')
```

```
loglog(tf,S_norm13,'+-')
loglog(tf,S_norm14,'+-')
loglog(tf,S_norm15,'+-')
loglog(tf,S_norm16,'+-')
hold off
set(gca,'xscale','log');
set(gca,'yscale','log');
xlabel('Time to rupture, t_f')
ylabel('stress /Elastic modulus')
legend('425^{\circ}C','450^{\circ}C','475^{\circ}C','500^{\circ}C','525^{\circ}C',

% stress rupture curve
figure(3)
box on
axis square
grid on
hold on
loglog(tf,S(:,1),'+-')
loglog(tf,S(:,2),'+-')
loglog(tf,S(:,3),'+-')
loglog(tf,S(:,4),'+-')
loglog(tf,S(:,5),'+-')
loglog(tf,S(:,6),'+-')
loglog(tf,S(:,7),'+-')
loglog(tf,S(:,8),'+-')
loglog(tf,S(:,9),'+-')
loglog(tf,S(:,10),'+-')
loglog(tf,S(:,11),'+-')
loglog(tf,S(:,12),'+-')
loglog(tf,S(:,13),'+-')
loglog(tf,S(:,14),'+-')
loglog(tf,S(:,15),'+-')
loglog(tf,S(:,16),'+-')
hold off
set(gca,'xscale','log');
set(gca,'yscale','log');
xlabel('Time to rupture, t_f')
ylabel('stress')
%legend('425^{\circ}C','450^{\circ}C','475^{\circ}C','500^{\circ}C','525^{\circ}C'
```

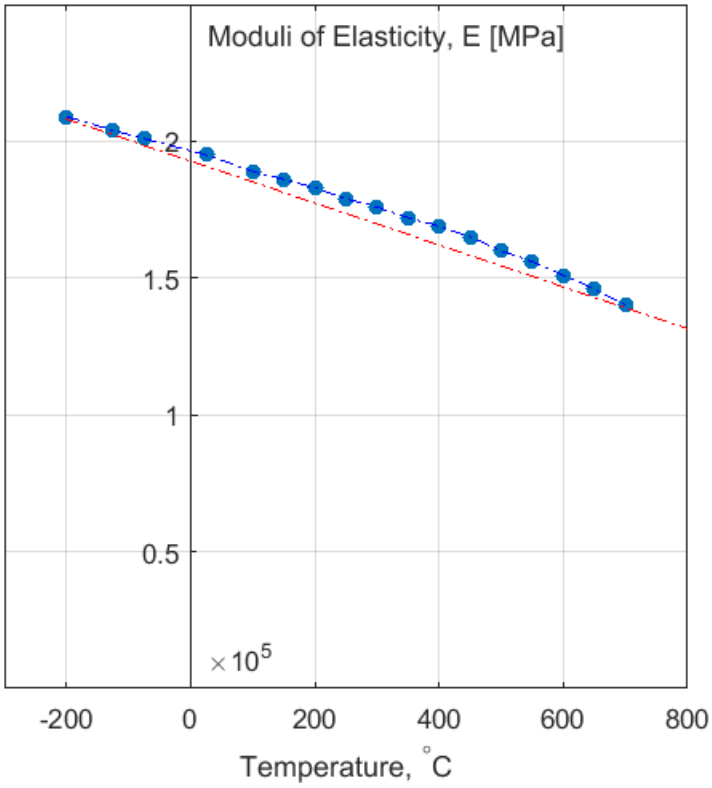
Moduli of Elasticity, E [MPa]
2
1.5
1
0.5
×10^5
-200
0
200
400
600
800
Temperature, °C

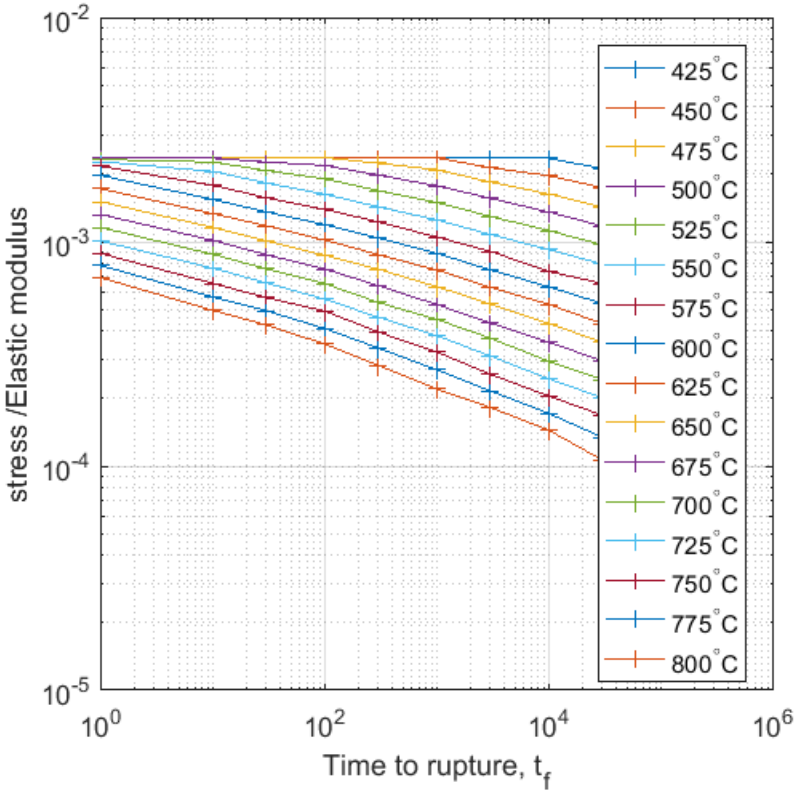
10^-2
10^-3
10^-4
10^-5
stress /Elastic modulus
10^0
10^2
10^4
10^6
Time to rupture, t_f
425°C
450°C
475°C
500°C
525°C
550°C
575°C
600°C
625°C
650°C
675°C
700°C
725°C
750°C
775°C
800°C

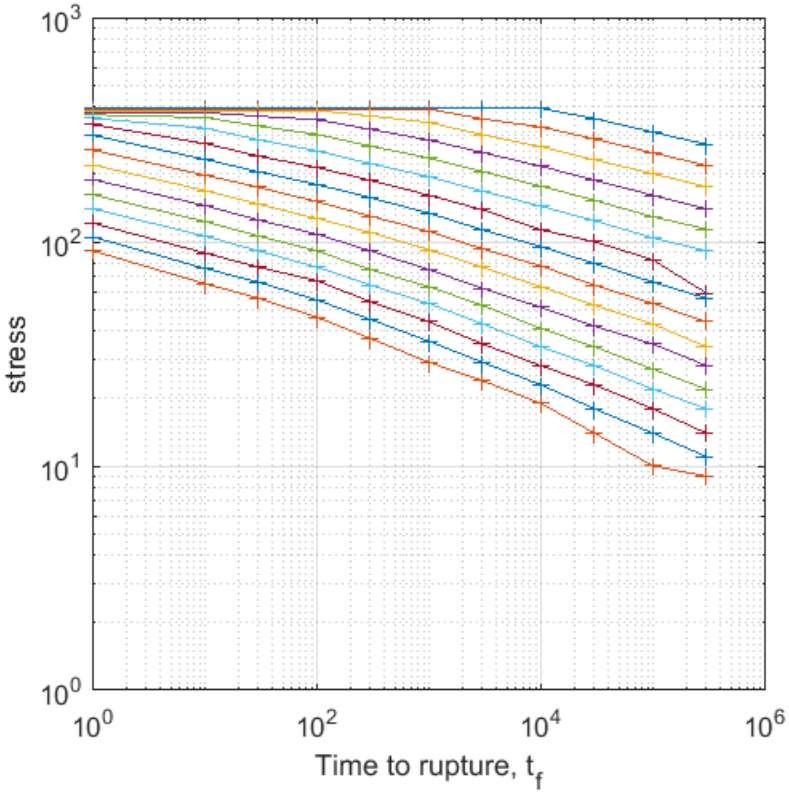

Published with MATLAB® R2016b

```
%=========================================================================
% Pavlou model vs. time fraction rule: sequence study
% Material: X8CrNiMoNb-16-16
%=========================================================================
close all;
clear all;

sigma=[120 150];    % Stress, sigma in [MPa]
T=[973 973];        % Temperature T in [K]

t_r1=[0:0.01:1];    % increment of ratio t1/tf1 between 0-1

% Fitting parameter

p=184.9160

for k=1:101

    for i=1:1

 % exponent for sequence L-H
    q(i)=T(i)*log10(sigma(i+1)/p)/(T(i+1)*log10(sigma(i)/p));

 % exponent for sequence H-L
    q(i+1)=T(i+1)*log10(sigma(i)/p)/(T(i)*log10(sigma(i+1)/p));

    t_r2(k)=1-t_r1(k)^q(i);   % remaining life L-H
    tr2(k)=1-t_r1(k)^q(i+1);  % remaining life H-L
    t_r2L(k)=1-t_r1(k);       % remaining life Robinson (linear)

    end
end

% plot of remaining life vs. consumed life

figure(1)
box on
grid on
axis square
hold on
plot(t_r1,t_r2,'b')
plot(t_r1,tr2,'r')
plot(t_r1,t_r2L, 'k')
hold off
%axis([0 1 0 1])
%axis([0 1 -1 1]) % for singularity load case
title('Constant temperature: case 4')
%title('Constant stress:Case 6')
xlabel('Consumed life t_1/t_f_1')
ylabel('Remaining life t_2/t_f_2')
legend('L-H','H-L','Linear summation')
```

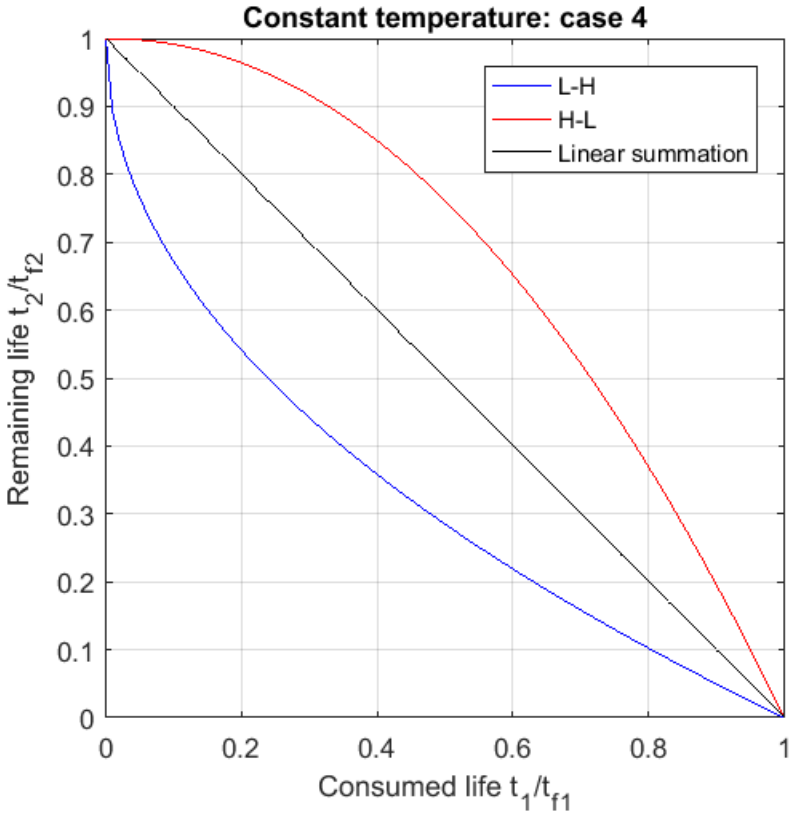

Published with MATLAB® R2016b

```
%=========================================================================
% Creep-Fatigue Damage Envelope
%=========================================================================

close all;
clear all;

% 304SS & 316SS, intersection (0.3, 0.3)

x = [0:0.01:0.3];
y = 1-7/3*x;          % first part of curve
x = [x,0.3];          % Cause a break in the line
y = [y,NaN];
x1 =[0.3:0.01:1];     % 2nd part of curve
x = [x,x1];
y = [y,3/7-x1.*3/7];
x1 = [x1,1];

% 21/4Cr-1Mo & 800H, intersection (0.1, 0.1)

r = [0:0.01:0.1];
s = 1-9/1*r;          % first part of curve
r = [r,0.1];          % Cause a break in the line
s = [s,NaN];
r1 =[0.1:0.01:1];     % 2nd part of curve
r = [r,r1];
s = [s,1/9-r1.*1/9];
r1 = [r1,1];

% 9Cr-1Mo-V, intersection (0.1, 0.01)
u = [0:0.001:0.1];
v = 1-9.9*u;          % first part of curve
u = [u,0.1];          % Cause a break in the line
v = [v,NaN];
u1 =[0.1:0.001:1];    % 2nd part of curve
u = [u,u1];
v = [v,1/90-u1.*1/90];
u1 = [u1,1];


% plot Creep-Fatigue Damage envelope

figure(1)
h1=plot(x,y,'b');
axis square
hold on
h2=plot(r,s, 'g');
h3=plot(u,v,'--r');
axis([0 1 0 1])
%title('Creep-Fatigue Damage Envelope')
xlabel('\Sigma n/ N_d')
ylabel('\Sigma \Deltat / T_d')
```

```
legend('304SS & 316SS','2 1/4Cr-1Mo & 800H','9Cr-1Mo-V')
grid on
set(gca,'xtick',[0.0 0.1 0.2 0.3 0.4 0.5 0.6 0.7 0.8 0.9 1])
set(gca,'ytick',[0.0 0.1 0.2 0.3 0.4 0.5 0.6 0.7 0.8 0.9 1])
set(gca,'xticklabel',
{'0.0' '' '0.2' '' '0.4' '' '0.6' '' '0.8' '' '1.0'})
set(gca,'yticklabel',
{'0.0' '' '0.2' '' '0.4' '' '0.6' '' '0.8' '' '1.0'})

set(h1,'LineWidth',1.2);
set(h2,'LineWidth',1.2);
set(h3,'LineWidth',1.2);
```

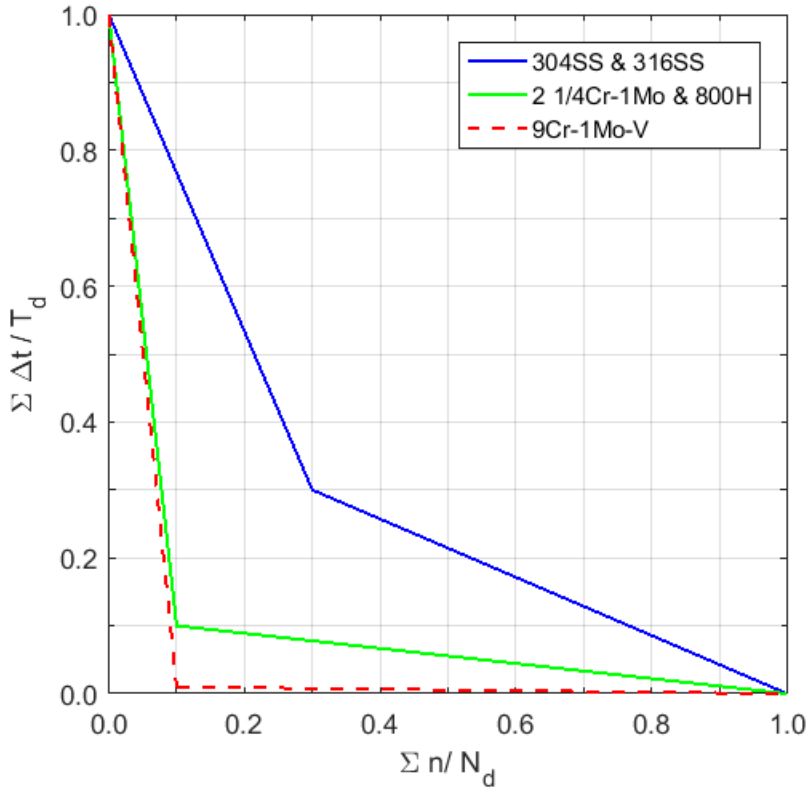

Published with MATLAB® R2016b

This page intentionally left blank

APPENDIX C – Remaining life calculations

Creep rupture: Remaining life t_2

CRS L-H linear elastic									**Pavlou model**	**Life Fraction Rule**		
		σ_1	σ_2	$\Delta\sigma$	q^{12}	t_1/t_{f1}	$(t_1/t_{f1})^{q12}$	t_{f2}	$t_{2p}=[1-(t_1/t_{f1})^{q12}]*t_{f2}$	$t_{2LFR}=(1-t_1/t_{f1})*t_{f2}$	$\Delta t_2=t_{2p}-t_{2LFR}$	$\Delta t_2/t_{2p}$
Von Mises	σ_{VM}	81.34	122.01	40.67	0.506	0.3	0.544	2665	1216	1865	-649	-53.4
Tresca	σ_{TR}	92.147	138.22	46.073	0.418	0.3	0.605	1567	619	1097	-477	-77.1
MPS	σ_{MPS}	84.162	126.24	42.078	0.485	0.3	0.558	2311	1022	1618	-596	-58.3
Mixed criteria α=0.8	σ_{eq}	81.896	122.84	40.944	0.502	0.3	0.546	2591	1176	1814	-638	-54.3
Mixed criteria α=0.9	σ_{eq}	81.618	122.43	40.812	0.504	0.3	0.545	2627	1196	1839	-644	-53.8
Huddleston	σ_{HUD}	83.843	125.76	41.917	0.487	0.3	0.556	2349	1043	1644	-601	-57.7
CRS H-L linear elastic									**Pavlou model**	**Life Fraction Rule**		
		σ_1	σ_2	$\Delta\sigma$	q^{12}	t_1/t_{f1}	$(t_1/t_{f1})^{q12}$	t_{f2}	$t_2=[1-(t_1/t_{f1})^{q12}]*t_{f2}$	$t_{2LFR}=(1-t_1/t_{f1})*t_{f2}$	$\Delta t_2=t_{2p}-t_{2LFR}$	$\Delta t_2/t_{2p}$
Von Mises	σ_{VM}	122.01	81.34	40.67	1.975	0.3	0.093	12690	11514	8883	2630	22.8
Tresca	σ_{TR}	138.22	92.147	46.073	2.393	0.3	0.056	8035	7585	5625	1960	25.8
MPS	σ_{MPS}	126.24	84.162	42.078	2.062	0.3	0.084	11220	10283	7854	2429	23.6
Mixed criteria α=0.8	σ_{eq}	122.84	81.896	40.944	1.991	0.3	0.091	12383	11257	8668	2589	23.0
Mixed criteria α=0.9	σ_{eq}	122.43	81.618	40.812	1.983	0.3	0.092	12536	11385	8775	2610	22.9
Huddleston	σ_{HUD}	125.76	83.843	41.917	2.052	0.3	0.085	11376	10414	7963	2451	23.5
CRS L-H elastic plastic									**Pavlou model**	**Life Fraction Rule**		
		σ_1	σ_2	$\Delta\sigma$	q^{12}	t_1/t_{f1}	$(t_1/t_{f1})^{q12}$	t_{f2}	$t_2=[1-(t_1/t_{f1})^{q12}]*t_{f2}$	$t_{2LFR}=(1-t_1/t_{f1})*t_{f2}$	$\Delta t_2=t_{2p}-t_{2LFR}$	$\Delta t_2/t_{2p}$
Von Mises	σ_{VM}	81.281	114.25	32.969	0.586	0.3	0.494	3487	1765	2441	-676	-38.3
Tresca	σ_{TR}	92.082	130	37.918	0.505	0.3	0.544	2042	931	1429	-499	-53.6
MPS	σ_{MPS}	84.098	119.47	35.372	0.554	0.3	0.513	2907	1416	2035	-619	-43.7
Mixed criteria α=0.8	σ_{eq}	81.836	115	33.164	0.583	0.3	0.496	3396	1712	2377	-665	-38.8
Mixed criteria α=0.9	σ_{eq}	81.559	114.62	33.061	0.584	0.3	0.495	3442	1739	2409	-671	-38.6
Huddleston	σ_{HUD}	83.782	117.94	34.158	0.568	0.3	0.505	3065	1518	2145	-627	-41.3
CRS H-L elastic-plastic									**Pavlou model**	**Life Fraction Rule**		
		σ_1	σ_2	$\Delta\sigma$	q^{12}	t_1/t_{f1}	$(t_1/t_{f1})^{q12}$	t_{f2}	$t_2=[1-(t_1/t_{f1})^{q12}]*t_{f2}$	$t_{2LFR}=(1-t_1/t_{f1})*t_{f2}$	$\Delta t_2=t_{2p}-t_{2LFR}$	$\Delta t_2/t_{2p}$
Von Mises	σ_{VM}	114.25	81.281	32.969	1.707	0.3	0.128	12724	11094	8906	2188	19.7
Tresca	σ_{TR}	130	92.082	37.918	1.979	0.3	0.092	8057	7313	5640	1673	22.9
MPS	σ_{MPS}	119.47	84.098	35.372	1.804	0.3	0.114	11251	9969	7876	2093	21.0
Mixed criteria α=0.8	σ_{eq}	115	81.836	33.164	1.716	0.3	0.127	12416	10844	8691	2152	19.8
Mixed criteria α=0.9	σ_{eq}	114.62	81.559	33.061	1.711	0.3	0.127	12568	10967	8798	2170	19.8
Huddleston	σ_{HUD}	117.94	83.782	34.158	1.760	0.3	0.120	11406	10036	7984	2052	20.4

1% strain: Remaining life t_2

Rp1 L-H linear elastic									**Pavlou model**	**Life Fraction Rule**		
		σ_1	σ_2	$\Delta\sigma$	q^{12}	t_1/t_{f1}	$(t_1/t_{f1})^{q12}$	t_{f2}	$t_{2p}=[1-(t_1/t_{f1})^{q12}]*t_{f2}$	$t_{2LFR}=(1-t_1/t_{f1})*t_{f2}$	$\Delta t_2=t_{2p}-t_{2LFR}$	$\Delta t_2/t_{2p}$
Von Mises	σ_{VM}	81.34	122.01	40.67	0.506	0.3	0.544	669	305	468	-163	-53.4
Tresca	σ_{TR}	92.147	138.22	46.073	0.418	0.3	0.605	347	137	243	-106	-77.1
MPS	σ_{MPS}	84.162	126.24	42.078	0.485	0.3	0.558	562	248	393	-145	-58.3
Mixed criteria α=0.8	σ_{eq}	81.896	122.84	40.944	0.502	0.3	0.546	646	293	452	-159	-54.3
Mixed criteria α=0.9	σ_{eq}	81.618	122.43	40.812	0.504	0.3	0.545	657	299	460	-161	-53.8
Huddleston	σ_{HUD}	83.843	125.76	41.917	0.487	0.3	0.556	573	254	401	-147	-57.7
Rp1 H-L linear elastic									**Pavlou model**	**Life Fraction Rule**		
		σ_1	σ_2	$\Delta\sigma$	q^{12}	t_1/t_{f1}	$(t_1/t_{f1})^{q12}$	t_{f2}	$t_2=[1-(t_1/t_{f1})^{q12}]*t_{f2}$	$t_{2LFR}=(1-t_1/t_{f1})*t_{f2}$	$\Delta t_2=t_{2p}-t_{2LFR}$	$\Delta t_2/t_{2p}$
Von Mises	σ_{VM}	122.01	81.34	40.67	1.975	0.3	0.093	4289	3892	3003	889	22.8
Tresca	σ_{TR}	138.22	92.147	46.073	2.393	0.3	0.056	2511	2370	1758	612	25.8
MPS	σ_{MPS}	126.24	84.162	42.078	2.062	0.3	0.084	3715	3405	2601	804	23.6
Mixed criteria α=0.8	σ_{eq}	122.84	81.896	40.944	1.991	0.3	0.091	4169	3790	2918	871	23.0
Mixed criteria α=0.9	σ_{eq}	122.43	81.618	40.812	1.983	0.3	0.092	4229	3840	2960	880	22.9
Huddleston	σ_{HUD}	125.76	83.843	41.917	2.052	0.3	0.085	3776	3456	2643	813	23.5
Rp1 L-H elastic-plastic									**Pavlou model**	**Life Fraction Rule**		
		σ_1	σ_2	$\Delta\sigma$	q^{12}	t_1/t_{f1}	$(t_1/t_{f1})^{q12}$	t_{f2}	$t_2=[1-(t_1/t_{f1})^{q12}]*t_{f2}$	$t_{2LFR}=(1-t_1/t_{f1})*t_{f2}$	$\Delta t_2=t_{2p}-t_{2LFR}$	$\Delta t_2/t_{2p}$
Von Mises	σ_{VM}	81.281	114.25	32.969	0.586	0.5	0.666	927	309	464	-154	-49.8
Tresca	σ_{TR}	92.082	130	37.918	0.505	0.3	0.544	482	220	337	-118	-53.6
MPS	σ_{MPS}	84.098	119.47	35.372	0.554	0.3	0.513	743	362	520	-158	-43.7
Mixed criteria α=0.8	σ_{eq}	81.836	115	33.164	0.583	0.3	0.496	898	453	629	-176	-38.8
Mixed criteria α=0.9	σ_{eq}	81.559	114.62	33.061	0.584	0.3	0.495	913	461	639	-178	-38.6
Huddleston	σ_{HUD}	83.782	117.94	34.158	0.568	0.3	0.505	793	393	555	-162	-41.3
Rp1 H-L elastic-plastic									**Pavlou model**	**Life Fraction Rule**		
		σ_1	σ_2	$\Delta\sigma$	q^{12}	t_1/t_{f1}	$(t_1/t_{f1})^{q12}$	t_{f2}	$t_2=[1-(t_1/t_{f1})^{q12}]*t_{f2}$	$t_{2LFR}=(1-t_1/t_{f1})*t_{f2}$	$\Delta t_2=t_{2p}-t_{2LFR}$	$\Delta t_2/t_{2p}$
Von Mises	σ_{VM}	114.25	81.281	32.969	1.707	0.3	0.128	4302	3752	3012	740	19.7
Tresca	σ_{TR}	130	92.082	37.918	1.979	0.3	0.092	2519	2286	1763	523	22.9
MPS	σ_{MPS}	119.47	84.098	35.372	1.804	0.3	0.114	3727	3302	2609	693	21.0
Mixed criteria α=0.8	σ_{eq}	115	81.836	33.164	1.716	0.3	0.127	4182	3652	2927	725	19.8
Mixed criteria α=0.9	σ_{eq}	114.62	81.559	33.061	1.711	0.3	0.127	4241	3701	2969	732	19.8
Huddleston	σ_{HUD}	117.94	83.782	34.158	1.760	0.3	0.120	3787	3332	2651	681	20.4